Queen Mary
University of London

School of Engineering and Materials Science (SEMS)

Engineered self-assembling peptide-hyaluronan hydrogels

for *in vitro* biomedical applications

Yichen Yuan

Primary Supervisor: Dr Helena Azevedo

Submitted in partial fulfillment of the requirements of the

Degree of Doctor of Philosophy

2022

Statement of Originality

I, Yichen Yuan, confirm that the research included within this thesis is my own work or that where it has been carried out in collaboration with, or supported by others, that this is duly acknowledged below, and my contribution indicated. Previously published material is also acknowledged below.

I attest that I have exercised reasonable care to ensure that the work is original and does not to the best of my knowledge break any UK law, infringe any third party's copyright or other Intellectual Property Right, or contain any confidential material.

I accept that the College has the right to use plagiarism detection software to check the electronic version of the thesis.

I confirm that this thesis has not been previously submitted for the award of a degree by this or any other university.

The copyright of this thesis rests with the author and no quotation from it or information derived from it may be published without the prior written consent of the author.

Signature: Yichen Yuan

Date: 20 February 2022

Acknowledgments

The four-year PhD at Queen Mary, University of London is a very special journey. Here I would like to first thank my supervisor Dr Helena Azevedo. I am so lucky to have you as my supervisor. I am grateful for your continuous guidance and generous support, and especially for your help during the thesis writing. You are always encouraging me to try something new and I am impressed with your enthusiasm about the research.

And I would like to thank China Scholarship Council and Queen Mary for the funding support and offering me this great opportunity for studying in London.

I would also thank everyone in MHAtriCell Group group. Yejiao: For your help with the research work, telling me a lot about the peptide characterization and we also spend a lot of great time hanging out. Xinqing: Thanks for showing me the cell work and for making our lunch time together so joyful. Yaqi: I will always remember the time when we were walking along the Regent canal. Jacob: thank you for telling me about Africa! I would also thank Ana, Arturo, Carlos, and Lourenco for the help in the lab. The support from SEMS is also important for me. I would thank every technician for the professional work. I would also thank Darren for the help with nanoindentation and Will for the help with the rheology work.

Finally. I would thank my family and friends for your continuous support. Thank you Mom, Dad, and Grandma for your unconditional love. Any all the friends-Rui, Mingyang, Xinru, Xuechun, Weidong and Yiyun - I'll always treasure those moments spent with you. I would also thank my flatmates in Cambridge House for sharing good food and interesting stories. This PhD journey must be the most unforgettable experience in my life.

Abstract

Self-assembling building blocks based on peptides have attracted great interest in tissue engineering due their intrinsic bioactivity. Supramolecular peptide-polymer assemblies have advantage of mimicking the natural protein-polymer complexes present in biological systems. Hyaluronic acid (HA) is an anionic, non-sulfated glycosaminoglycan involved in varied and essential biological activities, which is also one of chief components of the extracellular matrix (ECM) of tissues and the human vitreous. This thesis presents the fabrication of novel supramolecular hydrogels containing polyelectrolytes and rationally designed peptides and the exploitation of peptide-HA hydrogels as *in vitro* models.

In **Chapter 1** the research background of the project is introduced. It starts with a short review on self-assembling peptides and their hydrogel formation, followed by an overview about the HA macromolecule, and then finalised by discussing the research done on hybrid supramolecular peptide-polymer complexes. The objectives of the work described in the thesis are provided. **Chapter 2** describes in detail the materials and methods used in the project and in the work described in the following chapters (3, 4 and 5).

The design, synthesis and characterization of novel self-assembling cationic peptides [(KI)$_n$K] are described in **Chapter 3**, where the number (n) of repeating unit (lysine-isoleucine) varies from two to six. Peptides are found to behave as random coils at neutral pH, but form β-sheet rich fibrous nanostructures at basic pH. Several polyelectrolytes (HA, alginate, poly(styrene sulfonate and poly(acrylic acid)) are used to construct supramolecular peptide-polyelectrolyte hydrogel complexes, whereby the negative charge of the polyelectrolytes are used to screen the positive charges present on the peptides. The microstructures and mechanical properties of the peptide-polymer hydrogels are investigated in detail to identify hydrogel candidates for biomedical applications.

Chapter 4 focuses on the supramolecular peptide-HA hydrogels. This chapter describes the possibility of tuning the mechanical properties and morphology of peptide-HA hydrogels by changing the concentration of the components and the peptide sequence. In addition, the kinetic of the peptide-HA hydrogel formation, the hydrogel degradation in presence of hyaluronidase and its alignment under shear strain are also investigated.

Chapter 5 investigates the *in vitro* application of the supramolecular peptide-HA hydrogels, including their use as vitreous model and as platform for stem cell culture. HA is an essential polysaccharide of the ECM mediating activities in cellular signalling, wound repair, morphogenesis and matrix organization, and the supramolecular peptide-HA hydrogel provides a simple strategy to fabricate a synthetic ECM without chemical modification. It is found that human mesenchymal stem cells can form spheroids on peptide-HA hydrogels. The cell behaviour on peptide-alginate hydrogel and peptide-polymer coated surfaces, used as controls, was investigated to understand mechanism for the spheroid formation.

Chapter 6 summarizes the main findings reported in this thesis and suggests ideas for further investigation. As shown in the previous chapters, the peptide-polyelectrolyte complexes, in particular $(KI)_nK$-HA hydrogels, offer an opportunity to recapitulate the nanostructure and biofunction of the native ECMs, while enabling fine adjustments of their mechanical properties. While some potential biomedical applications of the peptide-HA hydrogels were exploited in this project, further applications are outlined in the final chapter, such as artificial substrate supporting neural differential and *in vitro* tumour models.

Table of contents

9

List of abbreviations

ACN	Acetonitrile
ATR	Attenuated total reflection
Boc	tert-Butyloxycarbonyl
CAC	Critical aggregation concentration
CD	Circular dichroism
CLSM	Confocal laser scanning microscopy
CPD	Critical point drying
DIC	N, N'-Diisopropylcarbodiimide
DIEA	N,N-Diisopropylethylamine
DMEM	Dulbecco's Modified Eagle Medium
DMF	Dimethylformamide
ECM	Extracellular matrix
ESI	Electrospray ionization
FBS	Fetal bovine serum
FF	Diphenylalanine
FGFβ	Fibroblast growth factor 2
Fmoc	Fluorenylmethoxycarbonyl
FTIR	Fourier-transform infrared

GAG	Glycosaminoglycan
HA	Hyaluronic acid or hyaluronan
HAase	Hyaluronidase
HOBt	1-Hydroxybenzotriazole hydrate
KGM	Konjac glucomannan
MBHA	4-Methylbenzhydrylamine
MS	Mass spectrometry
MSC	Mesenchymal stem cells
MDP	Multidomain peptide
NHS-rhodamine	5-(and 6)-Carboxytetra-methylrhodamine succinimidyl
NMR	Nuclear magnetic resonance
PA	Peptide amphiphile
PAA	Poly(acrylic acid)
PBS	Phosphate buffered saline
PDADMA	Poly(diallyldimethylammonium chloride)
PEs	Polyelectrolytes
PLL	Poly-L-lysine
PSS	Poly(sodium 4-styrenesulfonate)
RP-HPLC	Reversed phase high performance liquid chromatography
SEM	Scanning electron microscopy

TEM	Transmission electron microscopy
TFA	Trifluoroacetic acid
TGFβ1	Transforming growth factor beta 1
ThT	Thioflavin T
TIS	Triisopropylsilane
VEGF$_{165}$	Vascular endothelial growth factor 165

List of figures

19

20

shown. Red and green signals represent (KI)$_6$K and HA, respectively (scale bar=100 μm unless otherwise state).

Figure 5.16: *SEM images showing supramolecular peptide-alginate hydrogels with a dense surface.* *185*

List of tables

Chapter 1
Introduction

Chapter 1 Introduction

1. Introduction

Hierarchical materials, with dimensions of features ranging from the nano to the macroscale, are extremely common in nature to provide properties of interest. For example, macromolecules such as collagen and cellulose are nanoscale building blocks of human tissues and higher plants which play critical roles in their organization, properties, and function.

The extracellular matrix (ECM) of tissues is a dynamic and hierarchically organized nanocomposite that regulates essential cell functions such as adhesion, migration, proliferation, and differentiation. Engineering complex tissues requires biomaterial scaffolds that recapitulate the structure and composition of the ECM to provide cells with physical and biochemical signals that are important for tissue development and organization. Much of the functionality in cells and tissues are maintained and/or result from self-assembly of their individual constituents (1). In fact, self-assembly has been exploited to fabricate biomaterials as they are typically formed of a network of interwoven nanofibers reminiscent of the filamentous structures found in the ECM. Nano/microscale control over biomaterial composition and architecture may enable improved regulation of cell-material interactions and cell-cell contacts.

1.1. Self-assembly of peptides

Self-assembly, a fabrication method widely found in biological systems, is a spontaneous process by which molecules self-associate, adopting defined assemblies, through inter and intra-molecular interactions and without external guidance. Self-assembly has been proven to be a facile and versatile method for the bottom-up fabrication of functional biomaterials (2). Among all the building blocks used in molecular self-assembly, peptides have drawn great attention and been extensively utilized for diverse applications in biomedicine, because of

their good biocompatibility and biodegradability, structural and functional programmability, as well as their synthetic simplicity and affordability (3). Through rational design, a variety of peptide nanostructures, such as fibres, tubes, tapes, micelles, could be generated by self-assembly through the subtle balance of noncovalent forces, including electrostatic, hydrophobic, hydrogen bonding, van der Waals interactions and aromatic stacking (4).

1.1.1. Noncovalent forces

Though noncovalent forces are weaker (2–250 kJ mol^{-1}) compared to covalent bonds (100–400 KJ mol^{-1}), supramolecular self-assembly can be achieved by collective noncovalent interactions provided by having enough molecules (4). The noncovalent interactions in stable self-assemblies should be at least several order higher than the thermal energy, but not too strong so that reversible structures could self-optimize (5).

Electrostatic interactions are long range interactions with the strength of 50-250 KJ mol^{-1} (5). In supramolecular chemistry, electrostatic interactions are often accompanied with cooperative binding forces to achieve ionic self-assembly. For example, in the supramolecular polyelectrolyte-surfactant system (binding of charged surfactant to opposite charged polyelectrolyte), electrostatic interactions are acting combination with hydrophobic effects (6). In particular, the precipitation formed in the electrostatic self-assembling system could often redissolve in high concentration salt solution, as the electrostatic interactions are screened by salts (5). Hydrophobic effects are described by the association of two lipophilic molecules, where less water molecules are required for solvation compared to two separate solutes (7). Hydrophobic interactions are important driving forces in creating diverse supramolecular biological complexes. It has been described that the hydrophobic interaction is related to the chemical microenvironment, as the hydrophobic interaction generated by the nonpolar patch would be significant affected by the adjacent polar groups (8). Hydrogen bonding is a short-range directional interaction with the strength of 5-65 KJ mol^{-1} (5), derived from the electrostatic force of attraction between a hydrogen atom and another electronegative atom bearing a lone pair of electrons. Hydrogen bonding is one of the most

frequent used non-covalent interactions in supramolecular polymer chemistry, as supramolecular polymers could assemble from small molecules, or through hydrogen bonding between main chain and side chain based (9). In supramolecular peptide systems, various types of non-covalent interactions could mediate their synergistic self-assembly. In addition, aromatic interactions may also be involved in peptide self-assembly, which arise from the attractive forces between the π-electron clouds in the neighbouring aromatic groups of certain amino acids.

1.1.2. Amino acids as building blocks

Although the secondary structure of peptides can be predicted by amino acids it contains, the intrinsic propensity of amino acids for adopting certain secondary structures is influenced by the context of the sequence and the structural organization (10). Synthetic peptides can be built up using natural or non-natural amino acids. In nature, there are 20 different amino acids which have the same basic structure, with an amine group, a carboxyl group, a hydrogen atom, and a side chain covalently attached to a central carbon atom. Their unique characteristics derive from their variable side chains, which can be divided into 3 different categories (**Figure 1.1**) (11).

Hydrophobic amino acids with aliphatic side chains (A, V, L, I and M) can provide hydrophobic interactions, while hydrophilic amino acids with either positively charged (K, R and H) or negatively charged (E and D) can be involved in electrostatic interactions. In a protein, hydrophobic amino acids are often found in the interior, whereas hydrophilic amino acids are more likely to be in contact with the aqueous environment. Hydrophilic charged amino acids will be either protonated or deprotonated depending on environment pHs. K, R and H carry positively charges when pH is below their pK_a and change into uncharged status once pH is raised above the pK_a, while E and D transform from negatively charged to uncharged as the pH decreases below the pK_a. Therefore, the amine (-NH$_2$) and carboxylic acid (-COOH) groups of amino acids are not only working as donors or acceptors for intermolecular hydrogen bonds, but can also be involved in electrostatic interactions.
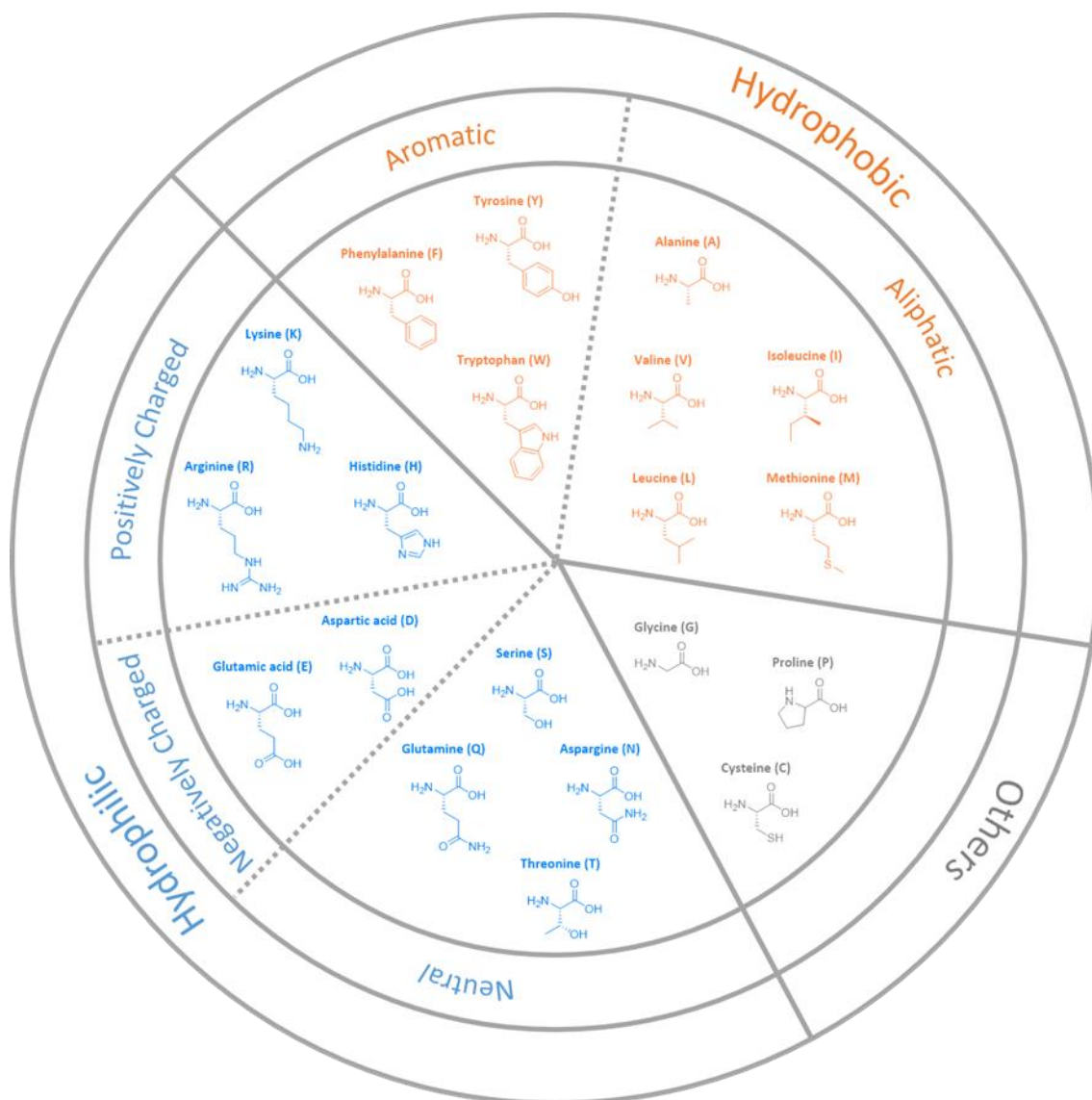
Figure 1.1: *The 20 natural amino acids grouped into 3 main categories: their common names, one letter abbreviations and chemical structures are given.*

Amino acids with aromatic side chains (F, Y and W) can be engaged in π-π stacking. Hydrophilic amino acids with uncharged side chains can create hydrogen bonds through either hydroxyl (S and T) or amide (N and Q) groups. On the other hand, glycine, with no side chain, and proline with its side chain being covalently linked to the amine terminus, can be utilized to

balance the structure rigidity of the peptide molecules due to its flexible and locked conformation, respectively. All these interactions and conformations imposed by the different amino acids can govern the self-assembly of peptides and influence the hierarchical order of peptide-based materials. Therefore, the realization of peptide self-assembly hinges upon rational molecular design of the peptide sequences and selection of specific building blocks, which can control the different noncovalent interactions.

pH changes can affect the self-assembly of charged peptides since the surface charge of the individual amino acids can be selectively altered as the pH is raised above or below their pK_a value (12, 13). Therefore, by rationally designing peptides with charged groups, the electrostatic interactions between neighbouring peptides can be controlled, which makes it possible to induce the self-assembly at certain pHs. Chen et al. designed a series of peptide amphiphiles (PAs) (C$_{16}$-AAAAKKKKG(RADA)$_n$-NH$_2$, n=1,2 and 3) with the charged region having four consecutive lysine residues and the surface region consisted of RADA segments (13). It was found that the PA nanofiber aggregated in a parallel fashion into a network of bundles when the pH was adjusted to 11. At such pH, the charge of K was screened, which encouraged the nanofiber formation, while R and D remained protonated. The alternating positive and negative charge of RADA sequence at the surface region promoted their lateral assembly. When pH increased to 13, the positive charges on both K and R were screened, leaving anionic D the only charged residue, so repulsive forces from negative charged peptide discouraged lateral assembly leading to the formation randomly dispersed nanofiber. Guo et al. developed C$_{12}$-GAGAGAGY-COOH PA and also observed a parallel nanoribbon aggregation at pH 8 because of hydrogen bonding formed between surface phenolic hydroxyl groups in Y and terminal –COO$^-$(14). However, when pH further increased to 11 the PA only self-assembled into randomly dispersed nanofiber, because of the dissociation of phenolic hydroxyl groups (pK_a value of phenolic hydroxyl group on Y is about 10).

1.1.3. Peptide secondary structure

Local segments of proteins may self-assemble into well-defined secondary structures, being α-helices and β-sheets the two most common secondary structures (**Figure 1.2-A**). α-Helical peptides make a completely turn every 3.6 residues, where hydrogen bonds between carbonyl oxygens and the hydrogens on the amide nitrogen of the fourth residue endow the structure with stability. Most coiled coils of α-helix are based on heptad sequence repeat, with the first and fourth positions being usually hydrophobic residues and the remaining sites largely polar (15). V, T, and I will disturb the α-helix because of steric clashes and serine, aspartate, and asparagine tend to destabilize the α-helical structure due to hydrogen-bond donors or acceptors on their side chain. Woolfson's group designed self-assembling fibrils with α-helical structures comprising two 28-residue peptides, where the α-helical fibrils interact to form self-supporting physical hydrogels (**Figure 1.2-C**) (16). Unlike coiled α-helical chains, the main chain of β-sheets, called β-strand, is fully extended. In the β-sheet, hydrogen bonds are formed between the carbonyl oxygen in one strand and the amino hydrogens of the adjacent strand. The two strands can be either parallel or anti-parallel depending on whether the strand directions are the same or opposite. Other secondary structure types such as beta turns and omega loops can occur as well, and some protein segments just exhibit random coils.

Many synthetic β-sheet forming peptides have been developed, where sequences contain repeating units of alternating hydrophilic and hydrophobic residues are frequented adopted. Hartgerink's group designed multidomain peptides (MDPs) with a central domain consisting of alternating hydrophilic-hydrophobic (e.g. glutamine-leucine) residues, encouraging β-sheet formation, and the charged residues at both termini to improve the solubility in water (17). In the process of supramolecular polymerization of the MDP monomers, hydrophobic interactions would act as main driving force to shield the hydrophobic face inside the core and expose the hydrophilic face to the outside aqueous environment, and the formation of intramolecular β-sheet hydrogen bonds elongate the supramolecular MDP nanofiber.

However, the repulsive charges from both charged termini would mitigate the self-assembly. Therefore, the self-assembling capacity of MDPs relies on the balance between the hydrophobic interaction provided by the repeating hydrophilic-hydrophobic unit and repulsive forces from charged residues. Zhang and colleagues used an ionic self-complementary peptide Ac-RADARADARADARADA-NH$_2$ (RAD16-I), which formed stable β-sheet structures and undergoes molecular self-assembly into nanofibers at neural pH (**Figure 1.2-C**) (18). Unlike MDPs, where the like-charges on hydrophilic face would inhibit self-assembly, in RAD16-I the opposite charges on the hydrophilic face are packed together through intermolecular ionic interactions in a checkerboard-like manner. Bowerman studied Ac-(XKXK)$_n$-NH$_2$ peptides (X=hydrophobic or aromatic residue) and found that the peptide β-sheet formation tendency would enhance as the hydrophobicity of X increased (19).

PAs developed by Stupp's group also self-assemble into β-sheet rich nanofibers. PAs consist of a linear hydrophobic tail coupled to a peptide block that includes β-sheet-forming segment, charged residues for solubility, and eventually a bioactive sequence (20, 21). Self-assembly of PAs can be triggered by charge screening induced by pH changes or the addition salts, forming high aspect ratio cylindrical nanofibril with alkyl chains buried in the core of the fiber (**Figure 1.2-D**).
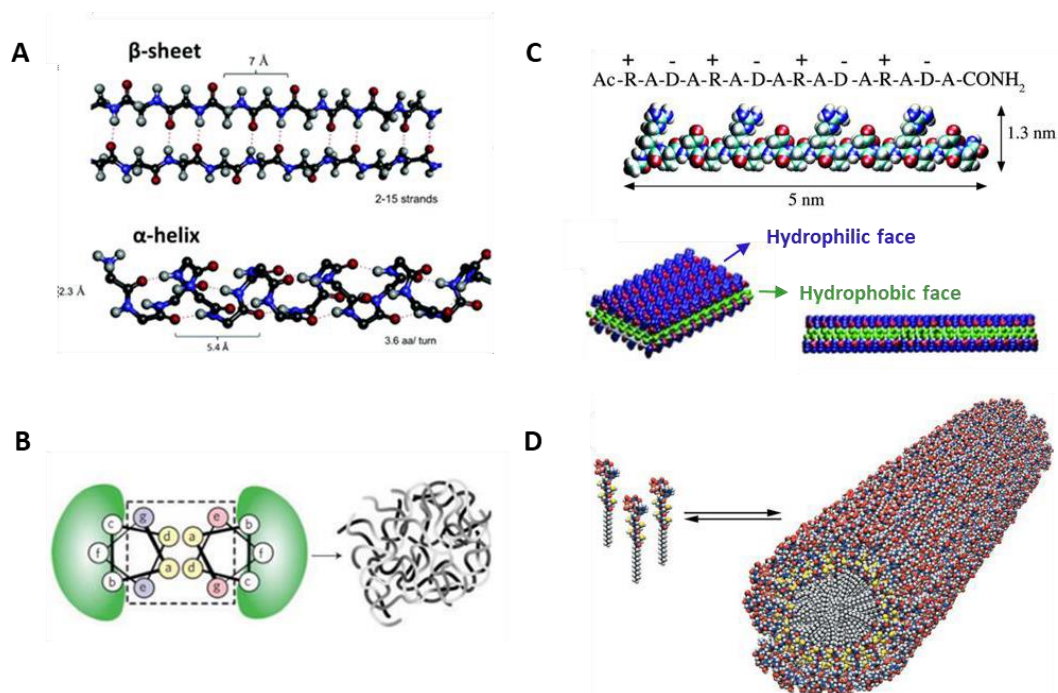
Figure 1.2: *Examples of nanofibrils formed by relatively short peptides. (A) Schematic representing α-helical and β-sheet structures (22). (B) Peptides with purely α-helical structures and their self-assembly into fibres, with interactions at all b, c and f sites (16). (C) RAD16-I peptide forms stable β-sheets and assemble into nanofibers (18). (D) Self-assembly of small PA molecules into β-sheet rich cylindrical nanofibril (21).*

1.2. Polymer networks

Polymers, either derived from natural or synthetic sources, have been elite materials for fabricating hydrogels, typically via covalent crosslinking chemistry. The selection of the polymer component (polymer composition, architecture, molecular weight, charge) and cross-linking method (physical vs chemical) enables a fine control over their structural (mesh size), mechanical (stiffness) and biochemical (biodegradability, swelling) properties. Biopolymers, such as hyaluronic acid (HA), alginate, chitosan, silk fibroin, offer great chemical diversity, while being obtained from renewable sources. When considering the use of natural-derived polymers for hydrogel fabrication, HA possesses inherent characteristics that make

this polysaccharide a unique candidate as starting material. Firstly, it is ubiquitously distributed in the tissues of the human body, being involved in many cellular processes and easily degraded *in vivo*. Secondly, HA repeating disaccharide unit is the same in all species and all tissues, posing low immunogenicity risks. Finally, its large size, anionic and hydrophilic properties, and easy chemical modification, enables the preparation of diverse HA biomaterials for a range of biomedical applications, from dermatology and ophthalmology to drug delivery and tissue engineering.

1.2.1. Hyaluronic acid

HA, also known as hyaluronan, was initially isolated from the vitreous of bovine eyes by Karl Meyer and his assistant John Palmer in 1934. It is an anionic, non-sulfated glycosaminoglycan (GAG) distributed widely throughout connective, epithelial, and neural tissues. HA molecules are straight chains containing hundreds or thousands of sugar units, which are of only two kinds: N-acetyl-D-glucosamine and D-glucuronate, in alternation as disaccharides (**Figure 1.3**) (23).
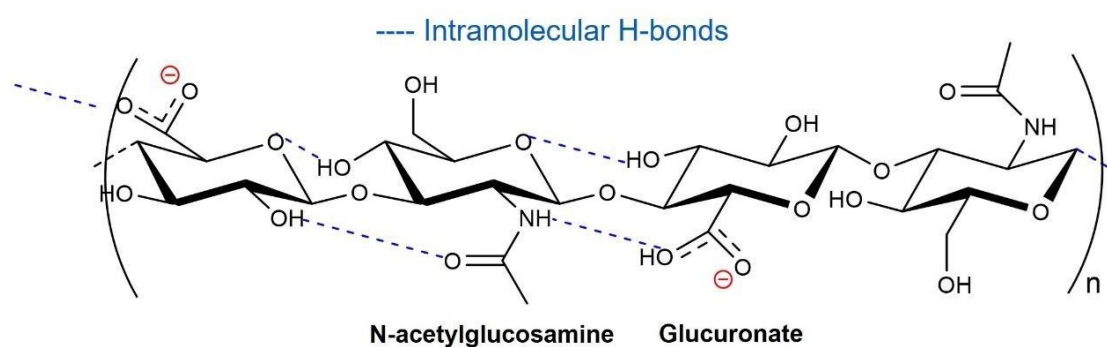
Figure 1.3: *Chemical structure of HA molecule showing the disaccharide repeating unit, anionic charge and intramolecular hydrogen bonds.*

HA chains are able to carry hundreds of negative charges at physiological pH because of the carboxylate groups on its glucoronate units. The presence of high number of hydroxyl and carboxylate groups in the HA chain makes the polymer highly soluble in water. It has been observed by nuclear magnetic resonance (NMR) spectroscopy that HA chains prefer to adopt a two-fold helix secondary structure due to extensive hydrogen-bonds that can be formed (**Figure 1.3**) and high molecular weight HA could aggregate into β-sheet like tertiary structures in aqueous solution (24). HA contains an extensive hydrophobic patch due to the presence of contiguous CH groups, and hydrophobic interactions could favour HA chain entanglement to form a polymer network. HA is known to exhibit non-Newtonian shear thinning behaviour, as HA chains are entangled at low shear rate but can disentangle and align in a strong shear field. In oscillation frequency sweep, HA acts as viscous liquid in low frequency regions, while showing an elastic behaviour in high frequency regions, and its viscoelastic behaviour is associated with its molecular weight and concentration (25, 26). The cross-over point observed in frequency sweep (when G'=G'') is found to decrease with increasing molecular weight (27), which means for longer HA chains the transition from liquid-like to solid-like behaviour occurs at longer relaxation time, because the longer entangled HA spends more time disentangling. HA with larger molecule weight has the greater chain entanglement, which leads to the higher zero-shear viscosity and stronger shear thinning behaviour (28). In dilute solution, when HA concentration is low, the HA chains do not overlap with each other, and the solution viscosity is proportional to the HA concentration (in high salt condition) (29). Once the HA concentration is above the entanglement concentration, HA can form viscoelastic networks, while the entanglement concentration is also determined by the molecular weight (entanglement concentration decreases with increased molecular weight) (30). Moreover, the rheological measurement of HA may also be affected by the shear history and the source of HA (e.g. protein contamination strongly influence HA rheology) (29). From a mechanical point of view, HA solutions have important biofunctions. For example, as one of the main components of synovial fluid, HA can behave as a lubricant and shock absorber (25). It was found that the

cross-over frequency of healthy synovial fluid from individuals over the age of 52 was 0.4 Hz, which is similar with HA with molecule weight of 2010 kDa (31). Therefore, during the walking and running frequency (with the range of 0.5 to 3 Hz), 2010 kDa HA is elastic-like and may function like synovial fluid to protect articular cartilage (31, 32). Many HA-based viscosupplements are commercially available for the symptomatic management of knee and hip osteoarthritis.

As a component of the ECM, HA is ubiquitously present in the human body. It serves a variety of functions within the ECM of nearly all tissues, and some of these functions have direct effects on cell behaviour. HA is capable of interacting with receptors on the cell surface, such as CD44, providing the means for interaction and communication between matrix and cells. HA's biological functions also involve modulation of complex processes such as cell migration, cell proliferation, inflammation and tumourigenicity, which have been described in detail in some review papers (33, 34). HA-based products also have a great influence in our daily lives (e.g. HA cosmetics are used to keep skin fresh-looking).

1.2.2. Hyaluronic acid-based hydrogels

Considering its beneficial properties, such as the biodegradability, biocompatibility and nonimmunity, HA has been widely used in pharmaceutical and tissue engineering applications (35, 36). To improve the mechanical strength and stability of HA network formed by the entangled HA chains, crosslinking is often required to generate HA hydrogels, where both covalent and non-covalent crosslinking approaches have been exploited. The most common sites on HA chain for chemical modification are -COOH, -OH and –NHCOCH3 groups (37). Covalent crosslinking is likely to produce strong and chemically robust hydrogels, whose mechanical properties can be modulated by changing the ratio between HA and crosslinking agents. However, the unreacted crosslinking agents (e.g. 1,4-butanediol diglycidyl ether) might raise safety concern limiting the biomedical usage, as they may affect

the integrity of drugs or protein entrapped in the HA gel in the drug delivery or tissue regeneration system (38). Non-covalent crosslinking of HA could be achieved via hydrogen bonding, hydrophobic interaction, ionic interaction, and host-guest interaction, which is safer than the covalent crosslinking. Stimuli like pH, temperature and shear pressure can affect these non-covalent interactions and thus lead to the sol-gel transition. Typical non-covalent crosslinking methods include ionic crosslinking by FeCl3 and host-guest crosslinking (HA chemically modified by a host molecule containing a cavity-like structure that can accommodate a certain guest molecule based on steric and chemical considerations) (37)

1.3. Supramolecular peptide-polymer biomaterials

The combination of polymers with self-assembling peptides has raised increasing attention in recent years (39), as the supramolecular peptide-polymer aggregates may retain structural similarity (e.g. nanofibrous structure) to the natural protein-polymer complexes in biological organisms. These supramolecular peptide-polymer systems can adopt a variety of shapes such as microcapsules, membranes, and hydrogels, which will be described in the following sections.

1.3.1. Supramolecular peptide-polymer hydrogels

The ECM of tissues is composed of a 3D network of fibrous proteins and GAGs, providing structural support for cells but also regulating cell activities such as adhesion proliferation and differentiation. Considering the dynamic nature of tissue ECMs, supramolecular hydrogels have attracted considerable research interests, compared to the permanent covalently cross-linked hydrogels, due to their resemblance to the structure and function of the native ECM. Supramolecular hydrogels are formed by self-assembly and hold by non-covalent interactions.

The dynamic nature of non-covalent interactions allows minimally invasive delivery by injection. In addition, noncovalent crosslinking also provides a compliant environment for cells to interact with, remodel and migrate, while performing normal functions (40, 41).

Self-assembling peptides with diverse design elements have been used to produce nanofibrous hydrogels and this topic has been covered in section 1.2 as well as in several reviews (42, 43). Biochemical functionality can be easily integrated into supramolecular peptide complex using known peptide sequences without disturbing their self-assembly ability. The mechanical properties of self-assembling peptide hydrogels can also be tuned through molecular structure, but within a certain range of storage modulus (3 – 80 kPa) (44). The addition of polymer into peptide self-assembling systems not only enhances the mechanical stiffness of the resulting hydrogels, but also provides a way to control the release of charged proteins (45), including growth factors (46), or creates a mimetic environment for tissue engineering (47). Benefiting from the diversity offered by both polymers and peptides (**Figure 1.4**), supramolecular peptide-polymer hydrogels can be obtained with desired properties by careful selection of the building blocks (e.g. polymer composition, architecture, molecular weight, charge, viscosity; peptide sequence, conformation) and their optimal combinations (peptide-polymer ratio, mixing order). Unlike traditional peptide/polymer conjugate hydrogels, obtained through covalent bond chemistry, supramolecular peptide-polymer hydrogels are formed via self-assembly, thereby avoiding the use of potentially non-biocompatible cross-linking agents, and providing a safer, more cost-effective and eco-friendly method to obtain hydrogels with tuneable properties.
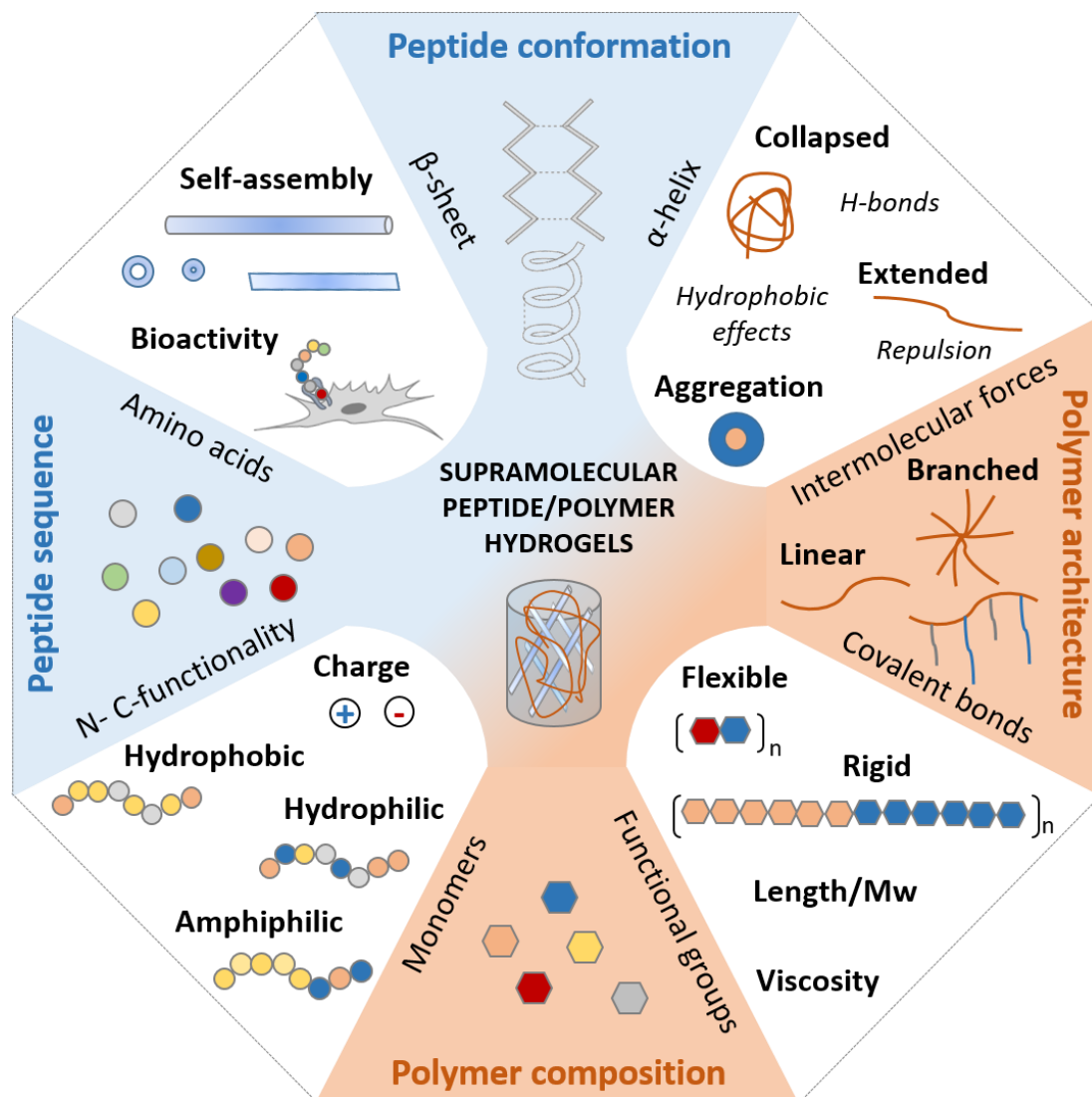
Figure 1.4: *Properties provided by peptides and polymers to fabricate supramolecular hybrid peptide-polymer hydrogels.*

1.3.1.1. Aromatic peptide-polymer hydrogels

Diphenylalanine (FF), an aromatic dipeptide derived from Alzheimer's β-amyloid, is considered as the simplest building block of supramolecular peptide-based materials and is known to self-assemble into varied well-ordered nanostructures (48). Noticeably, 9-fluorenylmethoxycarbonyl protected diphenylalanine (Fmoc-Phe-Phe-OH, or simply Fmoc-FF)

self-assembles into nanofibrous hydrogel at physiologic pH, triggered by a combination of non-covalent interactions like hydrogen bonding and π- π stacking (49). Two approaches have been described to fabricate Fmoc-FF hydrogels: one method, known as solvent switching, the Fmoc-FF solution is prepared in an organic solvent and then diluted with water or aqueous buffer, and the other, denominated as pH switching, the Fmoc-FF solution is prepared at high pH followed by lowering down the pH (50). Though Fmoc-FF hydrogel has received wide attention, its low stability and rigidity in physiological environment has been reported as limiting factor for its long-term usage (51, 52). The incorporation of polymers into the Fmoc-FF self-assembling system is expected to change the hydrogel structure, as the peptide-polymer ratio changes, and enhance their mechanical properties and stability.

Fmoc-FF-polymer hydrogels described in the literature were usually obtained by solvent switching method, where high concentration of Fmoc-FF solution (usually dimethyl sulfoxide) is diluted with aqueous polymer solution. The gelation time of hybrid peptide-polymer hydrogel is expected to be longer, compared to the pure Fmoc-FF hydrogel, due to steric effects of a long molecule which may slow down the self-assembly process. Fmoc-FF-polymer hydrogels were first investigated by Huang and co-workers, who combined konjac glucomannan (KGM), a non-ionic water-soluble polysaccharide, with Fmoc-FF (51). It was found that the addition of KGM decreased the size of assembled nanofibers, probably due to the reduced peptide diffusion rate, caused by the highly viscous polymer solution. However, the secondary structure of the self-assembling peptide was not altered by the presence of the polymer, as both Fmoc-FF and Fmoc-FF-KGM hydrogel had similar circular dichroism and Fourier transform infrared spectra.

Other polymers were also exploited to fabricate Fmoc-FF-polymer hydrogels, including, alginic acid, an anionic polysaccharide extracted from brown algae and widely applied as biomaterial because of its excellent biocompatibility. Gong et al. designed Fmoc-FF-alginate hydrogels showing different hydrogel nanostructure as the alginate concentration changed (53). The hydrogel also exhibited shear-thinning property, which enables its potential

application as injectable biomaterial (54). Alginate hydrogels are typically obtained by ionic cross-linking using divalent cations, such as Ca^{2+} (55). However, alginate-calcium hydrogels are not stable in physiological conditions as ion change can easily disrupt the ionic cross-linking. Hence, a more stable self-assembling gelling system has been developed combining Fmoc-FF, alginate and calcium ions (52). The peptide-polymer-ion hybrid hydrogel was formed by adding Fmoc-FF-alginate solution (at basic pH) into $CaCl_2$ solution, where gelation was achieved by synergistic effects of hydrogen bonding, π- π stacking and ionic interactions, as Ca^{2+} not only promoted Fmoc-FF nanofiber formation, by screening charges in Fmoc-FF, but also triggered the alginate cross-linking. As a result, the mechanical properties of the hybrid hydrogel were found to be enhanced in the presence of calcium ions (56).

HA was also utilized to produce Fmoc-FF-polymer hydrogels, as combining HA with the Fmoc-FF self-assembling system has the potential to enhance the physical properties of hydrogel while integrating the inherent bioactivity of HA. For example, Aviv et al. found that Fmoc-FF-HA hydrogel could be injected through a superfine needle, unlike Fmoc-FF hydrogel, whose rigid part remained inside the needles (57). Additionally, the swelling ratio of the hybrid hydrogel was significantly improved as the HA ratio increased, which is a beneficial property for its potential application as artificial cell scaffolds. Fmoc-FF-HA hydrogel could be degraded by hyaluronidase (HAase, an enzyme catalysing the HA degradation). However, the degradation rate was much slower compared to pure HA, probably because the enzyme diffusion was hindered by the dense hydrogel structure.

Since Fmoc-FF is negatively charged at neutral pH, due to the ionized carboxylic group at peptide C-terminus (**Table 1.1**), it is expected that the addition of a cationic polymers could induce electrostatic interactions between opposite charged molecules, producing a nanofibrous network with enhanced entanglement. Yan's group used Fmoc-FF and poly-L-lysine (PLL), a biocompatible polymer with high positive charge density, to fabricate the hybrid hydrogel (58, 59). Fmoc-FF-PLL hydrogel was shear-thinning, exhibiting a significantly higher stiffness and a much better recovery performance compared to pure Fmoc-FF hydrogel.

However, there was a major drawback regarding the fabrication of this hydrogel as it takes three days to be formed.

Inspired by the Fmoc-FF-polymer hydrogel system, additional aromatic peptide-polymer co-assembling systems were developed. Fmoc-FFpY (F: phenylalanine; Y: tyrosine; p: PO_4^{2-}), a water-soluble aromatic peptide usually gelled by alkaline phosphatase, which catalyses the removal of phosphate groups, was first introduced by Xu and co-workers (60). Instead of using the enzyme, Criado-Gonzalez et al chose polyallylamine hydrochloride (PAH), a cationic polymer commonly applied in cell encapsulation, to screen the negative charges of phosphate groups on Fmoc-FFpY, yielding a unique Fmoc-FFpY-PAH hybrid hydrogel (61). Unlike the enzymatically induced peptide hydrogel, Fmoc-FFpY-PAH hydrogel was triggered by electrostatic interactions. The hybrid hydrogel had a slightly higher ratio of β-sheet secondary structures and lower ratio of random coils, and also showed increased mechanical properties.

The tripeptide sequence RGD is a bioactive ligand functioning as a cell attachment site. As one of the simplest RGD-based peptides, Fmoc-RGD could self-assemble to form peptide hydrogel as the 'Fmoc' offered aromatic stacking interactions (62). However, the peptide hydrogel was not stable in the cell culture media, and it was found that the incorporation of chitosan could increase its stability (63). It was assumed that hydrogen bonds between chitosan and free carboxylic acid groups of Fmoc-RGD, as well as electrostatic interactions, were responsible for the formation of the hybrid Fmoc-RGD-chitosan network, whose storage modulus was almost six times higher than the native peptide hydrogel. Unlike many Fmoc-FF-polymer systems, where the polymer slowed down the gelation process, the formation of Fmoc-RGD-chitosan hydrogel was faster than the native Fmoc-RGD hydrogel.

1.3.1.2. Nonaromatic peptide-polymer hydrogels

Nonaromatic peptides, such as PAs, ionic self-complementary peptides and MDPs, were also used to create supramolecular hybrid peptide-polymer hydrogels. These hydrogels were easy to prepare as they could form by simply mixing aqueous solutions of the two components.

When a positively charged K_3 PA (C_{16}-$V_3A_3K_3$-NH_2) was combined with anionic HA, membranes and sacs were formed at the interface of the two liquids (64). Using a similar strategy, Radvar and Azevedo combined anionic poly(sodium 4-styrenesulfonate) (PSS) with the same PA and obtained a hybrid K_3-PSS hydrogel able to promote the deposition of calcium phosphate mineral after incubation in mineralization medium (39). Cotey et al. used the complexation between negatively charged E_3 PA (C_{16}-$V_3A_3E_3$–OH) and cationic chitosan polymer to fabricate E_3-chitosan hydrogels. The hydrogel exhibits a sheet-like morphology with fibrous textures, where the PA component was observed to be covered by chitosan layers under confocal microscopy (65).

The ionic self-complementary peptide RAD16-I is known to self-assemble into nanofibrous hydrogels at physiological condition (18). To develop a biofunctional nanofiber scaffold with growth factor binding affinity, the peptide, along with the growth-factor binding heparin polymer, were chosen to fabricate a novel supramolecular peptide-polymer hydrogel (66). Interestingly, although heparin was not interfering in the self-assembling process, it could weaken the β-sheet structures of the peptide. Vascular endothelial growth factor 165 ($VEGF_{165}$), fibroblast growth factor 2 (FGFβ) and transforming growth factor beta 1 (TGFβ1) contain heparin binding domains. However, heparin displayed on the hybrid scaffold could only specifically bind to $VEGF_{165}$ but not to FGFβ and TGFβ1. Rajangam et al. designed and heparin-binding PA (HBPA, $C_{16}A_4G_3LRK_2LGKA$-NH_2), displaying the heparin-binding sequence (LRKKLGKA), to create supramolecular HBPA-heparin hydrogels (46). With the addition of heparin, the PA secondary structure changed from predominantly α-helix to β-sheet. Unlike RAD16-I-heparin hydrogel, the HBPA-heparin hybrid hydrogel clearly showed the specific binding of FGFβ, promoting its retention in the network and delaying its release, and

demonstrating the benefit of using specific binding sequences. Hartgerink's group also utilized heparin to ionically cross-link the positively charged multidomain peptide (Ac-KSLSLSLRGSLSLSLKGRGDS-NH$_2$) to form the MDP-heparin hydrogels, which possess a nanofibrous structure and were mechanically robust (67). The hybrid hydrogel was also found to enable the slow release of growth factors (FGFβ, TGFβ1 and VEGF) (68).

1.3.1.3 The role of polymer characteristics in the formation and properties of supramolecular peptide-polymer hydrogels

As described above, different polymers have been combined with self-assembling peptides to create supramolecular hybrid hydrogels with properties distinct from their individual counterparts. Polymers have been selected based on their key characteristics, as summarized in **Table 1.1**. For example, charged polymers (polyelectrolytes) were widely used to favour electrostatic interactions between the polymer and peptides of opposite charge. Polymers can also be integrated into self-assembling peptide systems without the presence of electrostatic interactions, where their main function is to act as filler of the nanofibrous network, which might result in improved mechanical properties and enhanced stability of the hydrogel.

While polymer charge may play a prominent role in the formation of these hybrid hydrogels, polymer intrinsic properties, such as molecular weight and conformation, are expected to influence molecular diffusion and the assembly kinetics. Typically, polymers with higher molecular weight are more likely to form more robust hydrogels with peptides. For example, in the K$_3$-PSS system described above, hydrogel formed by 1 MDa PSS was more stable than the hydrogel with 70 kDa PSS, in both water and PBS environment (39). It was also found that in the Fmoc-FFpY-PAH system the peptide could self-assemble into a hydrogel only in presence of large PAH (120 kDa) while only forming viscous solution with smaller PAH (58 kDa) (61). Furthermore, the mechanical properties of self-assembling peptide-polymer hydrogels

can also be adjusted by changing the polymer molecular weight. Increasing molecular weight of PLL in Fmoc-FF-PLL hydrogel improved the cross-linking degree, resulting in higher moduli and better recovery performance (58). However, the impact of polymer molecular weight on Fmoc-FF-HA hydrogel was unexpected, as the rheological studies showed that the incorporation of extremely large HA (1-2 MDa) generally yielded a weaker hybrid network (69). Fmoc-FF-HA self-assembling system does not involve electrostatic interactions between the polymer and the peptide building blocks, and the hydrogel mechanical properties are mainly controlled by the peptide component, which is different from the other polymer-peptide hydrogel mentioned above (K_3-PSS, Fmoc-FFpY-PAH and Fmoc-FF-PLL) where the polymer played an important role in mediating hydrogel mechanical properties. The presence of HA, especially large molecular weight HA, could disturb diffusion and nucleation of the peptide phase. Though introducing HA into the Fmoc-FF network might weaken the hydrogel, it was found that the hybrid hydrogel had better ductility compared to the pure Fmoc-FF hydrogel, which facilitated its injection through thin needles.

Since large molecular weight polymers greatly increase the viscosity of the liquid in which they dissolve in, the formation of peptide-polymer hydrogel is often slower than the peptide-only hydrogel as the high viscosity retards the solution diffusion, which has been described above. The viscosity of peptide solutions would also affect the mechanical properties of resultant hydrogels. Cotey et al found E_3-chitosan hydrogels have lower storage modulus despite being formed with increased E_3 PA concentration, which was probably caused by the high-viscous E_3 PA solution reducing the mix between the two building blocks (65).

Polymer conformation could also play a role in determining the formation of supramolecular peptide-polymer. For example, no hydrogel was formed when combining Fmoc-FFpY with another polycation, poly(diallyldimethylammonium chloride) (PDADMA) (61). It was assumed that the rigid chain of PDADMA, compared to PAH, prevented the peptide self-assembly. Another example showing the effect of molecular size/conformation on the properties of resulting supramolecular hybrid hydrogels was reported by Hartgerink's group. MDPs formed

stronger hydrogels in presence of suramin (a multianionic drug) than with heparin, probably because suramin could conformationally fit in the MDP self-assembling system and screen the peptide charges more efficiently (67).

1.3.1.4. Biomedical applications of supramolecular peptide-polymer hydrogels

Most polymers used in peptide-polymer hydrogels are natural linear polymers present in living organisms which have good biocompatibility for their use in biomedical applications. Benefiting from a stable and dense network structure, peptide-polymer hydrogels could effectively encapsulate drugs and allow their sustainable release (52, 56). By mimicking the native ECM microenvironment, these hydrogels can also be used as 2D and 3D matrices for culturing multiple cell types, promoting their adhesion, proliferation and differentiation (39, 63).

Some bioactive polymers not only physically reinforce the non-covalent cross-linked network, but also provide their intrinsic biological function to the supramolecular hybrid hydrogels. For example, heparin is known to bind many soluble growth factors through their heparin binding domains. Therefore, peptide-heparin hydrogel (RAD16-I-heparin and HBPA-heparin) were shown to prevent the burst release of growth factors, proving better control over their release rate (46, 66). The heparin-growth factor complex is known to regulate cell activities, promoting, for example, the proliferation of endothelial cells leading to vascularization (70). It is expected that the biofunction of heparin would remain in the supramolecular peptide-heparin hydrogel. In fact, it was found that RAD16-I-heparin hydrogel, supplemented with growth factors, encouraged the formation of tubular-like structures from human microvascular endothelial cells and supported the chondrogenic differentiation of human adipose-derived stem cells (66). *In vivo* studies also showed significant neovascularization when growth factor loaded HBPA-heparin hydrogels were implanted in rat corneas (46). MDP-heparin hydrogels also showed potential in dental pulp engineering. Dental pulp stem cells

encapsulated in MDP-heparin hydrogel loaded with growth factors were able to form a vascularized soft connective tissue *in vivo* similar to dental pulp (68). Chitosan has a broad-spectrum antibacterial activity and low toxicity towards mammalian cells. Fmoc-RGD-chitosan hydrogel retained the antibacterial properties of chitosan, exhibiting significant inhibition of *Escherichia coli* growth (63, 71). PSS is capable of binding calcium ions, forming Ca-PSS complexes that can lead to the nucleation and growth of calcium carbonate mineral (72). K_3-PSS hydrogel were also able to promote deposition of calcium phosphate minerals when incubated in mineralization medium (39). Modified polymers could also be used to provide additional biofunction in supramolecular peptide-polymer, as hybrid hydrogels formed by Fmoc-FF and poly-L-lysine modified with thiol group (PLL-SH) were found to be a promising antitumor therapy (58). The formation of disulfide bonds between the thiol group was able to stabilize the helical fibrous structures, endowing Fmoc-FF-PLL-SH hydrogel with a helical nanofiber structure similar to fimbrial antigen, which could activate T cell response and suppress tumour growth.

Table 1.1: *Functionality provided by polymers and non-covalent forces involved in the formation of supramolecular peptide/polymer hydrogels.*

Peptide sequence (charge at neutral pH)	Polymer (charge at neutral pH)	Electrostatic interactions	Polymer functionality	Application	Ref.
Fmoc-FF-OH (anionic)	KGM (neutral)	No	Improve stability and mechanical properties	Controlled release of small drugs (docetaxel)	(51)
	Alginate (anionic)	No		Injectable scaffold for bone tissue regeneration	(53, 54)
	Alginate/Ca^{2+}	Yes	Improve stability and mechanical properties; Trigger the calcium-alginate network formation	Controlled release of small drugs docetaxel; *In vitro* 3D cell culturing scaffold	(52, 56)
	HA (anionic)	No	Enhance stability and swelling pressure	Controlled release of small drugs (curcumin); 2D cell culturing platform	(57, 69)
	PLL (cationic)	Yes	Increase network entanglement and mechanical properties	Injectable biomaterial for antitumor therapy	(58, 59)

Fmoc-FFpY-OH (anionic)	PAH (cationic)	Yes	Induce hydrogel formation	Not exploited	(61)
Fmoc-RGD-OH (anionic)	Chitosan (cationic)	Yes	Speed up gelation; Improve mechanical properties; Provide hydrogel with antibacterial function	*In vitro* 2D and 3D cell culturing model; exhibit antibacterial properties; produce silver nanoparticles for sensing and imaging	(63)
C_{16}-$V_3A_3K_3$-NH_2 (cationic)	PSS (anionic)	Yes	Induce hydrogel formation; Promote hydrogel mineralization and controlled release of charged proteins	3D encapsulation and culture of stem cells	(39)
C_{16}-$A_4G_3LRK_2LGKA$-NH_2 (cationic)	Heparin (anionic)	Yes	Induce hydrogel formation; Enable specific binding and controlled release of growth factors	Stimulate formation of new blood vessels *in vivo*	(46)

C_{16}-$V_3A_3E_3$–OH (anionic)	Chitosan (cationic)	Yes	Induce hydrogel formation	localizes both positive and negative charged protein (bovine serum albumin and lysozyme)	(65)
Ac-$(RADA)_4$-NH_2 (neutral)	Heparin (anionic)	Yes	Enable binding and controlled release of growth factors	3D cell culture scaffold supporting chondrogenesis and vasculogenesis *in vitro*	(66)
Ac-$K(SL)_3RG(SL)_3KGRGD$-NH_2 (cationic)	Heparin (anionic)	Yes	Induce the hydrogel formation	Dental pulp engineering	(67, 68)

1.3.2. Supramolecular peptide-polymer membrane

Supramolecular peptide-polymer membranes were first introduced in Stupp's lab, when a positively charged K_3 PA was combined with anionic HA, and membranes or sacs were formed at the interface of the two liquids due to the electrostatic interactions between opposite charged components (64). The membrane was formed by combining equal volumes of K_3 PA and HA, while adding viscous HA drops on the top of K_3 PA solution could lead to the formation of HA-filled sacs. In particular, it was found that the membrane had a highly ordered architecture containing three distinctive layers - amorphous zone (with random entangled fibrils), parallel layer (with oriented fibrils parallel to the interface) and perpendicular layer (with oriented fibrils perpendicular to the interface) (**Figure 1.5-B**). The amorphous zone

would form first with K_3 PA molecules rapidly interacting in the HA contact layer, following by the formation of parallel layer due to the self-assembly of K_3 PA creating the diffusion barrier, and then perpendicular layer were formed by HA strands crossing the diffusion barrier and nucleate K_3 PA nanofibers perpendicular to the interface, which is driven by the osmotic pressure forces (osmotic pressure at HA side is higher than K_3 PA side) (**Figure 1.5-A**). Moreover, conjugating integrin-binding motif RGDS to K_3 PA (K_3RGDS PA, C_{16}-$V_3A_3K_3$RGDS-NH_2) did not significantly affect the morphology of the PA-HA membrane, and it was found that PA and HA tend to locate at the different sides at the cross-section of the membrane (**Figure 1.5-C**) (73). It is also possible to produce the PA-HA membranes without the typical three-region architecture, as the membrane formed by HA and KLAK PA (C_{16}-$V_3A_3G_2$(KLAKLAK)$_2$-NH_2) shows non-fibrous homogeneous structure (74). Unlike K_3 PA, which self-assembles into cylindrical nanofibers, KLAK PA preferentially assemble into spherical aggregates, which is considered to be the major reason causing the PA-HA membrane structural difference. In KLAK-HA membrane, diffusion barrier did not form and there was also no perpendicular nanofibers growth. Instead, PA spherical micelle could diffuse into the HA solution. Mixing KLAK PA into K_3-HA self-assembling system resulted in the membrane becoming less ordered compared to the pure supramolecular K_3-HA membrane. Heparin- binding PA (HBPA) was found to form a membrane with HA, where the membrane shows a less ordered structure. However, incorporating heparin in the membrane would promote the formation of hierarchical distinct layers (containing perpendicular aligned fibril), and increasing heparin concentration would lead to the more predominant ordered structure. In HBPA-HA-heparin self-assembling system, the interaction between HBPA and heparin may dominate over the association between HBPA and HA, as the charge density of heparin is three times higher than HA (75). Therefore, the addition of heparin in HBPA-HA system may facilitate the formation of diffusion barrier which is believed to be an essential factor leading to the formation of hierarchical distinct layer structure.
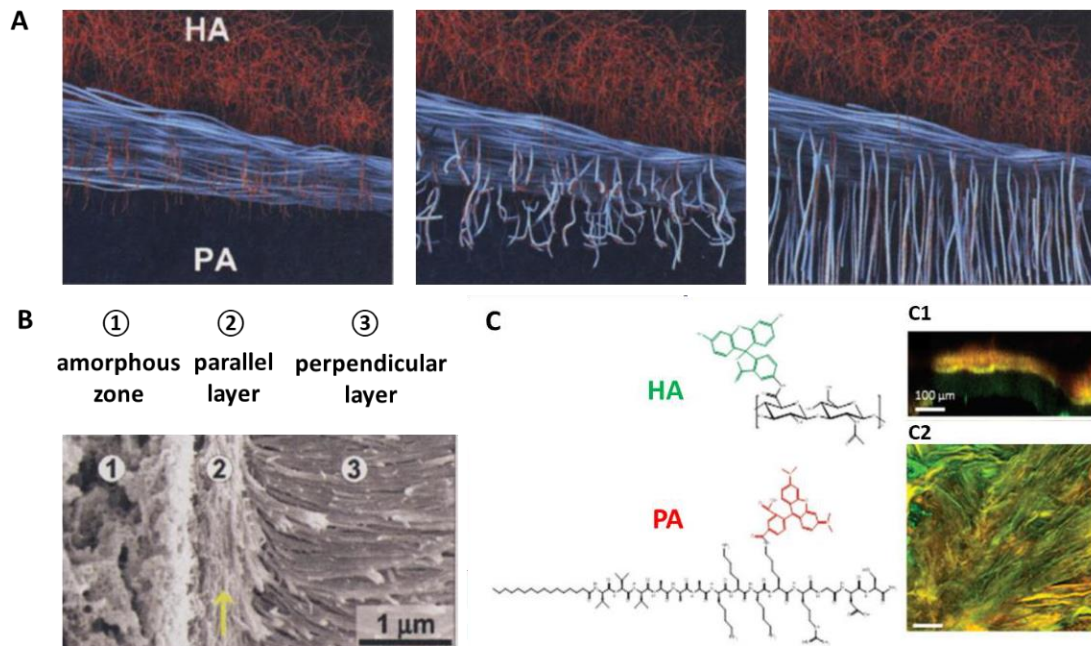
Figure 1.5: *(A) Schematic representation of the formation of supramolecular PA-HA membrane (64). (B) SEM image showed the three-layer structure at the cross-section of PA-HA membrane (64). (C) CLSM images demonstrate the distribution of PA (red, labelled with Rhodamine) and HA (green, labelled with fluorescein) at the (C1) cross-section and (C2) surface of the membrane (73).*

Apart from PAs, other cationic peptides, such as MDP (all MDPs contain an acetylated N-terminus and an amidated C-terminus), could also form a supramolecular membrane with HA. Supramolecular $K_2(QL)_6K_2$-HA membrane exhibits two distinctive layers, with HA aggregates on the one side (HA layer) and self-assembling MDP fibril rich in the other side (peptide layer) (15). The conjugation of bioactive osteogenic motif to MDP was shown to alter the structure of the supramolecular MDP-HA membrane, as $K_3(QL)_6E_2$YGFGG-HA membrane have a homogeneous cross-section, while HA in combination with $K_3(QL)_6E_2$, $K_2(VL)_6E_2$, $K_3(QL)_6E_2$RGDS all formed membranes showing featured distinct layers (76). However, the reason to cause the homogeneous morphology of $K_3(QL)_6E_2$YGFGG-HA membrane is still not fully understood. Additionally, it was found that the surface morphology of the peptide layer in MDP-HA membrane corresponded to the morphology of MDP observed under TEM.

The physical properties of the peptide-HA membrane could be affected by the component concentration, incubation time and temperature. Increasing the component concentration would lead to the formation of a thicker peptide-HA membrane, as the osmotic pressure forces would increase with the concentration, which encourages the component diffusion (77). Though the three-layer architecture could be detected at the cross-section of PA-HA membrane in a very short incubation time (three minutes), the longer incubation time promoted the strength and reduce the water permeability of the membrane (77). Increasing the incubation temperature from 4 °C to 21 °C was shown to thicken the MDP-HA membranes as well, since the higher temperature also promote the diffusion of the components (15).

Notably, the architecture of PA-HA membrane could be altered by the use of external forces. Electrical fields are known to influence the diffusion of charged species (78). By changing the direction of the electrical current, an electrical field applied perpendicular to the membrane interface could either encourage (in compressive field) or discourage (in pulling field) the membrane growth. Magnetic field was also used to direct the self-assembly of aromatic cationic peptides (e.g. Ac-$K_2A_5F_4$-NH_2) in presence of HA and align the surface nanofibril due to the diamagnetism effect (79).

1.3.2.1. Biomedical applications of supramolecular peptide-polymer membranes

The potential of the supramolecular peptide-polymer membranes in biomedical applications were investigated in angiogenesis, cancer therapy and serum-free cell culture studies. Like the supramolecular peptide-heparin hydrogel described above, supramolecular HBPA-HA-heparin membrane promoted rapid angiogenesis when utilizing heparin-binding growth factors (80). KLPA PA was shown to be cytotoxic against breast cancer cells at very low concentrations, and the enzymatic degradation of supramolecular KLAK-K_3-HA membrane by HAase was shown to effectively decrease the viability of breast cancer cells with the sustained release of KLAK-PA (74, 81). Therefore, the supramolecular KLAK-K_3-HA membrane could

potentially be used as enzyme- responsive platform for breast cancer therapy. In addition, the supramolecular peptide-HA membrane could present intrinsic bioactivity by displaying biochemical motifs. For example, incorporating 50% K_3RGDS PA into the supramolecular K_3-HA membrane significantly enhanced the cell adhesion and proliferation on the membrane in serum-free culture conditions (73). Cells were also seen to be more elongated on the supramolecular membrane formed by HA and RGDS conjugated MDP compared to ordinary MDP-HA membrane in the serum-free environment (76).

1.3.3. Supramolecular peptide-polymer microcapsules

With the usage of spray-based device, it was possible to fabricate supramolecular peptide-polymer microcapsule, which could be achieved by injecting alginate microdrops into low concentration K_3PA solution (0.1 wt%), while using higher concentration of K_3PA solution would lead to the formation of hydrogel (82). The self-assembly of K_3PA with alginate would enable the formation of the K_3-alginate shell separating the alginate liquid core from the exterior, where the liquid core could also be gelated by ionic cross-linking with Ca^{2+}. The supramolecular microcapsule could be further designed to be used in targeted drug delivery system. Boekhoven et al. developed anti-tumour K_3-alginate microcapsule by covalent modified alginate core with chemotherapy drug Doxorubicin and conjugating tumour targeting molecule folate to K_3PA, in which the microcapsule showed significant toxicity to the breast cancer cell (83). Supramolecular peptide-polymer microcapsules were also fabricated in a microfluidic device using cationic MDPs and the negatively charged polysaccharide xanthan gum (84). The microcapsules were shown to be mechanically stable, and their permeability could be tuned through the peptide-polymer ratio. Cell encapsulated in the microcapsules remained viable, indicating their potential use as 3D environments for cell culture.

1.4. Summary and objectives of the work

The previous sections described research activity on supramolecular peptide-polymer biomaterials and have highlighted some of their advantages over their single counterparts. However, the peptide and polymer landscapes are immense, suggesting opportunities for further exploitation and studies focusing on their self-assembly (kinetics) and rheological behaviour to identify their potential biomedical applications. The overall aim of this PhD project was to develop novel supramolecular peptide-polymer hydrogels with tailorable structural, rheological, and biochemical properties. The specific objectives of the work reported in this thesis were:

- Objective 1: To design and apply a library of novel cationic peptides to investigate their self-assembly behaviour and ability to form supramolecular hydrogels in presence of anionic polyelectrolytes.

- Objective 2: To apply the knowledge from the first objective to tune the properties of resulting peptide-polyelectrolyte materials.

- Objective 3: Identify promising peptide-polyelectrolyte systems for biomedical applications.

- Objective 4: To gain insights on the mechanism of hydrogel formation with particular focus on peptide-HA-based system.

- Objective 5: To exploit peptide-HA hydrogels for *in vitro* biomedical applications.

1.5. References

1. Azevedo HS. Biomaterials Inspired by Biology: From Molecules to Self-Assembly. In: Reis RL, editor. Encyclopedia of Tissue Engineering and Regenerative Medicine. Oxford: Academic Press; 2019. p. 109-17.

2.   Smith KH, Tejeda-Montes E, Poch M, Mata A. Integrating top-down and self-assembly in the fabrication of peptide and protein-based biomedical materials. Chemical Society Reviews. 2011;40(9):4563-77.

3.   Gazit E. Self-assembled peptide nanostructures: the design of molecular building blocks and their technological utilization. Chemical Society Reviews. 2007;36(8):1263-9.

4.   Mendes AC, Baran ET, Reis RL, Azevedo HS. Self-assembly in nature: using the principles of nature to create complex nanobiomaterials. Wiley Interdiscip Rev-Nanomed Nanobiotechnol. 2013;5(6):582-612.

5.   Faul CFJ, Antonietti M. Ionic Self-Assembly: Facile Synthesis of Supramolecular Materials. Advanced Materials. 2003;15(9):673-83.

6.   Antonietti M, Conrad J, Thuenemann A. Polyelectrolyte-Surfactant Complexes: A New Type of Solid, Mesomorphous Material. Macromolecules. 1994;27(21):6007-11.

7.   Biedermann F, Nau WM, Schneider H-J. The Hydrophobic Effect Revisited—Studies with Supramolecular Complexes Imply High-Energy Water as a Noncovalent Driving Force. Angewandte Chemie International Edition. 2014;53(42):11158-71.

8.   Zhang F, Yu L, Zhang W, Liu L, Wang C. A minireview on the perturbation effects of polar groups to direct nanoscale hydrophobic interaction and amphiphilic peptide assembly. RSC Advances. 2021;11(46):28667-73.

9.   Yang SK, Zimmerman SC. Hydrogen Bonding Modules for Use in Supramolecular Polymers. Israel Journal of Chemistry. 2013;53(8):511-20.

10.   Costantini S, Colonna G, Facchiano AM. Amino acid propensities for secondary structures are influenced by the protein structural class. Biochemical and Biophysical Research Communications. 2006;342(2):441-51.

11.   Fleming S, Ulijn RV. Design of nanostructures based on aromatic peptide amphiphiles. Chemical Society Reviews. 2014;43(23):8150-77.

12.   Aggeli A, Bell M, Carrick LM, Fishwick CWG, Harding R, Mawer PJ, et al. pH as a trigger of peptide beta-sheet self-assembly and reversible switching between nematic and isotropic phases. Journal of the American Chemical Society. 2003;125(32):9619-28.

13.   Chen YR, Gan HX, Tong YW. pH-controlled hierarchical self-assembly of peptide amphiphile. Macromolecules. 2015;48(8):2647-53.

14.   Guo H, Zhang JM, Xu T, Zhang ZD, Yao JR, Shao ZZ. The robust hydrogel hierarchically assembled from a pH sensitive peptide amphiphile based on silk fibroin. Biomacromolecules. 2013;14(8):2733-8.

15.   Mendes AC, Smith KH, Tejeda-Montes E, Engel E, Reis RL, Azevedo HS, et al. Co-Assembled and Microfabricated Bioactive Membranes. Advanced Functional Materials. 2013;23(4):430-8.

16.   Banwell EF, Abelardo ES, Adams DJ, Birchall MA, Corrigan A, Donald AM, et al. Rational design and application of responsive α-helical peptide hydrogels. Nature Materials. 2009;8(7):596-600.

17.   Dong H, Paramonov SE, Aulisa L, Bakota EL, Hartgerink JD. Self-Assembly of Multidomain Peptides: Balancing Molecular Frustration Controls Conformation and Nanostructure. Journal of the American Chemical Society. 2007;129(41):12468-72.

18.   Yokoi H, Kinoshita T, Zhang S. Dynamic reassembly of peptide RADA16 nanofiber scaffold. Proc Natl Acad Sci U S A. 2005;102(24):8414-9.

19.   Bowerman CJ, Liyanage W, Federation AJ, Nilsson BL. Tuning β-Sheet Peptide Self-Assembly and Hydrogelation Behavior by Modification of Sequence Hydrophobicity and Aromaticity. Biomacromolecules. 2011;12(7):2735-45.

20.   Behanna HA, Donners JJJM, Gordon AC, Stupp SI. Coassembly of Amphiphiles with Opposite Peptide Polarities into Nanofibers. Journal of the American Chemical Society. 2005;127(4):1193-200.

21.   Hartgerink JD, Beniash E, Stupp SI. Self-assembly and mineralization of peptide-amphiphile nanofibers. Science. 2001;294(5547):1684-8.

22.   Papapostolou D, Smith AM, Atkins EDT, Oliver SJ, Ryadnov MG, Serpell LC, et al. Engineering nanoscale order into a designed protein fiber. Proceedings of the National Academy of Sciences. 2007;104(26):10853.

23.   Scott JE. Secondary and tertiary structures of hyaluronan in aqueous-solution. Biochemical Journal. 1998;274:699-705.

24.   Scott JE, Heatley F. Biological properties of hyaluronan in aqueous solution are controlled and sequestered by reversible tertiary structures, defined by NMR spectroscopy. Biomacromolecules. 2002;3(3):547-53.

25.   Kobayashi Y, Okamoto A, Nishinari K. Viscoelasticity of hyaluronic acid with different molecular weights. Biorheology. 1994;31(3):235-44.

26.   Nijenhuis N, Mizuno D, Schmidt CF, Vink H, Spaan JA. Microrheology of hyaluronan solutions: implications for the endothelial glycocalyx. Biomacromolecules. 2008;9(9):2390-8.

27.   Falcone SJ, Palmeri DM, Berg RA. Rheological and cohesive properties of hyaluronic acid. J Biomed Mater Res A. 2006;76(4):721-8.

28.   Bhuanantanondh P, Grecov D, Kwok E, Guy P. Rheology of osteoarthritic synovial fluid mixed with viscosupplements: A pilot study. Biomedical Engineering Letters. 2011;1(4):213-9.

29.   Krause WE, Bellomo EG, Colby RH. Rheology of Sodium Hyaluronate under Physiological Conditions. Biomacromolecules. 2001;2(1):65-9.

30.   Dodero A, Williams R, Gagliardi S, Vicini S, Alloisio M, Castellano M. A micro-rheological and rheological study of biopolymers solutions: Hyaluronic acid. Carbohydrate Polymers. 2019;203:349-55.

31.   Rebenda D, Vrbka M, Čípek P, Toropitsyn E, Nečas D, Pravda M, et al. On the Dependence of Rheology of Hyaluronic Acid Solutions and Frictional Behavior of Articular Cartilage. Materials (Basel). 2020;13(11).

32.   Finelli I, Chiessi E, Galesso D, Renier D, Paradossi G. A new viscosupplement based on partially hydrophobic hyaluronic acid: A comparative study. Biorheology. 2011;48:263-75.

33.   Fraser JRE, Laurent TC, Laurent UBG. Hyaluronan: its nature, distribution, functions and turnover. Journal of Internal Medicine. 1997;242(1):27-33.

34.   Dicker KT, Gurski LA, Pradhan-Bhatt S, Witt RL, Farach-Carson MC, Jia X. Hyaluronan: A simple polysaccharide with diverse biological functions. Acta Biomaterialia. 2014;10(4):1558-70.

35.   Burdick JA, Prestwich GD. Hyaluronic acid hydrogels for biomedical applications. Advanced Materials. 2011;23(12):H41-H56.

36.   Stern R, Maibach HI. Hyaluronan in skin: aspects of aging and its pharmacologic modulation. Clinics in Dermatology. 2008;26(2):106-22.

37.   Khunmanee S, Jeong Y, Park H. Crosslinking method of hyaluronic-based hydrogel for biomedical applications. Journal of Tissue Engineering. 2017;8:2041731417726464.

38.   Kim M-H, Nguyen D-T, Kim D-D. Recent studies on modulating hyaluronic acid-based hydrogels for controlled drug delivery. Journal of Pharmaceutical Investigation. 2022;52(4):397-413.

39.   Radvar E, Azevedo HS. Supramolecular Nanofibrous Peptide/Polymer Hydrogels for the Multiplexing of Bioactive Signals. ACS Biomaterials Science & Engineering. 2019;5(9):4646-56.

40.   Saunders L, Ma PX. Self-Healing Supramolecular Hydrogels for Tissue Engineering Applications. Macromolecular bioscience. 2019;19(1):1800313.

41.   Perera MM, Ayres N. Dynamic covalent bonds in self-healing, shape memory, and controllable stiffness hydrogels. Polymer Chemistry. 2020;11:1410-23.

42.   Webber MJ, Appel EA, Meijer EW, Langer R. Supramolecular biomaterials. Nature Materials. 2016;15(1):13-26.

43.   Fichman G, Gazit E. Self-assembly of short peptides to form hydrogels: design of building blocks, physical properties and technological applications. Acta biomaterialia. 2014;10(4):1671-82.

44.   Pashuck ET, Cui H, Stupp SI. Tuning Supramolecular Rigidity of Peptide Fibers through Molecular Structure. Journal of the American Chemical Society. 2010;132(17):6041-6.

45.   Boekhoven J, Zha RH, Tantakitti F, Zhuang E, Zandi R, Newcomb CJ, et al. Alginate-peptide amphiphile core-shell microparticles as a targeted drug delivery system. RSC Advances. 2015;5(12):8753-6.

46.   Rajangam K, Behanna HA, Hui MJ, Han X, Hulvat JF, Lomasney JW, et al. Heparin Binding Nanostructures to Promote Growth of Blood Vessels. Nano Letters. 2006;6(9):2086-90.

47.   Ferreira DS, Marques AP, Reis RL, Azevedo HS. Hyaluronan and self-assembling peptides as building blocks to reconstruct the extracellular environment in skin tissue. Biomaterials Science. 2013;1(9):952-64.

48.   Yan X, Zhu P, Li J. Self-assembly and application of diphenylalanine-based nanostructures. Chemical Society Reviews. 2010;39(6):1877-90.

49. Jayawarna V, Ali M, Jowitt TA, Miller AF, Saiani A, Gough JE, et al. Nanostructured Hydrogels for Three-Dimensional Cell Culture Through Self-Assembly of Fluorenylmethoxycarbonyl–Dipeptides. Advanced Materials. 2006;18:611-4.

50. Raeburn J, Pont G, Chen L, Cesbron Y, Lévyc R, Adams DJ. Fmoc-diphenylalanine hydrogels: understanding the variability in reported mechanical properties. Soft Matter. 2012;8:1168-74.

51. Huang R, Qi W, Feng L, Sua R, Hea Z. Self-assembling peptide–polysaccharide hybrid hydrogel as a potential carrier for drug delivery. Soft Matter. 2011;7:6222-30.

52. Xie Y, Zhao J, Huang R, Qi W, Wang Y, Su R, et al. Calcium-Ion-Triggered Co-assembly of Peptide and Polysaccharide into a Hybrid Hydrogel for Drug Delivery. Nanoscale Research Letters. 2016;11(1):184.

53. Gong X, Branford-White C, Tao L, Li S, Quan J, Nie H, et al. Preparation and characterization of a novel sodium alginate incorporated self-assembled Fmoc-FF composite hydrogel. Materials science & engineering C, Materials for biological applications. 2016;58:478-86.

54. Ghosh M, Halperin-Sternfeld M, Grinberg I, Adler-Abramovich L. Injectable Alginate-Peptide Composite Hydrogel as a Scaffold for Bone Tissue Regeneration. Nanomaterials (Basel, Switzerland). 2019;9(4):497.

55. Wee S, Gombotz WR. Protein release from alginate matrices. Advanced Drug Delivery Reviews. 1998;31(3):267-85.

56. Çelik E, Bayram C, Akçapınar R, Türk M, Denkbaş EB. The effect of calcium chloride concentration on alginate/Fmoc-diphenylalanine hydrogel networks. Materials Science & Engineering C, Materials for Biological Applications. 2016;66:221-9.

57. Aviv M, Halperin-Sternfeld M, Grigoriants I, Buzhansky L, Mironi-Harpaz I, Seliktar D, et al. Improving the Mechanical Rigidity of Hyaluronic Acid by Integration of a Supramolecular Peptide Matrix. ACS Applied Materials & Interfaces. 2018;10(49):41883-91.

58. Xing R, Li S, Zhang N, Shen G, Möhwald H, Yan X. Self-Assembled Injectable Peptide Hydrogels Capable of Triggering Antitumor Immune Response. Biomacromolecules. 2017;18(11):3514-23.

59. Abbas M, Xing R, Zhang N, Zou Q, Yan X. Antitumor Photodynamic Therapy Based on Dipeptide Fibrous Hydrogels with Incorporation of Photosensitive Drugs. ACS Biomaterials Science & Engineering. 2018;4(6):2046-52.

60. Yang Z, Gu H, Fu D, Gao P, Lam JK, Xu B. Enzymatic Formation of Supramolecular Hydrogels. Adv Mater. 2004;16:1440-4.

61. Criado-Gonzalez M, Wagner D, Rodon Fores J, Blanck C, Schmutz M, Chaumont A, et al. Supramolecular Hydrogel Induced by Electrostatic Interactions between Polycation and Phosphorylated-Fmoc-Tripeptide. Chem Mater. 2020;32:1946-56.

62. Cheng G, Castelletto V, Jones RR, Connona CJ, Hamley IW. Hydrogelation of self-assembling RGD-based peptides. Soft Matter. 2011;7:1326-33.

63.   Chakraborty P, Ghosh M, Schnaider L, Adadi N, Ji W, Bychenko D, et al. Composite of Peptide-Supramolecular Polymer and Covalent Polymer Comprises a New Multifunctional, Bio-Inspired Soft Material. Macromolecular Rapid Communications. 2019;40(18):e1900175.

64.   Capito RM, Azevedo HS, Velichko YS, Mata A, Stupp SI. Self-assembly of large and small molecules into hierarchically ordered sacs and membranes. Science. 2008;319(5871):1812-6.

65.   Cotey TJ, Sai H, Perez C, Palmer LC, Stupp SI. Hybrid gels via bulk interfacial complexation of supramolecular polymers and polyelectrolytes. Soft Matter. 2021;17(19):4949-56.

66.   Fernández-Muiños T, Recha-Sancho L, López-Chicón P, Castells-Sala C, Mata A, Semino CE. Bimolecular based heparin and self-assembling hydrogel for tissue engineering applications. Acta Biomaterialia. 2015;16:35-48.

67.   Kumar VA, Shi S, Wang BK, Li IC, Jalan AA, Sarkar B, et al. Drug-triggered and cross-linked self-assembling nanofibrous hydrogels. Journal of the American Chemical Society. 2015;137(14):4823-30.

68.   Galler KM, Hartgerink Jd Fau - Cavender AC, Cavender Ac Fau - Schmalz G, Schmalz G Fau - D'Souza RN, D'Souza RN. A customized self-assembling peptide hydrogel for dental pulp tissue engineering. Tissue Eng Part A. 2012;18(1-2):176-84.

69.   Nadernezhad A, Forster L, Netti F, Adler-Abramovich L, Teßmar J, Groll J. Rheological analysis of the interplay between the molecular weight and concentration of hyaluronic acid in formulations of supramolecular HA/FmocFF hybrid hydrogels. Polym J. 2020;52:1007-12.

70.   Aslani S, Kabiri M, HosseinZadeh S, Hanaee-Ahvaz H, Taherzadeh ES, Soleimani M. The applications of heparin in vascular tissue engineering. Microvasc Res. 2020;131(1095-9319 (Electronic)):104027.

71.   Kong M, Chen XG, Xing K, Park HJ. Antimicrobial properties of chitosan and mode of action: A state of the art review. International Journal of Food Microbiology. 2010;144(1):51-63.

72.   Smeets PJM, Cho KR, Kempen RGE, Sommerdijk NAJM, De Yoreo JJ. Calcium carbonate nucleation driven by ion binding in a biomimetic matrix revealed by in situ electron microscopy. Nature Materials. 2015;14(4):394-9.

73.   Ferreira DS, Marques AP, Reis RL, Azevedo HS. Hyaluronan and self-assembling peptides as building blocks to reconstruct the extracellular environment in skin tissue. Biomaterials Science. 2013;1(9):952-64.

74.   Zha RH, Sur S, Stupp SI. Self-assembly of cytotoxic peptide amphiphiles into supramolecular membranes for cancer therapy. Advanced Healthcare Materials. 2013;2(1):126-33.

75.   Bitton R, Chow LW, Zha RH, Velichko YS, Pashuck ET, Stupp SI. Electrostatic Control of Structure in Self-Assembled Membranes. Small. 2014;10(3):500-5.

76.   Ribeiro S, Radvar E, Shi Y, Borges J, Pirraco RP, Leonor IB, et al. Nanostructured interfacial self-assembled peptide–polymer membranes for enhanced mineralization and cell adhesion. Nanoscale. 2017;9(36):13670-82.

77.   Carvajal D, Bitton R, Mantei JR, Velichko YS, Stupp SI, Shull KR. Physical properties of hierarchically ordered self-assembled planar and spherical membranes. Soft Matter. 2010;6(8):1816-23.

78.   Velichko YS, Mantei JR, Bitton R, Carvajal D, Shull KR, Stupp SI. Electric Field Controlled Self-Assembly of Hierarchically Ordered Membranes. Adv Funct Mater. 2012;22(2):369-77.

79.   Radvar E, Shi Y, Grasso S, Edwards-Gayle CJC, Liu X, Mauter MS, et al. Magnetic Field-Induced Alignment of Nanofibrous Supramolecular Membranes: A Molecular Design Approach to Create Tissue-like Biomaterials. ACS Applied Materials & Interfaces. 2020;12(20):22661-72.

80.   Chow LW, Bitton R, Webber MJ, Carvajal D, Shull KR, Sharma AK, et al. A bioactive self-assembled membrane to promote angiogenesis. Biomaterials. 2011;32(6):1574-82.

81.   Standley SM, Toft DJ, Cheng H, Soukasene S, Chen J, Raja SM, et al. Induction of cancer cell death by self-assembling nanostructures incorporating a cytotoxic peptide. Cancer Res. 2010;70(8):3020-6.

82.   Rożkiewicz DI, Myers BD, Stupp SI. Interfacial Self-Assembly of Cell-like Filamentous Microcapsules. Angewandte Chemie International Edition. 2011;50(28):6324-7.

83.   Boekhoven J, Zha RH, Tantakitti F, Zhuang E, Zandi R, Newcomb CJ, et al. Alginate–peptide amphiphile core–shell microparticles as a targeted drug delivery system. RSC Advances. 2015;5(12):8753-6.

84.   Mendes AC, Baran ET, Lisboa P, Reis RL, Azevedo HS. Microfluidic Fabrication of Self-Assembled Peptide-Polysaccharide Microcapsules as 3D Environments for Cell Culture. Biomacromolecules. 2012;13(12):4039-48.

Chapter 2
Materials and methods
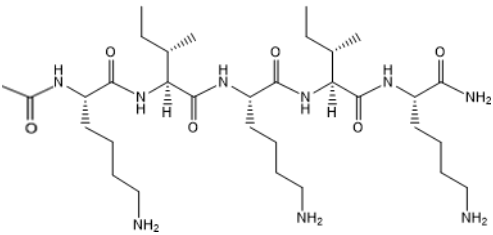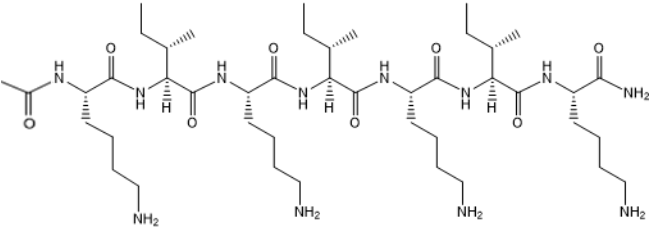
Chapter 2 Materials and methods
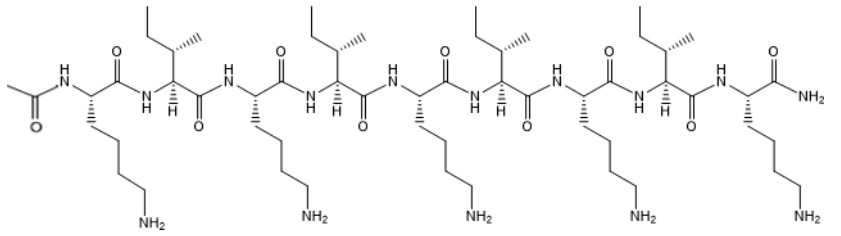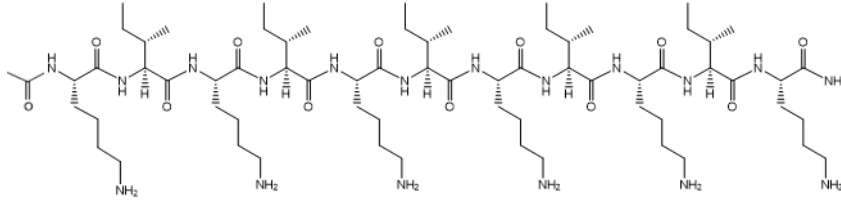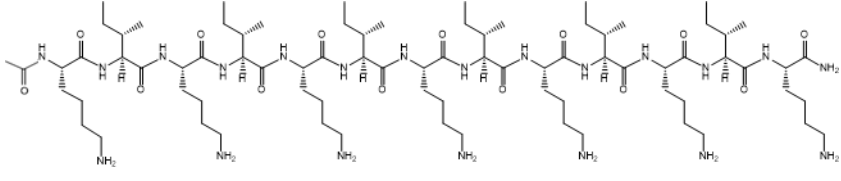
2.1. Self-assembling peptides

2.1.1. Peptide design

Peptides with the general chemical structure $(KI)_nK$ were designed in this work, where n represents the number of repeating units of alternating hydrophilic cationic lysine (Lys, K) and hydrophobic isoleucine (Ile, I) residues (**Table 2.1**). The peptides have an amidated C-terminus, where the uncharged C-terminus makes the peptide mimic the nature protein. The N-terminus of the peptide is acetylated is widely use protein modification while enhancing peptide stability. By eliminating additional charges at the N- and C-terminus, one can investigate the effect of charge derived from the amino side chains.

Table 2.1: *The chemical structure and molecular weight (Mw) of peptides.*

Peptide	Chemical structure	Mw (g/mol)
$(KI)_2K$	CH$_3$CONH-KIKIKIK-CONH$_2$	669.49
$(KI)_3K$	CH$_3$CONH-KIKIKIK-CONH$_2$	910.67

(KI)₄K   1152.58

CH₃CONH-KIKIKIKIK-CONH₂

(KI)₅K   1393.92

CH₃CONH-KIKIKIKIKIK-CONH₂

(KI)₆K   1634.21

CH₃CONH-KIKIKIKIKIKIK-CONH₂

2.1.2. Peptide synthesis by solid-phase method

Solid-phase peptide synthesis (SPPS, **Figure 2.1-A**) is a commonly used method to obtain peptides containing 4-30 amino acids. SPPS starts by attaching a fluorenylmethoxycarbonyl (Fmoc) protected amino acid (Fmoc-AA-OH) to a swollen solid resin where a covalent bond is formed between the carbonyl group of the protected amino acid and a free amino group in the resin, being usually carried out from the C- to the N-terminus.

The most common used resins are low cross-linked polystyrene beads. Effective solvation of resin/peptide is essential for efficient peptide synthesis, and properly swollen resin is almost as accessible to regents as if it is free in the solution (1). Since resins are an inert matrix passive to chemistry, linkers will be considered as immobilized protecting groups being able to provide linkage between the resin and the peptide chain (2). Common linkers typically result in peptide released as either peptide amide (e.g. Rink Amide resin) or carboxylic acid (e.g. Wang resin), and Fmoc and tert-butyloxycarbonyl (Boc) protected peptide synthesis also require the employment of different linkers. The coupling, which refers to the peptide bond formation between adjacent amino acids, can be achieved by the use of suitable coupling reagents. Piperidine easily removes the Fmoc group in Fmoc SPPS, and coupling involves attack of the amino group of one residue at the carbonyl group of the activated carboxy-containing component (1). The coupling reagent N, N'-Diisopropylcarbodiimide (DIC) is commonly used to produce amides, esters and acid anhydrides from carboxylic acids, and function as an activator in peptide synthesis, while 1-hydroxybenzotriazole hydrate (HOBt) not only supresses racemization caused by carbodiimide activation but also accelerates coupling (**Figure 2.1-B**).
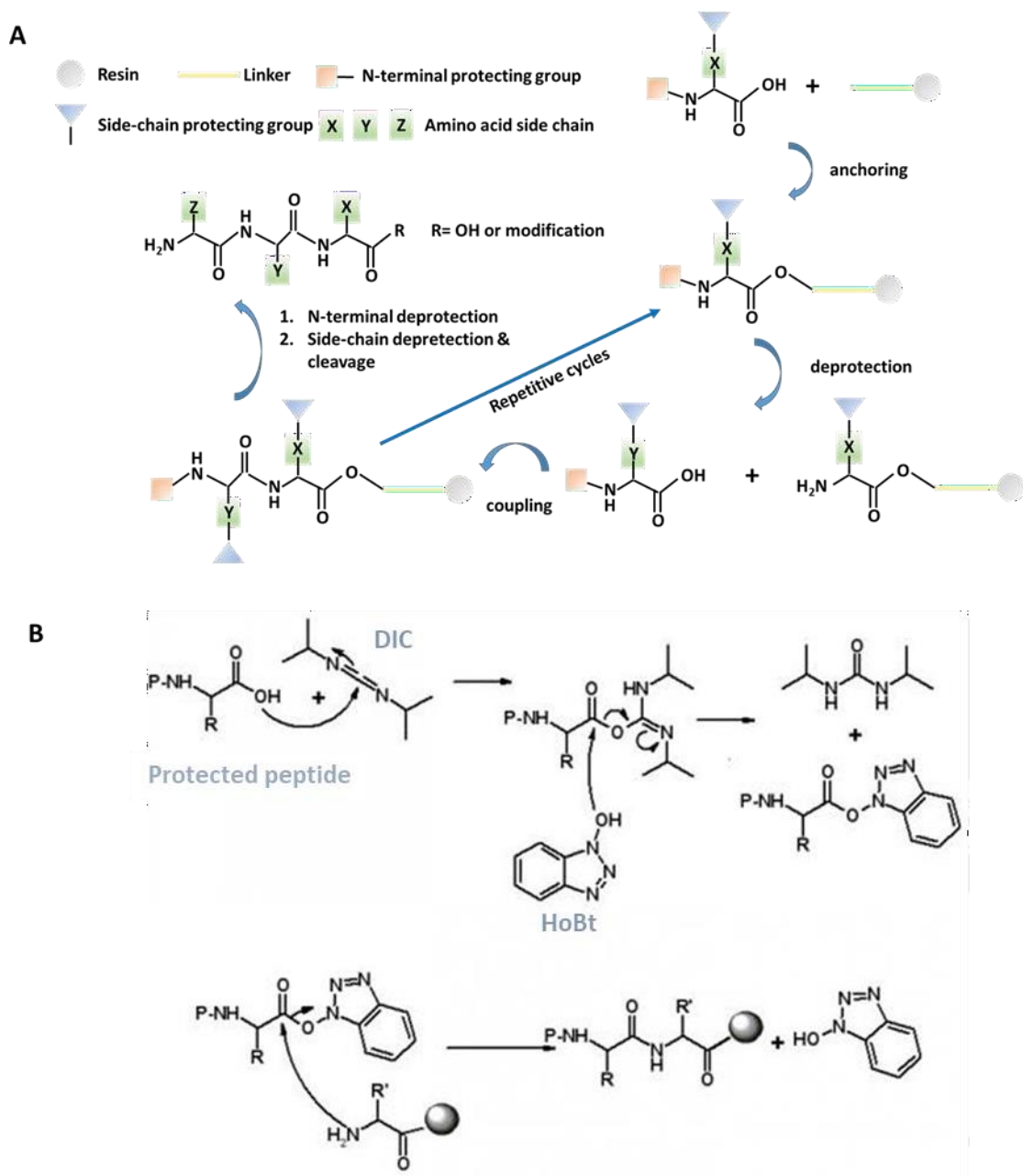
Figure 2.1: *(A) The general procedure of SPSS. (B) DIC and HOBt are used to produce activated ester reacting with the amino group of protected amino acid in peptide synthesis (3).*

Trifluoroacetic acid (TFA) is often used to remove side-chain protecting groups (e.g. Boc group) and cleave anchoring linkages connecting the resin and peptide. The selection of the cleavage

cocktail is determined by the nature of linker, where high-concentration TFA is required with Rink Amide linker.

Peptides, listed in **Table 2.1**, were synthesized in an automated peptide synthesizer (Liberty Blue, CEM, UK) using standard solid-phase Fmoc chemistry. Synthesis of 1 mmol was done using a 4-methylbenzhydrylamine (MBHA) rink amide resin with substitution degree of 0.52 mmol/g (Novabiochem, Merck, UK). The coupling was done with four equivalents of Fmoc-Ile-OH, Fmoc-Lys(Boc)-OH (Novabiochem, Merck, UK), HOBt (Carbosynth, UK) and DIC (Alfa Aesar, UK). Fmoc deprotections were performed with 20% piperidine (Alfa Aesar, UK) in dimethylformamide (DMF, Alfa Aesar, UK). Acetylation of N-terminus was performed using 10% acetic anhydride (Sigma-Aldrich, UK) in DMF. For the synthesis of fluorescent labelled peptide (Rhod-(KI)$_4$K, Rhod-(KI)$_5$K and Rhod-(KI)$_6$K), rhodamine dye was attached at peptide N-terminus, where 200 mg peptide-resin was swollen in 1200 μL DMF and 50 μL N,N-diisopropylethylamine (DIEA, Alfa Aesar, UK) with the addition of 10 mg of 5-(and 6)-carboxytetra-methylrhodamine succinimidyl ester (NHS-rhodamine, ThermoFisher, UK) and shaking at room temperature overnight. Peptides were cleaved from the resin using a cleavage cocktail composed of 95% TFA (Alfa Aesar, UK), 2.5% Triisopropylsilane (TIS, Alfa Aesar, UK) and 2.5% ultrapure water. The peptide-bound resin was incubated with the cleavage cocktail in a reaction vessel for 3 hours, at RT on a shaker (Stuart Wrist-Action Flask Shaker, UK). The peptide mixture was collected and excess TFA was removed by rotary evaporation. The resulting solution was transferred into cold diethyl ether (Alfa Aesar, UK), where a white peptide powder was precipitated. Peptides were collected by centrifugation, washed with cold ether, and allowed to dry overnight. Finally, peptides were dissolved in ultrapure water followed by freeze drying. For fluorescent labelled peptide sample, peptide powder was redissolved in ultrapure water and then transferred into dialysis tubing (500 Da MWCO, Sigma-Aldrich, UK) in which dialyzed against 100 mM NaCl (Sigma-Aldrich, UK), followed by dialysis against distilled water and lyophilisation.

2.1.3. Peptide purification by reversed phase high performance liquid chromatography (RP-HPLC)

The most used technique to analyse and purify peptides is RP-HPLC, which is suitable for both analytical and preparative separations. In HPLC, pumps pass a pressurized liquid (mobile phase) through a column filled with a solid adsorbent material (stationary phase). As each component in the sample interacts slightly differently with the adsorbent material, different components would have different retention times. For peptide purification, the overall peptide hydrophobicity/hydrophilicity are important factors in the peptide separation as it mainly determines its retention in the stationary phase (4). In RP-HPLC, active component of the column for the vast majority of peptide separations are silica-based supports containing covalently bound octyl (C_8) or octadecyl (C_{18}) functionalities, and C_{18} stationary phase works better for separating smaller peptide with molecular weight less than 2000-3000 Daltons (5). Peptides are eluted from the hydrophobic stationary phases in order of increasing peptide hydrophobicity, where the polarity of the gradient elution is reduced by adding increasing ratio of a less polar solvent (e.g. methanol, acetonitrile (ACN)). ACN is favoured to use as it has low viscosity (low pressure is required), is easily removed from samples and is relatively transparent to low wavelength UV light. Additives are also required in the mobile phase to improve the solubility of the peptides, and TFA is the most used acidic additive as it results in good peak shape in most columns (4). Ammonium hydroxide can also be added to the mobile phase once analysing negatively charged peptides to maintain them ionized and improve solubility in the mobile phase Detection of peptides is normally enabled by UV absorption at 220 nm, while the combination with MS provides a more powerful tool to purify peptides, as the mass of separated peptides can be analysed. Peak intensity appeared in MS may be increased compared to UV spectra, however, the existence of TFA might lead to the signal loss in MS due to the interaction between peptides and TFA, which can be solved by decreasing the TFA concentration or using formic acid as replacement.

Peptides were purified by preparative RP-HPLC system (with 2767 sample manager, 2545 binary gradient module), and a reverse-phase C_{18} column (X-bridge Prep OBD, 5μm, 30×150 mm, Waters, UK) was used. Peptides were dissolved in water/0.1% TFA solution (12 mg/mL), filtered before injection and eluted in a gradient of water/ACN (Alfa Aesar, UK) containing 0.1 % TFA (**Table 2.2**). UV detector (2489 UV/Vis detector, UK) in the in HPLC system was set at 220 nm to detect the peptide bond, mass spectrometer detector (SQ-2 mass detector, UK) was set up for mass analysis, and MassLynx software with the FractionLynx application manager was used for peptide fraction collection (**Figure 2.2**). After collecting the purified fractions, ACN was removed by rotary evaporation before freeze-drying to obtain peptides in the powder form.
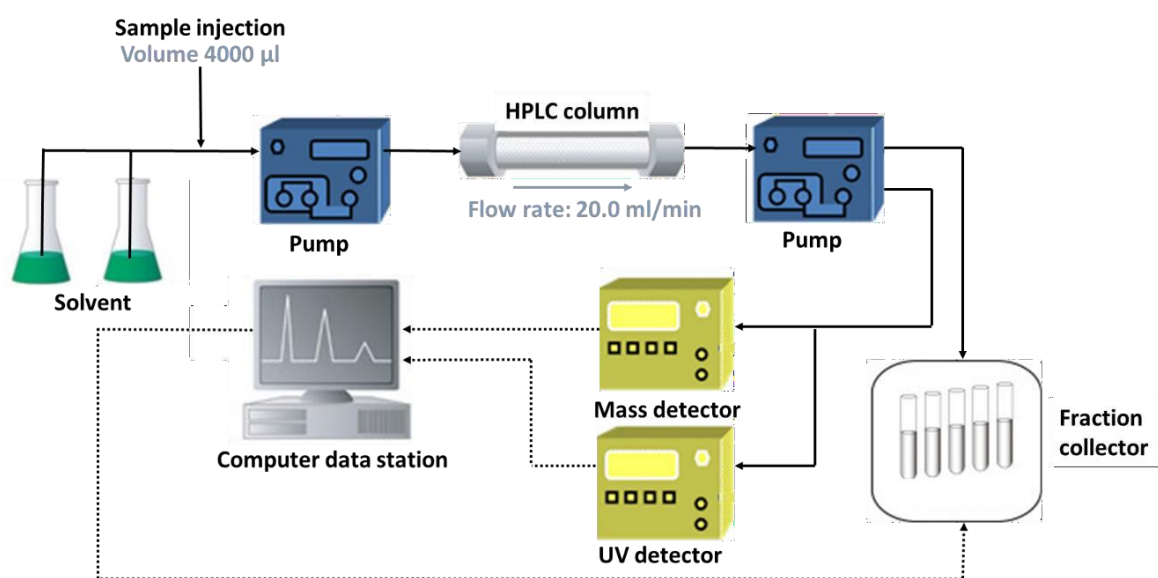
Figure 2.2: *Schematic of the main components and the path of flow in preparative RP-HPLC system used in this work.*

Table 2.2: *The mobile phase gradient used in preparative RP-HPLC.*

Time (min)	% (H$_2$O+0.1 % TFA)	% (ACN+0.1% TFA)
0	98	2
2	98	2
37	0	100
40	98	2
42	98	2

2.1.4. Peptide characterization

2.1.4.1. Confirmation of peptide identify by mass spectrometry (MS)

MS analyses the sample molecular weight by measuring the mass-to-charge ratio (m/z) of charged particles (ions). Samples are first ionized by varied techniques, such as electrospray ionization (ESI), atmospheric pressure chemical ionization and atmospheric pressure photoionization, where charged molecules can break into several fragments. Molecular fragment ions are separated in electronic or magnetic field by their mass-to-charge ratio and then detected by mass detector.

ESI is the most common mode when using in combination with HPLC. In ESI, a dilute solution is sprayed out from a fine tip at atmospheric pressure producing a mist of droplets, and droplets become highly charged by a high voltage between spray tip and the counter electrode (6). As droplets evaporate, single or multiplied charged ions form (e.g. [M+H]$^+$, [M+2H]$^{2+}$) and for peptide samples, normally maximum charged required is equivalent to the number of charged amino acids in the peptide. Methanol, ACN, and mixtures of water and ACN or methanol are ideal solvent for peptide mass analysis, as pure water could lead to low

sensitivity. The mass of the peptides was confirmed after synthesis and purification. Peptide samples were prepared by diluting 1 mg/mL peptide aqueous solutions in methanol to make a 0.1 mg/mL solution and then were analysed by ESI-MS (Bruker Esquire 3000 Plus Ion Trap, UK).

2.1.4.2. Determination of peptide purity by analytical RP-HPLC

Analytical RP-HPLC is typically used to analyse the purity of peptides. The general working principle of HPLC was described in section 1.2, but the diameter of columns used for analytical HPLC applications is usually 1-4 mm, which is much smaller than preparative HPLC column. The flow rate is also much lower than the one use in preparative HPLC and requires less sample volume.

Analytical HPLC (Alliance HPLC System, Waters, UK) with a reverse-phase C_{18} column (X-bridge, 3.5 μm, 4.6×150 mm, Waters, UK) was used to examine the purity of peptides before and after purification, using a gradient of water/acetonitrile (0.1% TFA). 100 μL of Peptide solution (1 mg/mL) was injected and analysed as described for the preparative HPLC. The gradient of the mobile phase (1 ml/min) used to purify peptides can be seen in **Table 2.3.** Purity of the peptides was calculated by integrating the peak area using Empower chromatography data software.

Table 2.3: The mobile phase gradient used in analytical HPLC.

Time (min)	% (H$_2$O+0.1 % TFA)	% (ACN+0.1% TFA)
0	98	2
5	98	2
35	0	100
40	0	100
42	98	2
45	98	2

2.1.4.3. Determination of peptide pK_a by base titration

Titration effectively determines the concentration of a dissolved substance in a known volume by reacting it against another substance of known volume and concentration. The acid-base titration is the most common titration type, which can also be used to determine the pK_a of a weak acid titrated by a strong base.

Equation 1.1 is the ionization equilibrium of a weak acid.

$$HA \Leftrightarrow H^+ + A^- \tag{1.1}$$

The apparent equilibrium constant K_a for this ionization is defined by

$$Ka=[H^+][A^-]/[HA] \tag{1.2}$$

Equation 1.2 illustrates that pK_a is the pH value in which the weak acid is half dissociated, which is when [A$^-$]=[HA].

The pH change can affect the ionization status of charged amino acid residues, therefore the self-assembly of pH-dependent peptides can be estimated based on the theoretical pK_a of containing amino acids. However, the amino acid pK_a is affected by the chemical environment. For example, self-assembly of Fmoc-peptide (with -COOH at the C-terminus) at pH above 3.5 is not favoured as pK_a values of N-protected nonpolar peptides is around 3.5, but Fmoc-FF is found to assemble at neutral pH, where the titration experiment reveals dramatic pK_a shifts toward higher values (7). Titration curves allows to investigate the ionization of peptide at different pHs.

100 mM NaOH solution in 1 µL steps were added to a 1 mL peptide aqueous solution with a 1 mM starting concentration. After each NaOH addition, vortex was used to vigorously agitate the sample to enable homogenous mixing. The pH was measured using a pH meter (FiveGo Cond meter F3, Mettler-Toledo Ltd, UK).

2.1.4.4. Analysis of peptide secondary structure by circular dichroism (CD) spectroscopy

In CD, a sample is analysed by differential absorption of left- and right-handed circular polarized light. When circularly polarized light interacts with an absorbing optically active matter, the absorbance of left- and right-handed circular polarized light could be different, which is used to determine the molecule conformation.

CD is very useful to gain structural information on the conformation of peptides, as each of the secondary structure has a characteristic spectrum. Peptides with α-helix secondary structure have CD spectrum with negative bands at 208 and 222 nm and positive band at 193 nm, while the spectrum of β-sheet forming peptides shows positive band at 195 nm and negative band at 218 nm. Random coil conformation is characterized by a negative band at 195 nm and a weak ellipticity above 210 nm in the CD spectrum (8). It is also possible to determine the content of each secondary structure using quantitative analysis (9).

The buffers used in the sample analysis are critical in obtaining high-quality CD spectra. Buffers for CD samples should be free of optical active molecules. Distilled water is ideal as peptides dissolved in water have the highest transparency. For peptide samples where salts are required, there are low wavelength limits for spectrum analysis. Bubbles should also be avoided as oxygen would affect the CD spectra below 200 nm.

Peptide solutions for CD measurements were prepared at 0.1 mM in ultrapure water and the pHs were adjusted by NH_4OH (Alfa Aesar, UK) to 7, 9, 9.5, 10 and 11, and pHs were confirmed by pH meter. Peptide solutions were incubated overnight before the measurement was performed in a Chirascan CD spectrometer (Applied Photophysics, UK) under a continuous flow of nitrogen at a constant pressure. Far-UV spectra were recorded at 25 °C from 190 to 270 nm in a quartz cuvette with 1 mm path-length. Each presented spectrum is an average of 3 spectra.

2.1.4.5. Determination of beta-sheet content of peptide assemblies by thioflavin T (ThT) assay

Introduced in 1959, ThT is a fluorescent probe used to detect amyloid fibres in cortex tissue. It binds to the side chain channels along the long axis of the amyloid fibrils and the fluorescence signal is enhanced at approximately 482 nm when excited at 450 nm, due to the rotational immobilization of the central C–C bond connecting the benzothiazole and aniline rings (10, 11). ThT can also be used to monitor the real-time aggregation, since fluorescence intensity of ThT correlates linearly with amyloid fibril concentration (11). Generally, ThT does not affect the amyloid fibre aggregation at low concentration.
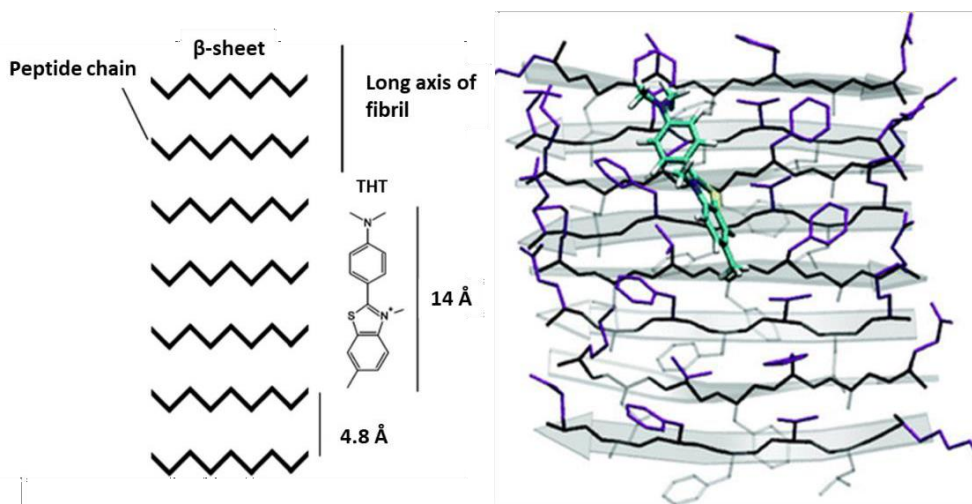
Figure 2.3: *Schematic illustrating ThT oriented with their long axis parallel to the long axis of the β-sheet forming fibril (12).*

It was found that ThT can bind to β-sheet-rich assemblies when staining the amyloid deposit in tissue samples, and the minimal four consecutive β-strands were required for ThT binding (**Figure 2.3**) (13). The flatness of β-sheet fibril also affects the ThT binding affinity, as THT favours more rigid and less twisted fibril. Peptides with side chains containing aromatic rings also tend to have stronger peptide-ThT interaction. ThT can be used to determine the critical aggregation concentration (CAC) of β-sheet rich peptides as the fluorescence intensity dramatically increases once β-sheet aggregation forms (14).

However, ThT was found not only bind to amyloid fibres but also other structures such as DNA and polymer membranes (15). The inhibition of ThT rotation also derives from both amyloid fibre absorption and solvent viscosity. The self-assembly study of β-sheet forming peptides assessed by ThT assay was in agreement with the internal viscosity of the peptide nanofiber (16).

ThT was used in this work to study the amyloid formation ability of $(KI)_nK$ peptides. Peptides were dissolved in ultrapure water at varied concentrations and the pHs were adjusted to 7 and 11 using NH_4OH. Equal volumes of 50 μM ThT (Sigma-Aldrich, UK) solution were mixed

with peptide solutions. After one-day incubation protected from the light, the fluorescence of solutions was measured in a Luminescence spectrometer (PerkinElmer, US) with an excitation wavelength of 440 nm and an emission wavelength range from 460 nm to 520 nm.

2.1.4.6. Analysis of peptide secondary structure by Fourier-transform infrared (FTIR) spectroscopy

FTIR analyses sample absorbance or transmittance within infrared spectrum, and Fourier transform is then used to turn the raw data into the actual spectrum. Attenuated total reflection (ATR) is one of the accessories allowing a direct sample examination, where the evanescent wave penetrates into samples between 0.5-2 mm.

FTIR is very powerful in obtaining structural information of self-assembling peptides. To get high-quality spectra, high peptide concentration (>10 mg/ml) is often required (17). The amide I absorbance region of peptide is at 1600-1700 cm^{-1}, mainly due to the stretching vibrations of the C=O bonds of the amino acids. The strength of hydrogen bonds in self-assembling peptide systems can be affected by the secondary structure, which results in varied absorption frequency of the C=O vibration (18). Therefore, the secondary structure of self-assembling peptides can be determined by the absorbance range in amide I region. However, it is worth noting that that there are no simple correlations between FTIR spectra and secondary structure, so FTIR would be more reliable if used in combination with other peptide characterization technique (e.g. CD) (19).

For peptides in solution with α-helix secondary structure, the band centre occurs at 1650-1655 cm^{-1}, while the component centred between 1640-1648 cm^{-1} is assigned to random coils. However, the overlap of the α-helical and random structure absorption frequency range often makes the 1640–1660 cm^{-1} a region difficult to analyse. Peptides with β-sheet conformation often see the absorbance region between 1620 and 1640 cm^{-1}, while the assignment of parallel and antiparallel β-sheets remains controversial. Meanwhile, absorbance bands of

native β-sheet proteins and amyloid fibrils are not exactly the same, where the absorbance region of amyloid fibrils (containing β-sheet structures) is at 1611-1630 cm^{-1} and native β-sheet proteins produce peak from 1630 cm^{-1} to 1643 cm^{-1} (19, 20). An absorption band near 1673 cm^{-1} can be seen in the IR spectra, caused by the CH_3COOF^- counterions associated with the peptide purification.

In this work, the peptide secondary structures were investigated in solution by FTIR-ATR. Stock peptide solutions of 20 mM were prepared by dissolving peptides in D_2O (Sigma-Aldrich, UK). To study the peptide self-assembly at different ionic strength, stock peptide solutions were diluted to 10 mM using equal volume of NaCl solutions (in D_2O). The final NaCl concentrations in the peptide solutions were 0, 50, 100, 200, 300 and 400 mM. Secondary structures of peptides were also investigated at different pHs by diluting stock peptide solutions with D_2O and pHs were adjusted to 7 and 11 using ND_4OD (Sigma-Aldrich, UK). Solutions were analysed using a Brukler Tensor 27 FTIR spectrometer equipped with a diamond ATR accessory. Absorbance spectra were obtained with a 4 cm^{-1} resolution and D_2O was used as the background.

2.1.4.7. Morphological analysis of peptide assemblies by transmission electron microscopy (TEM)

As the resolution of optical microscopy is limited by the wavelength of light, electron microscopy can produce high magnification imaging due to the small wavelength of electron beam. TEM enables visualization of samples by electron beams which can pass through a very thin sample. For non-conductive samples, such as peptide assemblies, negative staining with uranium is required to increase the image contrast. Samples are placed on a meshed area of TEM grid.

Peptides were dissolved in deionized water to obtain the concentration of 1 mM and the pH was adjusted to 11 using NH_4OH. Samples for TEM analysis were prepared by placing a drop

of peptide solution directly on the 400-mesh carbon-coated copper TEM grid (Agar Scientific, UK). For negative staining, a drop of a 2 wt% uranyl acetate (Agar Scientific, UK) aqueous solution was placed on the samples. The excess solution was wiped away with a piece of filter paper, and the sample was allowed to dry under ambient conditions for 3 hours. All images were collected with a JEOL 1230 transmission electron microscope at 100 kV (JEOL, USA) with a SIS Megaview III wide angle CCD camera. The images were analysed in ImageJ software to determine the nanofiber diameter.

2.1.4.8. Determination of surface charge by zeta potential measurements

Zeta potential characterizes the stability of particles in colloidal systems, and it provides the electrical potential of the double layer by velocity measurement of the charged particles moving toward the electrode in the presence of an external electric field (21). Zeta potential is associated with interfacial charge which reflects the potential of the particle plane where the liquid velocity relative to the particle is zero (22). Zetasizer could measure the electrophoretic mobility of the charged particle and zeta potential could thus be estimated according to electrokinetic model. Stable suspensions typically have an absolute zeta potential of more than 30 mV, while particles with absolute zeta potential less than 30 mV are considered as unstable.

The degree of the stability of charged peptide aggregates was measured by Zetasizer (Nano ZS series, Malvern Panalytical, UK). Peptides were dissolved at 1 mM in ultrapure water and the pHs were adjusted by ammonium hydroxide (NH_4OH) and the measurement was carried out immediately after the pH adjustment. Three repeated measurements were conducted for each sample.

2.2. Polyelectrolytes (PEs)

PEs are polymers with repeating units bearing an electrolyte group including polycations and polyanions, and they often combine the physical and chemical properties of both polymer and electrolyte. PEs can be naturally occurring (e.g. hyaluronic acid and alginate) or synthetic (e.g. polystyrene sulfonate and poly(acrylic acid)).

2.2.1. Hyaluronic acid (HA)

HA (**Figure 2.4-A**) is a weak natural PE which properties are described in detail in the Chapter 1 (section 1.2.1.). HA used in this work was mostly sodium hyaluronate with molecular weight of 2 MDa (Lifecore, USA). HA was dissolved in ultrapure water or PBS at desired concentration.

To monitor the formation of peptide-HA hydrogel along the time, HA was fluorescently labelled with fluoresceinamine (fluorescein–HA) using EDC chemistry (23). 50 mg HA was dissolved in 20 mL ultrapure water and then mixed with a solution of 5 mg of fluoresceinamine (Sigma-Aldrich, UK) in 20 mL of DMF. Next, 100 mg of NHS (Sigma-Aldrich, UK) was added, and the solution pH was adjusted to 4.75 with 0.01 M HCl. Finally, 50 mg of EDC (Sigma-Aldrich, UK) was added maintaining the solution pH at 4.75. After 12 h, the solution was transferred to dialysis tubing (2000 Da MWCO, Sigma-Aldrich, UK) and dialyzed exhaustively against 100 mM NaCl for 2 days, followed by dialysis against distilled water for another 2 days and then lyophilization.

2.2.2. Alginate

Alginate is a polysaccharide extracted from seaweeds and can be considered as block copolymer composed of L-guluronate and D-mannuronate residues (**Figure 2.4-B**) whose ratio is determined by the natural source. Alginate can also be produced by bacterial biosynthesis which provide alginate with a more defined chemical structure. Commercial alginate has the

molecular weight between 32-400 kDa, and pK_a of –COOH on alginate is at 3-3.5. Being an anionic polyelectrolyte, alginate can be easily ionically cross-linked by divalent cations such as Ca^{2+}. Alginate has shown to be biocompatible being widely exploited in biomedical applications (24).

Sodium alginate used in this work was extracted from brown algae with 'medium viscosity' (Sigma-Aldrich, UK). Alginate was dissolved in ultrapure water or PBS to obtain the desired concentration.

2.2.3. Polystyrene sulfonate (PSS)

PSS is a synthetic polymer derived from polystyrene by the addition of sulfonate functional groups (**Figure 2.4-C**). Clinically it is used to treat high blood potassium. Ions such as Ca^{2+} and Mg^{2+} would adhere to the anionic sulfonate groups replacing Na^+, and it was found that the formation of PSS-Ca globules was an important precursor in biomineralization systems (25). As sulfonic acids tend to be strong acids, PSS would completely disassociate in water for most pH values. In this work, PSS with molecular of 1 MDa (sodium salt, Sigma-Aldrich, UK) was dissolved in ultrapure water or PBS with desired concentration.

2.2.4. Poly(acrylic acid) (PAA)

PAA can be viewed as a polyethylene polymer with carboxylic acid substituents on alternating carbons (**Figure 2.4-D**). It can form hydrogel at neutral pH as the pK_a of PAA is at 4.75 (26). PAA hydrogels have an excellent swelling ability as they can absorb many times their weight in water (27), being used as a drug carrier due to the good bioadhesive properties and enhanced drug penetration (28).

PAA with molecular of 1.25 MDa (Sigma-Aldrich, UK) was used in this work by dissolving the polymer powder in ultrapure water or PBS with desired concentration.
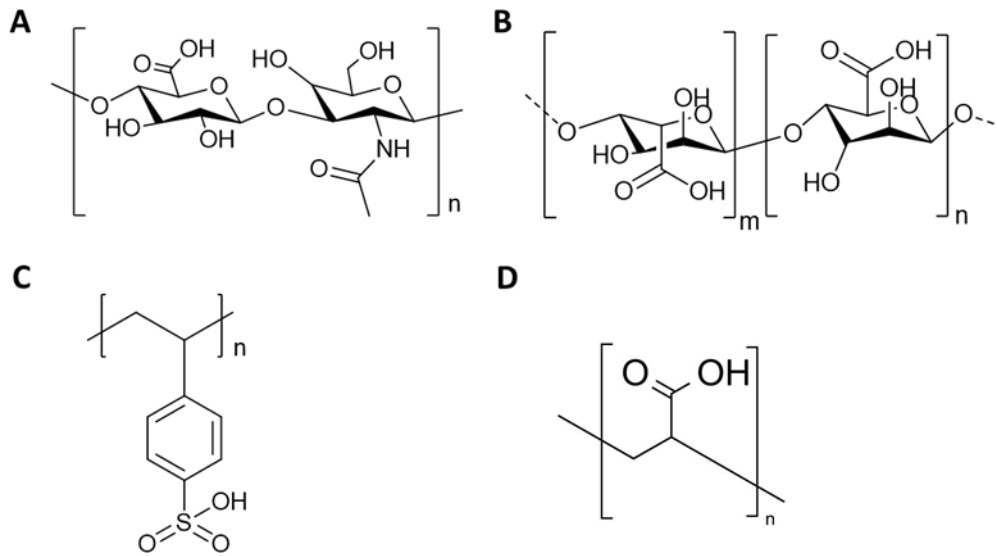
Figure 2.4*: Chemical structures of (A) HA, (B) Alginic acid, (C) PSS and (D) PAA.*

2.2.5. Characterization of PEs

The coefficient of proportionality between the shear stress and shear rate is defined as the shear viscosity or dynamic viscosity (η). Fluids are normally divided into two broad categories, Newtonian and non-Newtonian fluids. Typical Newtonian fluids include water and oil, which show shear stress linearly related to the shear rate, with the viscosity being independent of shear rate. Viscosities of non-Newtonian fluids vary at different shear rate, and the most common type of non-Newtonian fluids behave as shear-thinning. Shear-thinning fluid has a constant viscosity when shear rate is close to zero (zero shear viscosity, η_0), and the viscosity is observed to dramatically decrease within the shear-thinning range, where Power law model could be used for fitting (equation (2.1)).

$$\sigma = K\dot{y}^n \tag{2.1}$$

Where σ is shear stress, K is cross constant, $\dot{y}$ is shear rate and n represents power low index.

When shear rate is high enough, the relative constant viscosity is observed again (infinite shear viscosity, η_∞). However, some shear-thinning fluid would exhibit different behaviour, where viscosity becomes infinite at a very low shear rate (**Figure 2.5-A**).

Most polymer solutions show shear-thinning behaviour, as polymer chains would be in disordered status at rest, stretching out and aligning when shear stress is applied (**Figure 2.5-B**). Shear-thickening behaviour may also occur in some polymer solutions but is less common.
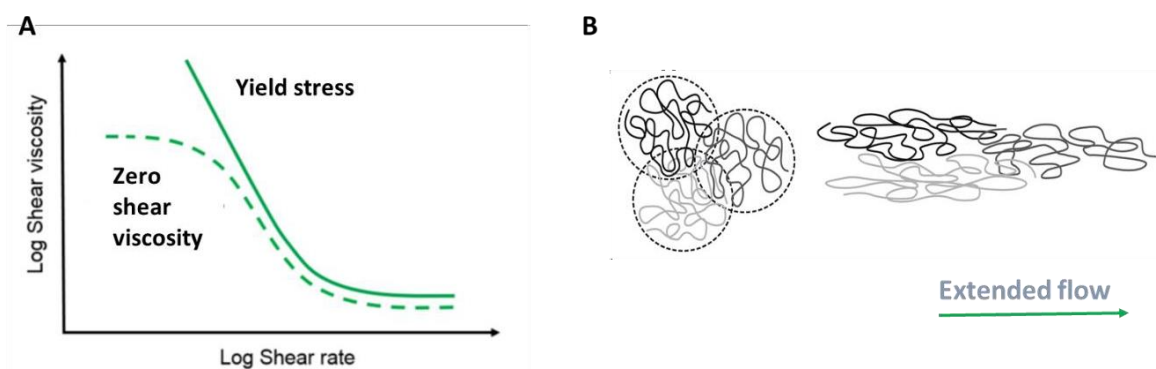
Figure 2.5: (A) Two typical curves exhibit shear-thinning fluid behaviour (29). (B) Shear-thinning behaviour is exhibited where polymer chains extend along the external shear (30).

In this work, the viscosity of 2 wt% polymer solutions (in water or phosphate buffered saline (PBS)) was measured at room temperature using a Discovery Hybrid Rheometer (TA instruments, USA) with a 20 mm parallel plate. For each measurement, 1 mL of polymer solution was loaded and a shear rate of 10-1000 s^{-1} was applied. Triplicate measurements were conducted for each polymer solution. PBS contains 0.01 M phosphate buffer, 0.0027 M potassium chloride and 0.137 M sodium chloride with pH 7.4 (at 25 °C).

Polyelectrolyte solutions could also be characterized by zetasizer, which measures the electrophoretic mobility, indicating the charge status of polyelectrolyte. However, the polyelectrolytes alone do not have zeta potential due to the lack of interfaces

are permeable to electrolyte ions thus an interface does not exist between polyelectrolyte and surrounding environment).

2.3. Peptide-PE hydrogels

2.3.1. Hydrogel preparation

Hydrogels were typically prepared by adding 75 µL of peptide solution on top of 75 µL of either electrolyte or polyelectrolyte solution in a 96 well plate (flat bottom) unless otherwise noted. Electrolyte-induced peptide hydrogels were obtained by adding 2 wt% $(KI)_4K$ and $(KI)_5K$ aqueous solution on top of 1600 mM NaCl (Sigma-Aldrich, UK) and 50 mM Na_2HPO_4 (Sigma-Aldrich, UK).

$(KI)_nK$-PSS, $(KI)_nK$-PAA and $(KI)_nK$-alginate hydrogels were prepared by adding 2 wt% $(KI)_nK$ water solution on top of 2 wt% polyelectrolyte water or PBS solution.

$(KI)_nK$-HA hydrogels were made by either adding 1 wt% or 2 wt% of $(KI)_nK$ aqueous solutions (in water or PBS) on top of 1 wt% or 2 wt% HA solutions (in water or PBS), or with the opposite order, which is adding 1 wt% HA water solution on the 2 wt% $(KI)_nK$ aqueous solution.

The corresponding molar concentrations for 1 wt% $(KI)_2K$, $(KI)_3K$, $(KI)_4K$, $(KI)_5K$ and $(KI)_6K$ are 14.9 mM, 11.0 mM, 8.7 mM, 7.2 mM and 6.1 mM, respectively. For 2 wt% $(KI)_2K$, $(KI)_3K$, $(KI)_4K$, $(KI)_5K$ and $(KI)_6K$, the molar concentrations are 29.8 mM, 22.0 mM, 17.3 mM, 14.3 mM and 12.2 mM. All hydrogels were incubated at room temperature overnight (without mixing) before further characterization.

2.3.1.1. Formation of peptide-HA strings

To exploit the possibility of shear-inducing fibre alignment, liquid-like peptide-HA complex was first made by adding 2 wt% $(KI)_4K$ aqueous solution on the top of 2 wt% HA aqueous solution. After incubation at room temperature overnight, the peptide-HA complex was slowly injected into PBS solution through the tip using micropipette and peptide-HA 'string' was formed.

2.3.2 Hydrogel characterization

2.3.2.1. Examination of hydrogel structure by scanning electron microscopy (SEM)

SEM utilizes a high-energy electron beam that interacts with the sample surface, producing a variety of signals including secondary electrons, backscattered electrons, diffracted backscattered electrons, photons, visible light, and heat. The secondary electron is an electron from the sample excited by the primary electron beam, where the path length of secondary electrons is about 1 nm making them ideal for examining topography. Backscattered electrons are scattered primary electrons rebounded from the sample surface, capable of showing both specimen composition and topography, but it gives poorer image resolution than secondary electrons. X-ray would be emitted when electron beam strikes the sample, which can be measured by dispersive x-ray spectroscopy detector characterizing element present in the sample.

Conventional SEM is conducted under vacuum, allowing the examination of dry samples only. For hydrogel samples with high water content, sample drying causes collapse of the hydrogel 3D shape and dramatic structural changes, being necessary appropriate techniques to preserve the hydrogel 3D structure and dimensions. The most common methods used for preparation of hydrogel samples before SEM observation includes glutaraldehyde fixation to stabilize the 3D shape, removal of water by dehydration using gradated ethanol series, solvent evaporation through a drying process (drying in hexamethyldisilazane, critical point

drying (CPD) or freeze-drying), and additional metal or carbon coating to make the sample conductive to electrons (31). CPD is ideal for drying biological samples where liquid CO_2 is often used, because critical point of CO_2 is 31 °C and 1072 psi which is relatively easy to reach. At the critical point, samples can be dried without suffering from the surface tension effect, since equal density of liquid and gas result in zero surface tension. However, CO_2 is not miscible with water so the third medium (e.g. ethanol) is introduced which is miscible with both water and CO_2.

However, the drying methods used for hydrogel samples can still alter their structure cause artifacts. For example, sample shrinkage and densification can be observed during the dehydration in graded. Therefore, SEM imaging may not reflect the original sample structure due to the changes caused by the sample preparation method.

The micro/nanostructure of the hydrogels prepared in this work was analysed by SEM. Peptide-polyelectrolyte hydrogel samples were fixed in 2.5% glutaraldehyde in ultrapure water for 1 h at 5 °C, while salt-induced peptide hydrogels were fixed in 2.5% glutaraldehyde in PBS. Subsequently, sequential dehydration in increasing ethanol concentrations (20%, 40%, 60%, 75%, 90% to 100%, sample incubation at each concentration is 15 min) was conducted. To avoid collapse of the gel structure, CPD (EMS 850, Electron Microscopy Sciences, USA) was used to remove ethanol. Prior to observation, samples were coated with a gold layer for 1 minute and imaged on a field emission scanning electron microscope (FEI Inspect F, The Netherlands) using 5.0 kV beam.

2.3.2.2. Rheological analysis of the peptide-PE hydrogels

Rheology, the science of flow and deformation of materials, is often used to measure the way in which a liquid, suspension or slurry flows in response to applied forces, which is especially useful to characterize the viscoelastic property of hydrogels. To measure the rheological

properties of hydrogels, rheometers are used, which can either measure shear strain, with known shear stress, or testing shear stress with controlled shear strain.

In a rheology test, oscillation sweep is often performed. For pure elastic material, stress and strain are in phase, as maximum stress occurs at the maximum strain (**Figure 2.6-B**). G (elastic modulus) can be express in equation (3.1)

$$G = \frac{\sigma}{\gamma}$$

(3.1)

Where σ represents shear stress and γ represents shear strain.

For the pure viscous materials (Newtonian fluid), stress and strain are out of phase by 90° (**Figure 2.6-C**), as stress is proportional to the shear rate (equation (3.2)).

$$\eta = \frac{\sigma}{\dot{y}}$$

(3.2)

$$\dot{y} = \frac{d\gamma}{dt}$$

(3.3)

Where η is viscosity and $\dot{y}$ is strain rate determined by the rate of strain change with time (equation (3.3)). **Figure 2.6-A** illustrates the sample loading between the parallel plates, where h is the measurement gap and ω is angular velocity of the upper plate. Considering r as the radius of the plate, shear rate can be calculated by equation (3.4)

$$\eta = \frac{\omega r}{h}$$

(3.4)

For the viscoelastic materials, the phase angle (δ) between shear stress and strain is 0-90° (**Figure 2.6-D**). If the change of shear stress with time and angular velocity follows $\gamma(\omega, t) = \gamma_0 \sin(\omega t)$, G' (storage modulus) and G'' (loss modulus) can be introduced in the equation (3.5):

$$\sigma(\omega, t) = G' \gamma_0 \sin(\omega t) + G'' \gamma_0 \cos(\omega t)$$

(3.5)

Phase angle (δ) is often expressed as the loss factor (tan δ) evaluating elastic and viscous contribution (equation (3.6))

$$\tan \delta = \frac{G''}{G'} \qquad\qquad (3.6)$$

G', G'' and tan δ are essential rheological parameters monitoring changes in the hydrogel mechanical property against strain, time and frequency. A typical rheology test protocol often performs amplitude sweeps at first, to determine the linear viscoelastic regime (G' and G'' independent of strain or stress) and study yield stress/strain (**Figure 2.7-A**). Following amplitude sweep, time sweep can be conducted evaluate the mechanical behaviour (e.g. hydrogel formation kinetic and time stability).
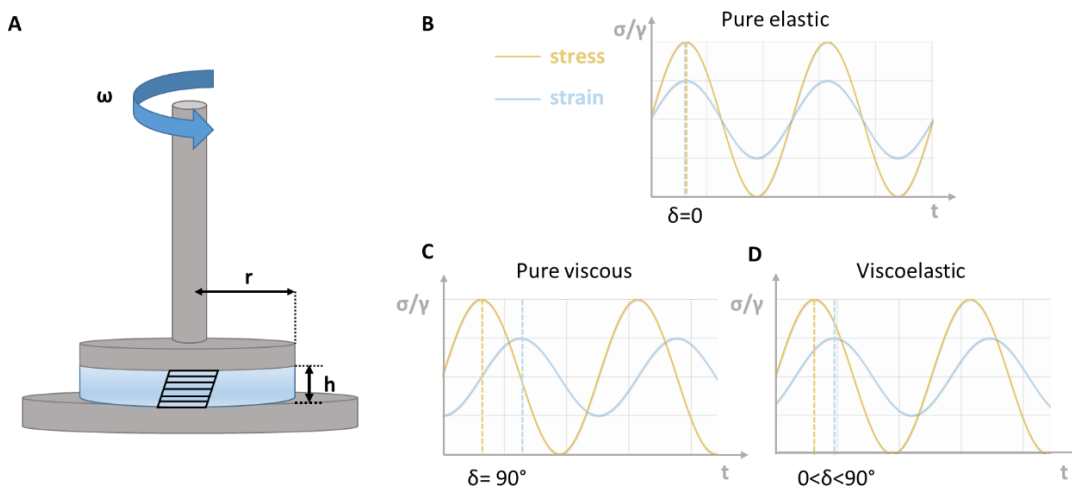
Figure 2.6: *(A) Schematic of rheometer using parallel plate and stress-strain wave of (B) pure elastic materials (C) pure viscous materials and (D) viscoelastic materials.*

To evaluate the gel status, it is critical to examine the frequency dependence of G', G'' and tanδ, rather than simply comparing values of G' and G in amplitude or time sweep, as viscoelastic materials show time dependent rheology properties thus G' and G'' would change as the time scale varies. In the frequency sweep, high frequencies correspond to short time scales and low frequencies to longer time scales. Viscoelastic liquid (e.g. polymer solution) often shows higher G' than G'' at higher frequencies and the situation is reversed at lower frequencies, whereas viscoelastic solid has a parallel G' and G'' and tanδ is constant, independent of frequencies with a value between 0 and 1. For viscoelastic solid (e.g. glass-

like material), G' is constant and frequency independent, while G'' would be linearly increasing with the frequency (**Figure 2.7-B**). Frequency sweeps can be performed at varied stress/strain within the linear viscoelastic regime, and for practical reasons, requiring a stiff hydrogels as biomaterial, having G' > G'' at all frequencies studied is usually qualitatively sufficient (32).
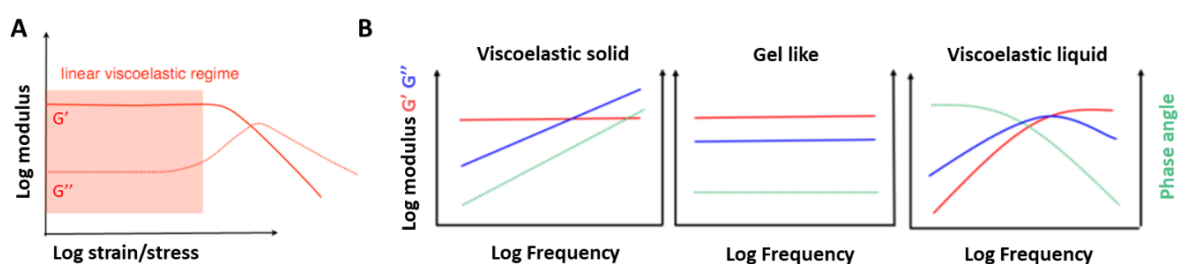
Figure 2.7: *(A) Typical amplitude sweep curve exploring the LVR (33). (B) Frequency dependency of G' and G'' with viscoelastic solid, viscoelastic liquid and gel like material (29).*

Rheological properties of hydrogel samples were first assessed by performing an oscillatory amplitude sweep, from 0.01% to 100%, at a fixed frequency of 1 Hz using a Discovery Hybrid Rheometer (TA instruments, USA) with an 8 mm parallel plate at the room temperature. Following the amplitude sweep, samples were subjected to a frequency sweep at a strain from the linear viscoelastic region (LVR) of the amplitude sweep. The dehydration of hydrogel was prevented by addition of water at the exposed sides of the gel.

2.3.2.3. Monitoring hydrogel formation by confocal laser scanning microscopy (CLSM)

To monitor the formation of $(KI)_nK$-HA hydrogel, fluorescent labelled HA (fluorescein-HA) and peptide (Rhod-$(KI)_nK$ were used and the hydrogel assembly followed by CLSM. Individual aqueous solutions (2 wt%) of the hydrogel components were first prepared by mixing 10% fluorescein-HA with 90% of native HA and 1 % Rhod-$(KI)_nK$ was combined with non-labelled peptide. 25 µL of HA solution was first added into a plastic ring adhered to a glass slide (**Figure**

2.8) and then 25 µL of peptide solution was added on the top. The sample was immediately observed under CLSM (Zeiss LSM710, Germany) and images were taken every 20 minutes. 3D structure was reconstructed using Zeiss Data analysis Workstation for LSM 710.
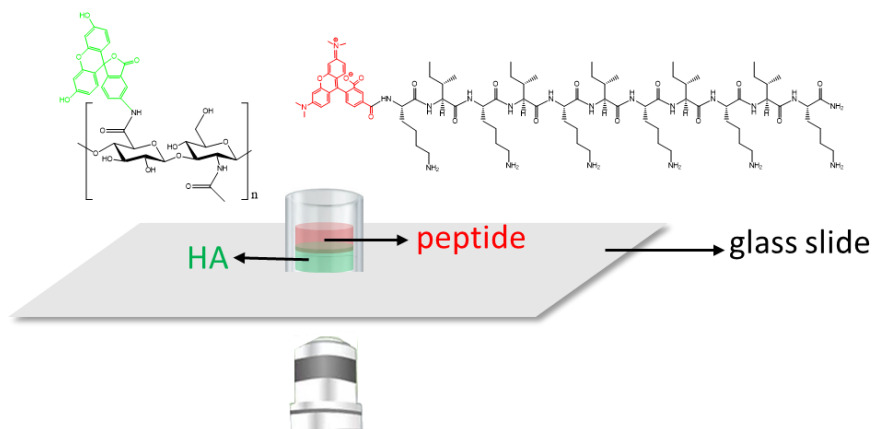
Figure 2.8: *Experimental set up for monitoring the hydrogel assembly using CLSM.*

2.3.2.4. Degradation of peptide-HA hydrogels in presence of hyaluronidase

To assess the enzymatic degradation of peptide-HA hydrogels, hydrogel samples were incubated with hyaluronidase (HAase), the enzyme that catalyses the hydrolysis of HA by cleavage of β(1,4) glycosidic linkages (**Figure 2.9-A**). The hydrogels were first prepared by adding 2 wt% (KI)$_5$K aqueous solution on top of 1 wt% HA aqueous solutions. After 24 h, they were incubated at 37 °C in 24 well plate containing 1 ml PBS or PBS with 2.6 U/mL (simulate physiological conditions in human plasma) and 50 U/ mL of bovine testicular HAase (Type IV-S, 700-3000 units/mg, Sigma-Aldrich, UK) (23). Enzyme solutions and PBS were refreshed every 3 days, collected, and then stored at -20 °C until further quantification of N-acetylamino reducing sugars. Hydrogels were also retrieved at each time point for microstructure analysis using SEM. Experiments were done in triplicate.
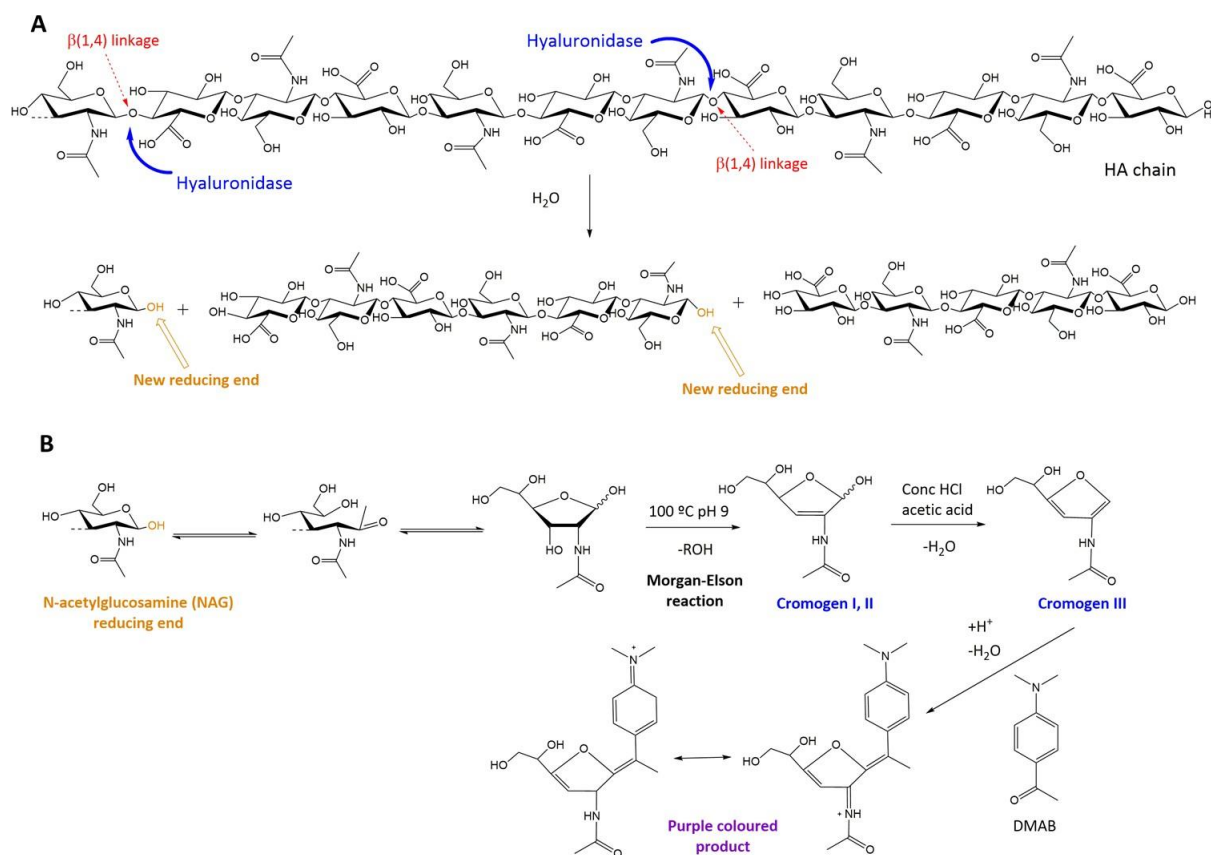
Figure 2.9: *(A) The degradation of HA by HAase generating HA fragments of variable size. (B) In the Morgan-Elson reaction, the reducing end of N-acetylglucosamine results in purple coloured product (34).*

Quantification of HA hydrolysis was done by the Morgan–Elson assay method (**Figure 2.9-B**) (35). Stock solutions of borate and Ehrlich's reagent were first prepared. Borate solution was made by dissolving 4.94 g of boric acid (Sigma-Aldrich, UK) and 1.98 g of potassium hydroxide (Sigma-Aldrich, UK) in 100 mL ultrapure water. The Ehrlich's stock reagent was prepared by dissolving 5 g of 4-(Dimethylamino)benzaldehyde (DMAB, Sigma-Aldrich, UK) in 6.25 mL HCl (12 M, VWR, UK) and 43.75 mL glacial acetic acid (VWR,UK). Ehrlich's reagent was diluted 10 times with glacial acetic acid before using. N-acetyl-D-glucosamine (NAG, Sigma-Aldrich, UK) standard solutions with concentrations of 0-0.5 mg/mL were also prepared to make the calibration curve. For the NAG quantification, 50 μL of borate solution were mixed with 200

μL of sample or standard NAG solutions in a glass tube and boiled in a water bath for 3 min, followed by transferring into cold water bath. 1.5 mL of Ehrlich's reagent was added to each tube. Glass tubes were finally incubated at 37 °C for 15 min and 200 μL of the solution transferred into 96 well plate for measuring the absorbance at 585 nm a using plate reader (SPECTROstar® Omega Absorbance Plate Reader, UK).

2.3.2.5. Birefringence analysis by polarized microscopy

Polarized light microscopy is often used to identify organized domains in solutions or materials. Polarized light is especially effective to analyse anisotropic samples such as biological macromolecular assemblies as they are structurally birefringent. These anisotropic samples can separate the incident light into two rays with orthogonal vibration directions and different refractive indices, named ordinary ray and extraordinary ray. The anisotropy of the bulk sample could be observed by directly placing the sample between cross polarizers, which has the advantage of revealing the anisotropy of the whole sample instead of focusing on a small local area (36).

The birefringence of peptide-HA 'string' and the eventual nanofibre alignment was examined under a polarized microscope (Olympus BX60 upright compound microscope, UK).

2.4. Animal vitreous

2.4.1. Sources and isolation of animal vitreous

Eyes of porcine (age 3-9 months) and ovine (age 3-5 months) were sourced from local slaughterhouse. Eyes were used within 3 hours after arriving at the lab. A scalpel blade was used to make an incision of the sclera midway, between the cornea and optic nerve, and then the point of the scissors was inserted into the slit to cut the sclera all the way around the ball of the eye. Vitreous were carefully removed for further characterization.

2.4.2. Morphological and rheological analysis of animal vitreous samples

2.4.2.1. Scanning electron microscopy (SEM)

Fresh vitreous were analysed by SEM following the procedures described in section 2.3.2.1 without the fixation step to avoid artefacts. Fresh vitreous were dehydrated in graded ethanol series and dried by CPD. Prior to observation, samples were coated with a gold layer.

2.4.2.2. Rheology

The mechanical properties of the vitreous samples were analysed by rheology following the procedure described in section 2.3.2.2, and using a 40 mm parallel plate (instead of 8 mm) to match the size of the vitreous.

2.5. Cell culture

2.5.1. Cell maintenance and materials sterilization

Human mesenchymal stem cells (hMSCs, passage number 4 and 5, PromoCell GmbH, Germany) were used for the cell culture studies. Cells were cultured in 75 cm^2 flasks at density of 5×10^3 cells cm^{-2} and were maintained in DMEM culture medium (Dulbecco's Modified Eagle Medium, low glucose, GlutaMAX supplement, Gibco, Thermo Fisher, UK) supplemented with 10% fetal bovine serum (FBS), 1% Penicillin-Streptomycin. Flasks were incubated at 37 °C, 5% CO_2. Medium was refreshed every three days, and cells were trypsinized when reached 80% confluency.

Sterilization of hydrogel components for cell culture was done by dissolving HA or alginate in ultrapure water, filtering the polymer solution through a 0.22 µm sterile filter, followed by lyophilization in sterile falcon tubes (TubeSpin® Bioreactors, Switzerland). Peptide powders

were sterilized by UV exposure for 15 minutes. Hydrogels were then prepared in 96-well plates under sterile environment (cell culture hood).

2.5.2. Monolayer culture

In monolayer culture experiments, PLL hydrochloride (Mw=15-30 kDa, Sigma-Aldrich, UK) was used as control of positive charged peptides. Prior to cell culture, 40 μL of aqueous solutions of peptides ((KI)$_4$K, (KI)$_5$K and (KI)$_6$K) and PLL (0.1 mg/ml and 1 mg/ml), or peptide-polyelectrolyte mixtures were cast on 96 well plate and allowed to dry overnight. For the peptide-polyelectrolyte coating, the final concentration of peptide and polyelectrolyte are 0.1 mg/mL and 0.2 mg/mL respectively. MSCs were then cultured on the coated wells at the density of 5000/cm^2.

2.5.3. Hydrogel culture

Peptide-PE hydrogels for cell culture were prepared by adding 25 μL 1 wt% or 2 wt% peptide ((KI)$_5$K or (KI)$_6$K) aqueous solution on the top of 25 μL 2 wt% HA and alginate solution in 96 well plate and incubated at room temperature overnight, followed by adding 200 μL culture media allowing for gelation of peptide-HA complex and swelling of peptide-alginate hydrogel. After 1 h, the extra liquid around the gel was removed before adding 200 μL MSCs suspension on top of the gel. 10^4 cells were seeded on each hydrogel.

Cells were also seeded on alginate hydrogels crosslinked with calcium ions (alginate-Ca), as control, and in the same way as described above. Alginate-Ca gels were made by adding 25 μL CaCl$_2$ aqueous solution (100 mM or 500 mM) on top of 25 μL alginate solution (2 wt%).

2.5.4. Cell viability and morphology

The viability of hMSCs was assessed using LIVE/DEAD Viability/Cytotoxicity Kit for mammalian cells (Invitrogen, UK). Briefly, each hydrogel sample or monolayer was treated with 4 µM calcein AM and 2 µM ethidiumhomodimer-1 and incubated for 20 min at room temperature. Stained cells on the hydrogels were imaged using confocal microscopy on day 1, 3 and 7, and cells on monolayer were observed using fluorescent microscopy (Leica DMi8) on day 7.

The morphology of cells cultured on the hydrogels was observed using both SEM and CLSM on day 7. Hydrogel samples for SEM were first fixed in 2.5% glutaraldehyde in PBS for 1 h at 5 °C, and then following the protocol steps were same as described in section 2.3.2.1. The formation of cell sphere-like aggregation was monitored by optical microscope (Leica DMIL, Germany).

F-actin staining was also conducted to observe cytoskeleton fibres of hMSCs. hMSCs on hydrogel or monolayer were washed in PBS, fixed in 4% paraformaldehyde at room temperature for 20 min and permeabilised using 0.1 wt% Trition X-100 for 20 min. They were then stained with 1:100 Alexa Fluor phalloidin (Invitrogen, UK) and 1:1000 Dapi (Invitrogen, UK) in PBS at room temperature for 40 min. Samples were then washed with PBS twice before examination by CLSM (for hydrogel sample) or fluorescent microscopy (for monolayer sample). For CLSM, 3D structure was reconstructed using Zeiss Data analysis Workstation for LSM 710.

2.5.5 Fluorescence image analysis

To quantify cell density and cell area, the confocal images of hMSCs were analysed in MATLAB R2019b based on the work by Rabbani (37) to calculate cell area and cell number, where F-actin staining area was measured and the number of nuclei was counted.

2.6. Statistical Analysis

Data are presented as mean ± standard error (SEM). Statistical differences were obtained with MATLAB R2019b software using two-tailed Student's t-tests for comparison between two experimental groups or a one-way analysis of variance (ANOVA) with a Bonferroni's multiple comparison test. ****=$p<0.0001$, ***=$p<0.0002$, **=$p<0.0021$, and *=$p<0.0332$

2.7. References

1.   Fields GB. Introduction to Peptide Synthesis. Current Protocols in Protein Science. 2001;26(1):18.1.1-.1.9.

2.   Guillier F, Orain D, Bradley M. Linkers and Cleavage Strategies in Solid-Phase Organic Synthesis and Combinatorial Chemistry. Chemical Reviews. 2000;100(6):2091-158.

3.   Al-Warhi TI, Al-Hazimi HMA, El-Faham A. Recent development in peptide coupling re-agents. Journal of Saudi Chemical Society. 2012;16(2):97-116.

4.   Sikora K, Jaśkiewicz M, Neubauer D, Migoń D, Kamysz W. The Role of Counter-Ions in Peptides—An Overview. Pharmaceuticals. 2020;13(12):442.

5.   Mant CT, Chen Y, Yan Z, Popa TV, Kovacs JM, Mills JB, et al. HPLC Analysis and Purification of Peptides. In: Fields GB, editor. Peptide Characterization and Application Protocols. Totowa, NJ: Humana Press; 2007. p. 3-55.

6.   Zhang G, Annan RS, Carr SA, Neubert TA. Overview of Peptide and Protein Analysis by Mass Spectrometry. Current Protocols in Protein Science. 2010;62(1):16.1.1-.1.30.

7.   Tang C, Smith AM, Collins RF, Ulijn RV, Saiani A. Fmoc-Diphenylalanine Self-Assembly Mechanism Induces Apparent pKa Shifts. Langmuir. 2009;25(16):9447-53.

8.   Greenfield NJ. Using circular dichroism spectra to estimate protein secondary structure. Nature Protocols. 2006;1(6):2876-90.

9.   Micsonai A, Wien F, Kernya L, Lee Y-H, Goto Y, Réfrégiers M, et al. Accurate secondary structure prediction and fold recognition for circular dichroism spectroscopy. Proceedings of the National Academy of Sciences. 2015;112(24):E3095-E103.

10.   Krebs MRH, Bromley EHC, Donald AM. The binding of thioflavin-T to amyloid fibrils: localisation and implications. Journal of Structural Biology. 2005;149(1):30-7.

11.   Xue C, Lin TY, Chang D, Guo Z. Thioflavin T as an amyloid dye: fibril quantification, optimal concentration and effect on aggregation. Royal Society Open Science. 2017;4(1):160696.

12.   Groenning M. Binding mode of Thioflavin T and other molecular probes in the context of amyloid fibrils—current status. Journal of Chemical Biology. 2010;3(1):1-18.

13.   Biancalana M, Makabe K, Koide A, Koide S. Molecular mechanism of thioflavin-T binding to the surface of beta-rich peptide self-assemblies. J Mol Biol. 2009;385(4):1052-63.

14.   Edwards-Gayle CJC, Barrett G, Roy S, Castelletto V, Seitsonen J, Ruokolainen J, et al. Selective Antibacterial Activity and Lipid Membrane Interactions of Arginine-Rich Amphiphilic Peptides. ACS Applied Bio Materials. 2020;3(2):1165-75.

15.   Amdursky N, Erez Y, Huppert D. Molecular Rotors: What Lies Behind the High Sensitivity of the Thioflavin-T Fluorescent Marker. Accounts of Chemical Research. 2012;45(9):1548-57.

16.   Shi Y, Summers PA, Kuimova MK, Azevedo HS. Unravelling the Enzymatic Degradation Mechanism of Supramolecular Peptide Nanofibers and Its Correlation with Their Internal Viscosity. Nano Letters. 2020;20(10):7375-81.

17.   Kong J, Yu S. Fourier transform infrared spectroscopic analysis of protein secondary structures. Acta Biochim Biophys Sin (Shanghai). 2007;39(8):549-59.

18.   Jackson M, Mantsch HH. The use and misuse of FTIR spectroscopy in the determination of protein structure. Crit Rev Biochem Mol Biol. 1995;30(2):95-120.

19.   Shai Y. ATR-FTIR studies in pore forming and membrane induced fusion peptides. Biochim Biophys Acta. 2013;1828(10):2306-13.

20.   Zandomeneghi G, Krebs MR, McCammon MG, Fändrich M. FTIR reveals structural differences between native beta-sheet proteins and amyloid fibrils. Protein Sci. 2004;13(12):3314-21.

21.   Shnoudeh AJ, Hamad I, Abdo RW, Qadumii L, Jaber AY, Surchi HS, et al. Chapter 15 - Synthesis, Characterization, and Applications of Metal Nanoparticles. In: Tekade RK, editor. Biomaterials and Bionanotechnology: Academic Press; 2019. p. 527-612.

22.   Ohshima H. Electrophoresis of soft particles: Analytic approximations. ELECTROPHORESIS. 2006;27(3):526-33.

23.   Ferreira DS, Marques AP, Reis RL, Azevedo HS. Hyaluronan and self-assembling peptides as building blocks to reconstruct the extracellular environment in skin tissue. Biomaterials Science. 2013;1(9):952-64.

24.   Lee KY, Mooney DJ. Alginate: Properties and biomedical applications. Progress in Polymer Science. 2012;37(1):106-26.

25.	Smeets PJM, Cho KR, Kempen RGE, Sommerdijk NAJM, De Yoreo JJ. Calcium carbonate nucleation driven by ion binding in a biomimetic matrix revealed by in situ electron microscopy. Nature Materials. 2015;14(4):394-9.

26.	Lin H-R, Wang S-H, Chiang C-C, Juang Y-C, Yu F-A, Tsai L. High strain-rate response of injectable PAA hydrogel. Journal of Biomaterials Science, Polymer Edition. 2015;26(9):534-44.

27.	Elliott JE, Macdonald M, Nie J, Bowman CN. Structure and swelling of poly(acrylic acid) hydrogels: effect of pH, ionic strength, and dilution on the crosslinked polymer structure. Polymer. 2004;45(5):1503-10.

28.	Jeong J-O, Park J-S, Kim EJ, Jeong S-I, Lee JY, Lim Y-M. Preparation of Radiation Cross-Linked Poly(Acrylic Acid) Hydrogel Containing Metronidazole with Enhanced Antibacterial Activity. International Journal of Molecular Sciences. 2020;21(1):187.

29.	Huang D, Chen Y-S, Xu Q, Hanes J, Rupenthal ID. Effects of enzymatic degradation on dynamic mechanical properties of the vitreous and intravitreal nanoparticle mobility. European Journal of Pharmaceutical Sciences. 2018;118:124-33.

30.	Xu Q, Boylan NJ, Suk JS, Wang YY, Nance EA, Yang JC, et al. Nanoparticle diffusion in, and microrheology of, the bovine vitreous ex vivo. J Control Release. 2013;167(1):76-84.

31.	Bhattacharya R, Saha S, Kostina O, Muravnik L, Mitra A. Replacing critical point drying with a low-cost chemical drying provides comparable surface image quality of glandular trichomes from leaves of Millingtonia hortensis L. f. in scanning electron micrograph. Applied Microscopy. 2020;50(1):15.

32.	Yan C, Pochan DJ. Rheological properties of peptide-based hydrogels for biomedical and other applications. Chemical Society Reviews. 2010;39(9):3528-40.

33.	Käsdorf BT, Arends F, Lieleg O. Diffusion Regulation in the Vitreous Humor. Biophys J. 2015;109(10):2171-81.

34.	Takahashi T, Ikegami-Kawai M, Okuda R, Suzuki K. A fluorimetric Morgan-Elson assay method for hyaluronidase activity. Anal Biochem. 2003;322(2):257-63.

35.	Elson LA, Morgan WT. A colorimetric method for the determination of glucosamine and chondrosamine. Biochem J. 1933;27(6):1824-8.

36.	Zhou J, Du X, Gao Y, Shi J, Xu B. Aromatic–Aromatic Interactions Enhance Interfiber Contacts for Enzymatic Formation of a Spontaneously Aligned Supramolecular Hydrogel. Journal of the American Chemical Society. 2014;136(8):2970-3.

37.	Rabbani A, Salehi S. Dynamic modeling of the formation damage and mud cake deposition using filtration theories coupled with SEM image processing. Journal of Natural Gas Science and Engineering. 2017;42:157-68.

Chapter 3

Self-assembly of cationic/hydrophobic peptides into complexes and hydrogels

3. Self-assembly of cationic/hydrophobic peptides into complexes and hydrogels

3.1. Introduction

As described in chapter I, amino acids have been gathered into innovative peptide designs to create diverse and versatile nanomaterials by self-assembly. Cationic/hydrophobic β-sheet forming peptides are very promising building blocks for the bottom-up fabrication of complex biomaterials. This class of self-assembling peptides are soluble in the water, due to the high content of polar and charged amino acids, but can self-assemble into amyloid-like nanofibers when increasing the pH or ionic strength as the peptide charges become screened. Hartgerink's group designed multidomain peptides (MDPs) with a central domain consisting of alternating hydrophilic and hydrophobic residues and positively charged termini (1). In the process of supramolecular polymerization of the MDP monomer, hydrophobic interactions act as the main driving force to shield the hydrophobic face inside the core and expose the hydrophilic face to the outside aqueous environment, while the formation of intramolecular β-sheet hydrogen bonds elongate the supramolecular MDP nanofiber. Schneider and co-workers developed β-hairpin peptides, which contain alternating hydrophobic residue valine and cationic residue lysine as well as a β-turn forming domain V^{D}PPT (2), which self-assemble into nanofiber in a similar way. Nilsson's group developed Ac-(XKXK)$_2$-NH$_2$ peptides where X is a hydrophobic or aromatic amino acid, and the self-assembly is induced with increasing ionic strengths (3). At physiological condition, multiple counterions reduced intramolecular and intermolecular electrostatic repulsion, which enables the self-assembly of multicationic β-sheet forming peptides providing opportunities for a sol-gel transition. These supramolecular peptide hydrogels have wide biomedical applications such as artificial extracellular matrix (ECM) for the encapsulation of cells (4), delivering drugs to a particular tissue through injection (5), and as antimicrobial biomaterials (6). Self-assembly behaviour of cationic/hydrophobic β-sheet forming peptides was found to be closely related to the peptide sequence, and the effect of hydrophobicity, aromaticity and terminal amino acid on the

peptide self-assembly have been explored (3, 7). However, the effect of sequence length and charge/hydrophobic ratio on the peptide β-sheet forming ability has been less clear.

The mechanical properties of the resulting hydrogels are expected to be affected by not only the peptide sequence itself (e.g. charge, length, hydrophilicity/hydrophobicity ratio), but also by the type of the electrolyte ions used to trigger gel formation. Monovalent counterions (such as Cl^-) can screen the peptide charge which makes it more likely for the nanofiber formation and entanglement, while multivalent counterions (such as phosphate) act as ionic cross-linker making stiffer hydrogels (8). Though many studies have been reported using phosphate-buffered saline (PBS) or cell culture media, which contains a variety of electrolytes, to gelate multicationic β-sheet forming peptide solutions, the use of polyelectrolytes (PEs) to induce peptide gelation has been less exploited (9). In this work, four different PEs, from synthetic and natural origin (PSS, PAA, alginate and HA), were used as trigger to induce gelation of multicationic β-sheet forming peptides [$(KI)_nK$] to obtain a hybrid hydrogel that combines the properties of both peptide and PE. These PEs, which are biocompatible and widely used in tissue engineering, carry negative charges at neutral pH, while high concentration $(KI)_nK$ peptide aqueous solution could be considered as positive charged colloid system. The viscosity and zeta potential of the PEs were analysed to investigate the effect of PE intrinsic properties on the supramolecular formation of hybrid hydrogels as well as their properties. $(KI)_nK$ is a series of peptides designed in this study having different lengths and charge density as the number of lysine (K)-Isoleucine (I) unit (n) changes (n=2-6). The self-assembly behaviour of individual $(KI)_nK$ peptides at different pHs and ionic strengths was studied as well as the effect of sequence length on the peptide β-sheet forming propensity and the formation of supramolecular hybrid hydrogels. The formation of supramolecular peptide-PE system was then studied in both salt-free and PBS environment, and their microstructure as well as mechanical properties were investigated for potential biomedical applications.

3.2. Cationic/hydrophobic self-assembling peptides $(KI)_nK$

$(KI)_nK$ peptides possess varying number of a repeating unit containing alternating hydrophilic cationic residue lysine (K) and hydrophobic residue isoleucine (I). Increasing the number of repeating unit (n) is expected to generate peptides with stronger driving forces for β-sheet formation, but as the number of charges also increases, it will favour repulsive forces preventing their self-assembly. Therefore, studying how these two counteracting forces affect the self-assembly of $(KI)_nK$ can reveal new insights to design self-assembling biomaterials with innovative properties. In this study, five peptides $(KI)_2K$, $(KI)_3K$, $(KI)_4K$, $(KI)_5K$ and $(KI)_6K$ were synthesised and their self-assembly behaviour investigated under different environmental conditions.

3.2.1. Confirmation of peptide mass and purity

The $(KI)_nK$ peptides were synthesized and purified, whose molecular masses were confirmed by ESI-MS, and their purity was analysed by analytical HPLC (**Figure 3.1**). For example, the expected mass of $(KI)_2K$ peptide was calculated to be 669.49 (**Table 3.1**) and its mass spectrum (**Figure 3.1**) shows peaks at 670.86 m/z, 336.20 m/z and 224.41 m/z, corresponding to $[M+H]^+$, $[M+2H]^{2+}$ and $[M+3H]^{3+}$, respectively. Analytical HPLC shows a quite pure product with purity calculated as 95%. The same analysis was performed for the other peptides and a summary of this analysis is given in Table 3.1.

Table 3.1: *Characterization of the peptides synthesized and purified in this work.*

Peptide	Chemical formula	Expected mass (g/mol)	Observed mass (g/mol)	Purity (%)	Retention time (min)
$(KI)_2K$	$C_{32}H_{63}N_9O_6$	669.49	670.86 $[M+H]^+$ 336.20 $[M+2H]^{2+}$ 224.41 $[M+3H]^{3+}$	95	7.5
$(KI)_3K$	$C_{44}H_{86}N_{12}O_8$	910.67	912.21 $[M+H]^+$ 456.83 $[M+2H]^{2+}$ 304.98 $[M+3H]^{3+}$	94	8.5
$(KI)_4K$	$C_{56}H_{109}N_{15}O_{10}$	1152.58	577.49 $[M+2H]^{2+}$ 385.45 $[M+3H]^{3+}$ 289.26 $[M+4H]^{4+}$	99	9.0
$(KI)_5K$	$C_{68}H_{132}N_{18}O_{12}$	1393.92	349.68 $[M+3H]^{3+}$ 465.91 $[M+4H]^{4+}$	97	9.5
$(KI)_6K$	$C_{80}H_{155}N_{21}O_{14}$	1634.21	546.32 $[M+3H]^{3+}$ 410.11 $[M+4H]^{4+}$ 328.20 $[M+5H]^{5+}$	98	9.9
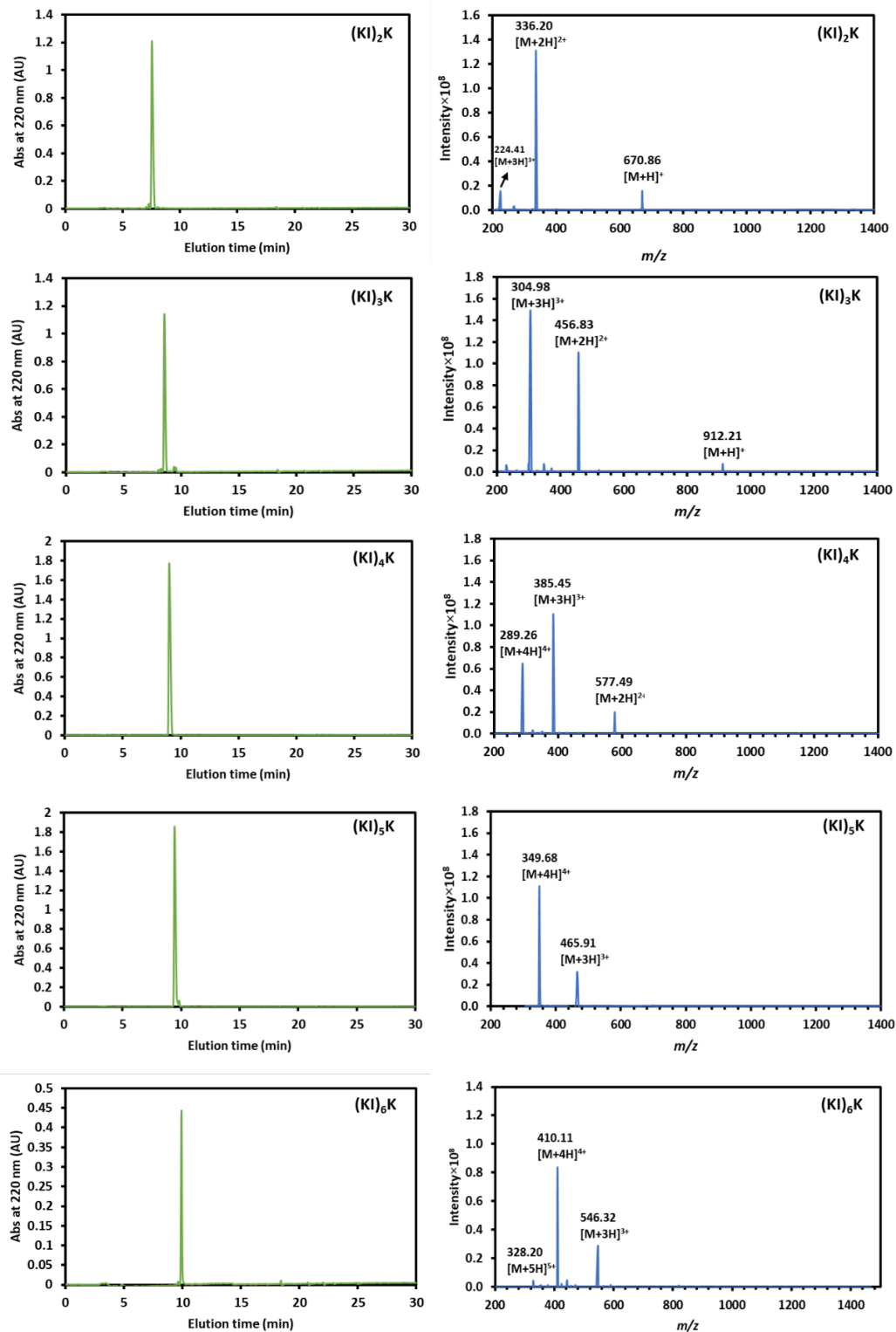
Figure 3.1: *Analytical RP-HPLC traces and ESI mass spectra of purified (KI)ₙK peptides.*

103

3.2.2. pH as a trigger for the self-assembly of cationic/hydrophobic peptides

Cationic (KI)$_n$K peptides could self-assemble into amyloid-like nanofiber with increasing pH as the peptide charges are neutralized. The pH-dependence of peptide self-assembly can be estimated based on the theoretical pK_a of containing amino acids. However, different microenvironments can lead to a shift in the theoretical pK_a(10). The ionic groups in t (KI)$_n$K peptides are on the side chain of lysine residues, whose theoretical pK_a is 10.53. Therefore, it is assumed that the peptide self-assembly is not favoured at pH below 10.53 due to electrostatic repulsion. Interestingly, the titration curves (**Figure 3.2**) suggest that longer peptides showed increased pK_a shifts. The titration curve of (KI)$_2$K showed a reduced pH change at around pH 10.5, indicating a transition at this pH, in good agreement with the theoretical pK_a value, while in (KI)$_3$K and (KI)$_4$K 'plateau' with less pH change were observed below their theoretical pK_a, where the pK_a-like transition for (KI)$_3$K was at around pH 10.1 and at pH 9.7 for (KI)$_4$K. (KI)$_5$K and (KI)$_6$K exhibited greater pK_a shifts towards lower pH as pK_a-like transitions were found to be at pH 9.1 and 8.8, respectively. In (KI)$_n$K peptides, the proximity of hydrophobic residue (I) and hydrophilic charged residue (K) promotes hydration competition between them, which results in the elevated apolar-polar repulsive free energy of hydration inducing the pK_a shift (11). It is noticeable that the ratio of hydrophobic residue to the total amino acid number in (KI)$_2$K, (KI)$_3$K, (KI)$_4$K, (KI)$_5$K and (KI)$_6$K peptides are 0.40, 0.43, 0.44, 0.45 and 0.46, respectively. Thus, the overall peptide hydrophobicity is expected to increase as the number of the repeating unit (n) becomes higher, also confirmed by the RP-HPLC profiles (**Figure 3.1**) where longer (KI)$_n$K peptides show increased retention times. Since the greater peptide pK_a shift is expected to be found in a more hydrophobic background (10, 11), it is suggested that the lower pK_a of longer (KI)$_n$K peptides might be ascribed to its increased hydrophobicity.
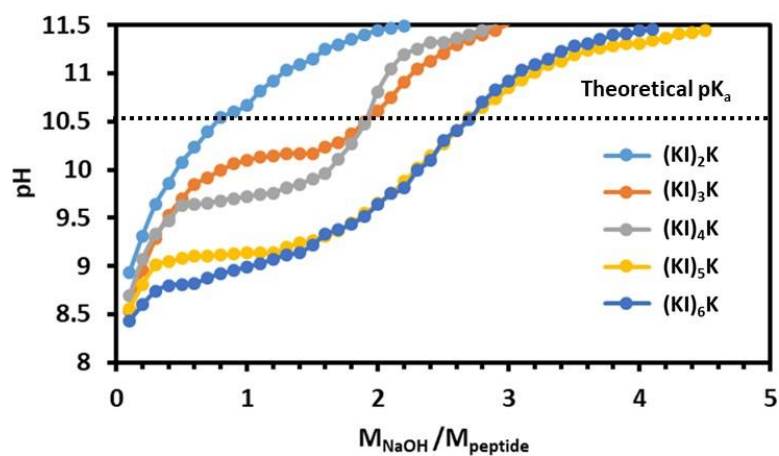
Figure 3.2: *The titration curves of (KI)$_n$K peptides (1 mM) determining their pK$_a$.*

The effect of pH on peptide self-assembly was further investigated by measuring the zeta potential of peptide aqueous solutions at different pHs (**Figure 3.3**). (KI)$_2$K and (KI)$_3$K peptides had a very low absolute zeta potential at pH 7-8.5, which might suggest the peptide molecules were not aggregating and remained as monomers in these conditions. While (KI)$_4$K shows small positive zeta potential of 4.2 ± 0.8 mV at neutral pH, suggesting minimal self-assembly, the zeta potential increases to 29.8 ± 0.6 mV once pH reached 8 due to peptide aggregation. The higher zeta potential values of (KI)$_5$K (26.9 ± 1.9 mV) and (KI)$_6$K (36.5 ± 1.5 mV) indicates relatively stable peptide colloids with high number of positive charges at neutral pH. Zeta potential of each peptide declines at the pH is close to their individual pK_a, showing the deprotonation of $-NH_3^+$ on the lysine side chain, and continuously decreases when the pH was risen to 11, in which amino groups become deprotonated (neutral). Generally, the longer (KI)$_n$K peptide is likely to have higher positive zeta potential, consistent with the higher number of lysine residues in the sequence.
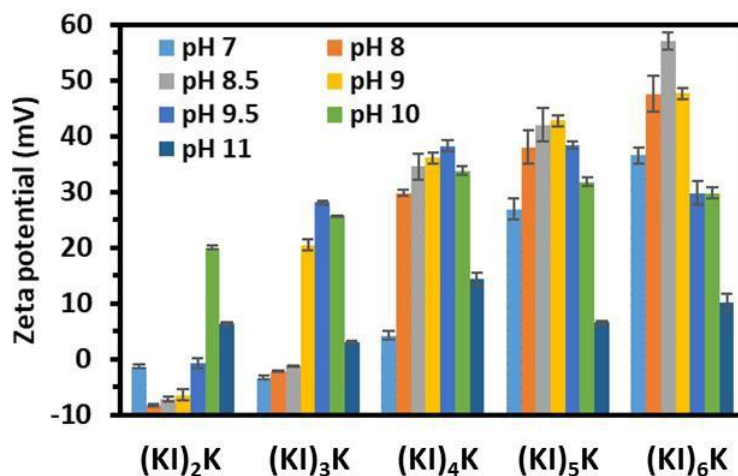
Figure 3.3: *Zeta potential of (KI)ₙK peptides (1 mM) at varied pHs. Standard deviation is indicated by error bars and measurements were performed in triplicate.*

The secondary structures of $(KI)_nK$ peptides with pH change were then evaluated by CD (**Figure 3.4**). The CD spectra of $(KI)_2K$ (pK_a ~ 10.5) and $(KI)_3K$ (pK_a ~ 10.1) displayed a characteristic profile of random coils with negative band at 195 nm at pH 7, 9, 9.5 and 10. However when pH increased to 11, over the pK_a of both peptides, $(KI)_2K$ showed the weak negative bands at both 199 and 216 nm, indicating mixture of random coil and β-sheet structures (12), and $(KI)_3K$ had a maximum at 194 nm and a minimum at 216 nm corresponding to a dominant β-sheet structure. $(KI)_4K$ (pK_a ~ 9.7) mainly shows a secondary structure of random coils at pH 7, 9 and 9.5 and a typical β-sheet conformation at pH 11, while a mixture of α-helix and β-sheet conformation was observed at pH 10 with a positive band at 194 nm and a broad minimum at around 210 nm (13), which may reflect an unstable state occurring during the structural transition from random coils to β-sheets. $(KI)_5K$ (pK_a ~ 9.1) has a random coil structure at pH 7 and 9 and changes to β-sheet at pH 9.5 and above, while $(KI)_6K$ (pK_a ~ 8.8) is only disordered at neutral pH and shows the intermediate stage of β-sheet formation at pH 9 and 9.5. At pH 10 and 11, $(KI)_6K$ finally adopts a well-defineβ-sheet conformation. Generally, CD spectra observed for $(KI)_nK$ peptides show they are as random

coil structures at pHs below their individual pK_a and gradually formed a β-sheet structure when the pH is increased, where the conformation transition is observed at around their pK_a. $(KI)_nK$ peptides can form β-sheet structures at basic pH due to the reduced intermolecular electrostatic repulsion, encouraging the self-assembly, and longer $(KI)_nK$ peptides form β-sheet structures at relative lower pHs corresponding to the pK_a value.
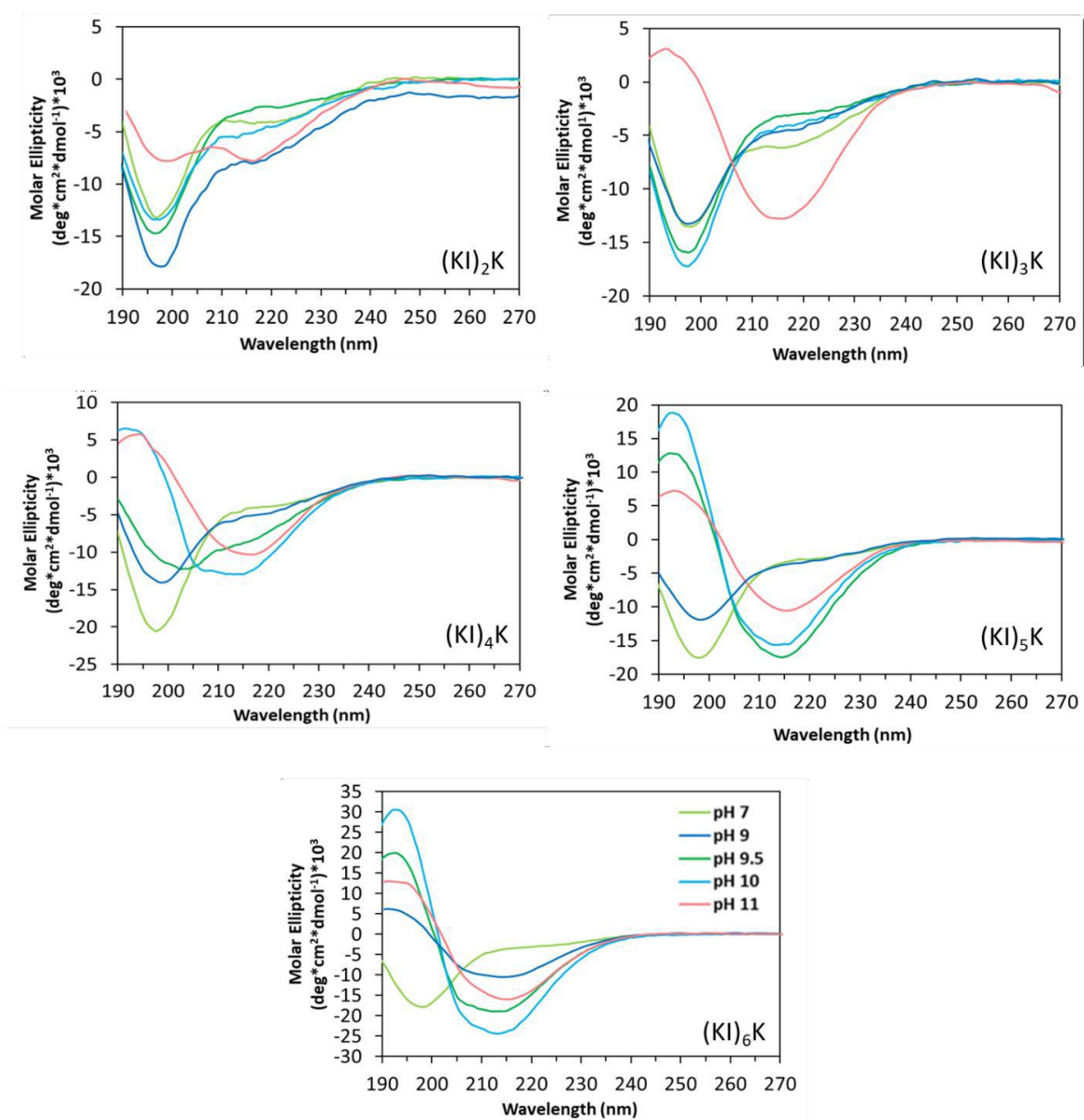
Figure 3.4: CD spectra of $(KI)_nK$ peptides (0.1 mM) at pHs 7, 9, 9.5, 10 and 11.

FTIR was also used to study the secondary structure of peptides at both neutral and basic pHs (**Figure 3.5**), where peptides present an absorbance signal at 1673 cm^{-1} from residual TFA after HPLC purification (14). At pH 11, all peptides exhibited apparent amide I absorbance region at 1616-1620 cm^{-1} indicating β-sheet formation. At neutral condition (pH 7) no peak was assigned to β-sheet, indicating the minimal self-assembly.
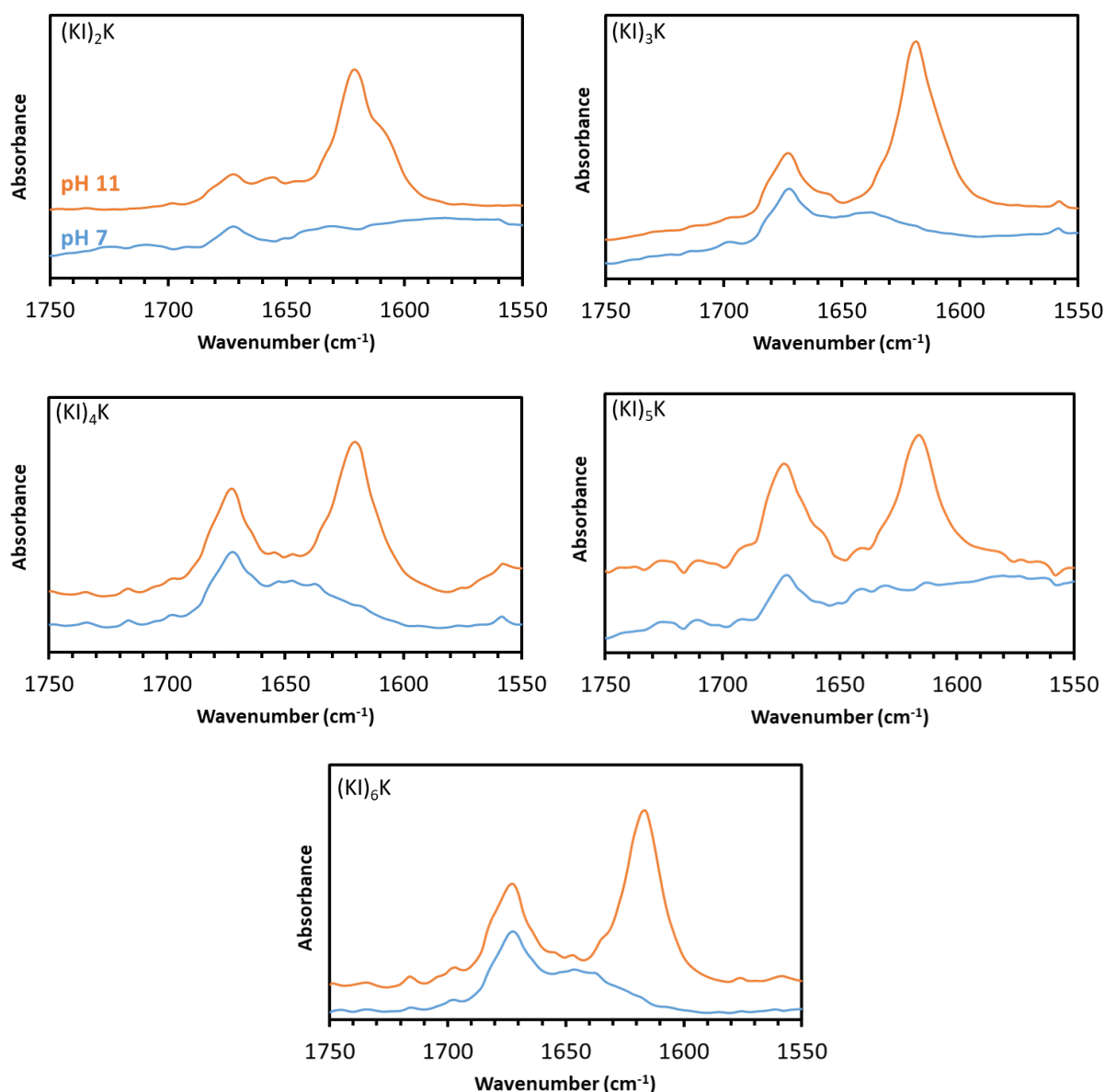
Figure 3.5: *FTIR spectra of (KI)$_n$K peptides (10 mM) at pHs 7 and 11.*

TEM was used to confirm the morphology of peptide supramolecular assemblies at basic condition (pH 11, **Figure 3.6**). $(KI)_2K$ peptide forms very thin fibrils which are difficult to distinguish from each other (being challenging for quantification) due to the limited β-sheet forming capability. The quantification of diameter of $(KI)_3K$, $(KI)_4K$, $(KI)_5K$ and $(KI)_6K$ fibrils is given as well. $(KI)_3K$ and $(KI)_4K$ formed long and twisted fibres with an average width of 12.4 ± 3.0 nm and 7.6 ±3.0 nm, respectively, which appears to be bundles of smaller fibrils. Entangled long nanofibrils could also be found in $(KI)_5K$, while $(KI)_6K$ only assembled into short worm-like fibril structures. The average fibril diameter of $(KI)_5K$ and $(KI)_6K$ dramatically decreased to 4.3 ± 0.8 nm and 4.6 ± 1.0 nm, which is consistent with the estimated length of linear peptide chain (the length of one amino acid is 0.35 nm). The fibril bundling effect is less evident as the peptide length increases, probably due to the stronger repulsive interactions, as longer peptides carry more charged residues (3).

The mechanical properties of supramolecular peptide assemblies were assessed by measuring the viscoelasticity of peptide solutions at pH 11 (**Figure 3.7**). All peptides displayed much larger G' than G'' independent of frequency, indicating the formation of peptide hydrogel, where $(KI)_3K$ hydrogel is the most rigid one, with G' close to 2 kPa, followed by $(KI)_4K$ and $(KI)_5K$ exhibiting G' around 1 kPa, while $(KI)_2K$ and $(KI)_6K$ gels are the weakest, whose G' are only around 0.8 kPa. $(KI)_3K$, $(KI)_4K$ and $(KI)_5K$ gels are relatively stronger probably because they formed longer fibrils (**Figure 3.6**) leading to the enhanced fibril entanglement.
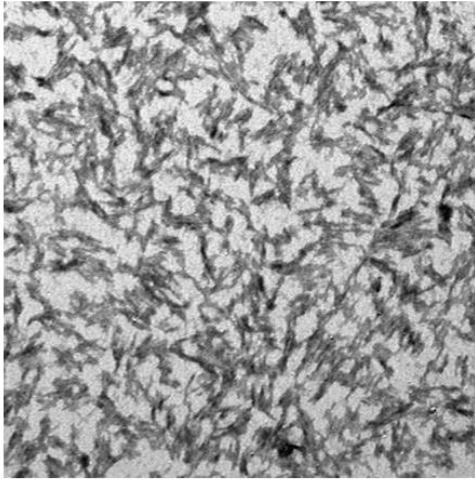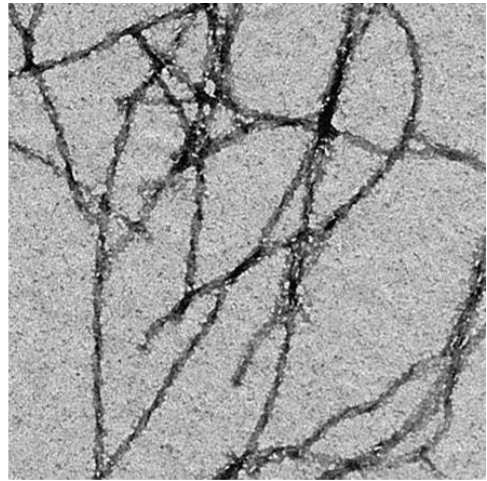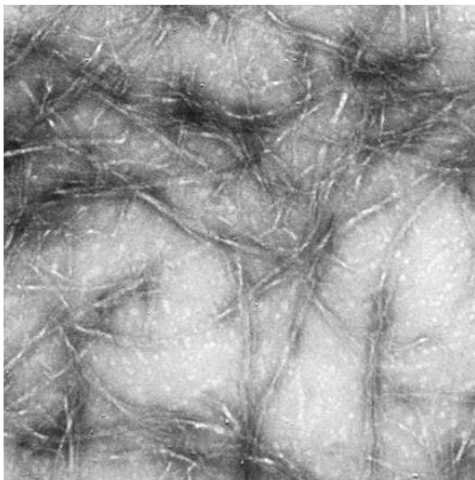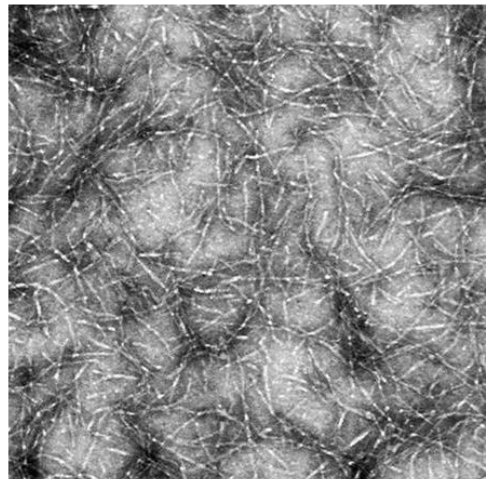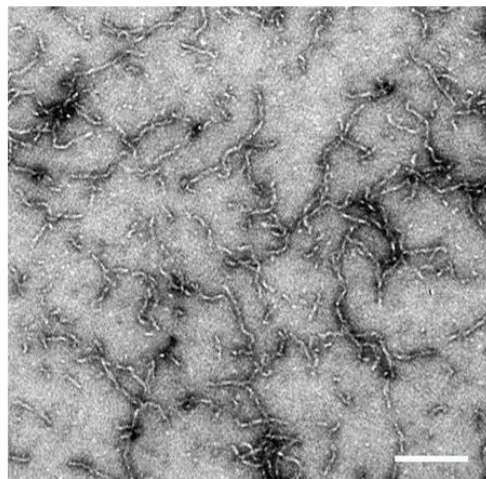
Figure 3.6: *TEM micrographs of (A) (KI)$_2$K, (B) (KI)$_3$K, (C) (KI)$_4$K, (D) (KI)$_5$K and (E) (KI)$_6$K peptides (1 mM) at pH 11. Scale bar=100 nm.*
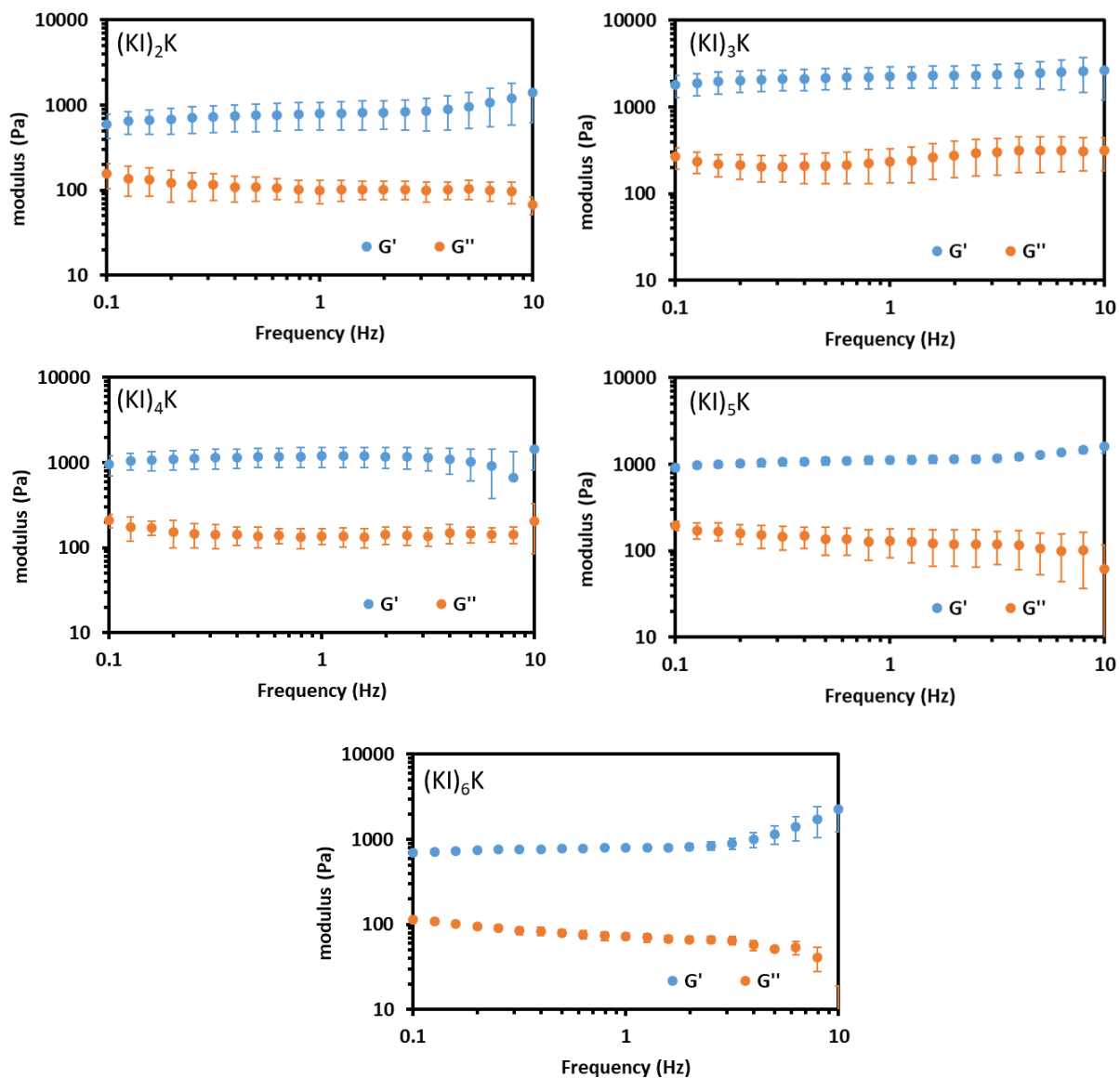
Figure 3.7: *Rheology analysis of (KI)ₙK (1 mM) at pH 11. Standard deviation is indicated by error bars and measurements were performed in triplicate.*

ThT is a commonly used probe to monitor *in vitro* amyloid fibril formation which shows a strong fluorescence signal when bound to β-sheet structures and once excited at 480 nm. The self-assembly of peptides was investigated across a gradient of concentrations using the ThT

assay (**Figure 3.8**). At pH 7, all peptides did not show strong fluorescent signal in all concentrations (0.0075 mM-1 mM). When the pH increases to 11, the ThT fluorescent signals of $(KI)_2K$ and $(KI)_6K$ remains relatively low, revealing weak β-sheet formation. $(KI)_3K$, $(KI)_4K$ and $(KI)_5K$ peptides show significant fluorescent signal intensity increase at pH 11, while $(KI)_4K$ has the strongest fluorescent signal. It is known that fluorescence intensity of ThT correlates linearly with amyloid fibril concentration (15). However, $(KI)_4K$ does not show significantly larger fibril size in the TEM images or much more rigid structures in the rheology measurements compared to other peptides. A recent study has shown that the electrostatic interactions between ThT and amyloid fibrils could affect the ThT binding to β-sheet domains, as the repulsion between positive charge of ThT and cationic amyloid fibrils could inhibit ThT binding (16). Therefore, the binding between ThT and $(KI)_nK$ peptides might be reduced by electrostatic repulsion, especially for longer peptide $(KI)_5K$ and $(KI)_6K$ which carry more positive charges.
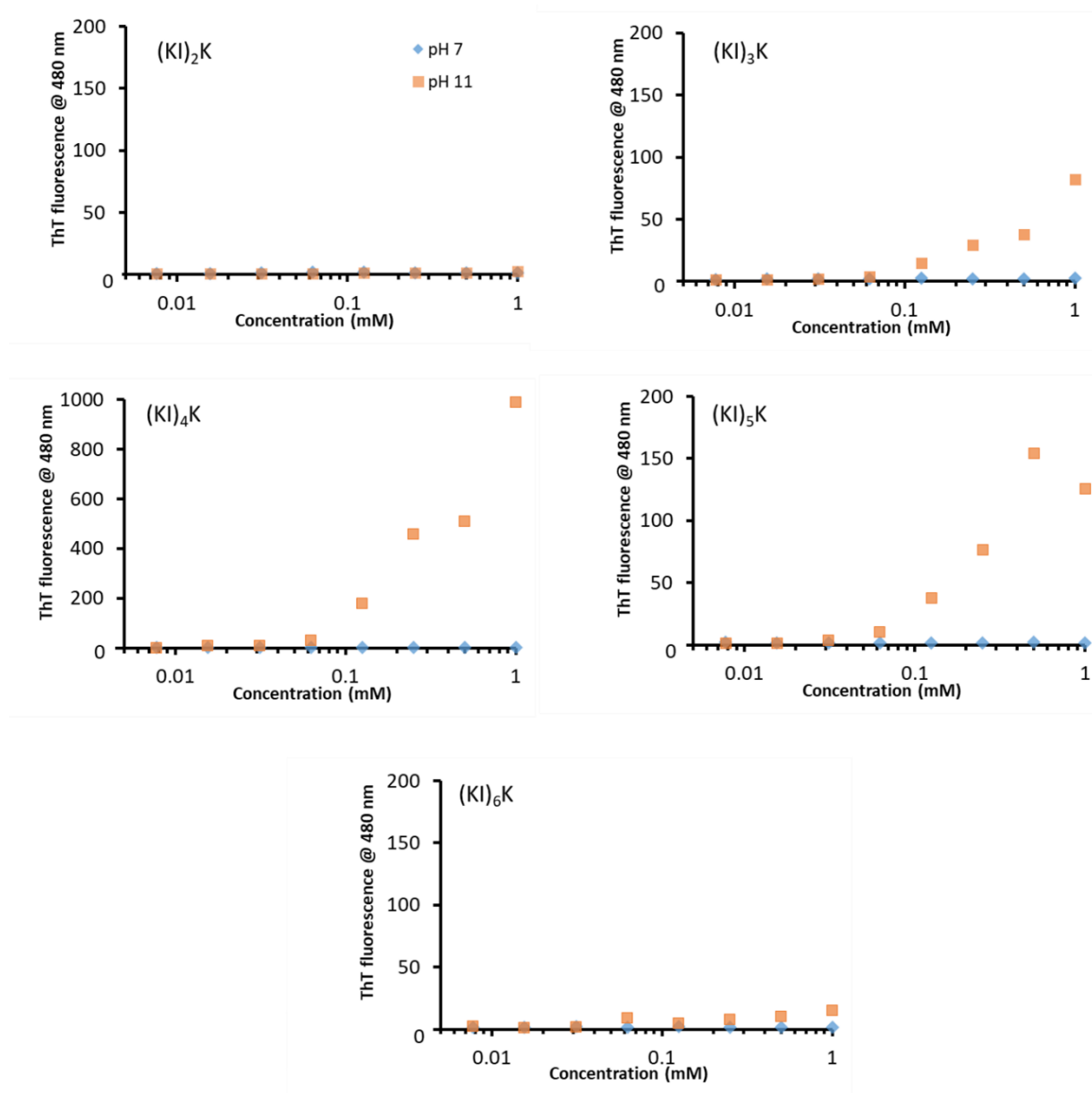
Figure 3.8: ThT assay showing the binding between $(KI)_nK$ peptides (1 mM) and ThT at pHs 7 and 11.

3.2.3. Ionic strength as a trigger for the self-assembly of cationic/hydrophobic peptides

Increasing ionic strength can also lead to peptide self-assembly as the presence of counterions can shield the positive charges on the side chain of lysine residues. In this study, both monovalent counterions (Cl^-) and multivalent (HPO_4^{2-}) counterions were used to regulate the ionic strength. Peptide solutions with increasing concentrations of NaCl were analysed by FTIR to assess the minimal concentration of monovalent counterions required to trigger the peptide self-assembly (**Figure 3.9**). Peptide solutions present absorbance signal at 1673 cm^{-1} in the FTIR spectra, from residual TFA after HPLC purification. $(KI)_2K$ showed no evident β-sheet formation with increased NaCl concentration up to 400 mM, and self-assembly was also disfavoured for $(KI)_3K$ at low NaCl concentration below 300 mM. However, an amide I stretch at 1616 cm^{-1} was observed at 400 mM NaCl for $(KI)_3K$, which is the typical absorbance region of β-sheet in amyloid fibrils (17). NaCl promotes $(KI)_4K$, $(KI)_5K$ and $(KI)_6K$ peptides to form β-sheet structures as amide I absorbance bands at 1614 cm^{-1}-1618 cm^{-1} were found, and the minimal NaCl concentration required for the β-sheet assembly for $(KI)_4K$, $(KI)_5K$ and $(KI)_6K$ is 300, 100 and 50 mM, respectively. It is known that the β-sheet propensity of ionic self-complementary peptides increases with the peptide hydrophobicity and the number of repeating hydrophilic-hydrophobic residue units (3, 18). The enhanced hydrophobicity, as well as the extended sequence length, can trigger a β-sheet assembly of $(KI)_nK$ peptides at lower ionic strength in a synergistic effect, even if longer $(KI)_nK$ would carry more like-charges.
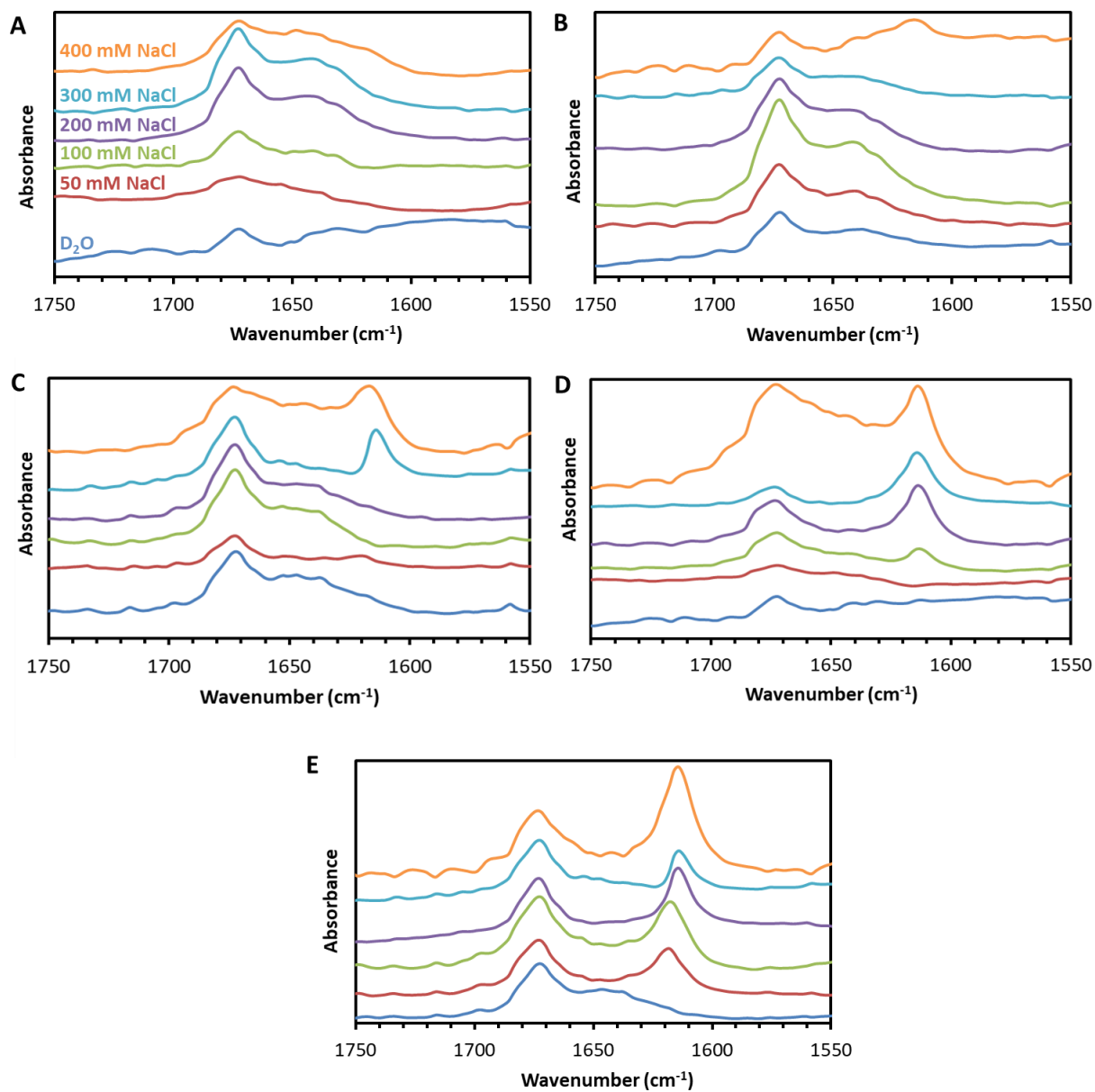
Figure 3.9: FTIR spectra of (A) $(KI)_2K$, (B) $(KI)_3K$, (C) $(KI)_4K$, (D) $(KI)_5K$ and (E) $(KI)_6K$ peptide solutions (10 mM) with different NaCl concentrations.

Among all $(KI)_nK$ peptides, $(KI)_3K$, $(KI)_4K$ and $(KI)_5K$ is expected to self-assemble into long fibrils and forming a relatively stiff network when charges are screened, while $(KI)_4K$ and $(KI)_5K$ peptides require less counterions to achieve β-sheet formation. Therefore, $(KI)_4K$ and $(KI)_5K$ were chosen to fabricate supramolecular peptide-electrolyte hydrogel with the addition of

NaCl and Na_2HPO_4 whose microstructures were examined by SEM. $(KI)_4K$ and $(KI)_5K$ hydrogels formed by high NaCl concentration (800 mM) were found to have a dense structure, consisting of entangled thin fibrils (**Figure 3.10**). Hydrogels formed in the presence of Na_2HPO_4 (50 mM) have a relatively looser fibrous structure, and the fibrils appeared to be thicker compared to NaCl-induced hydrogel, probably because of the fibril bundling. HPO_4^{2-} are multivalent counterions considered as an ionic cross-linkers to provide patches of negative charges once interacting with positive charged peptides, where the strong electrostatic interactions might encourage the fibril bundling. No evident differences are observed between $(KI)_4K$ and $(KI)_5K$ hydrogels induced by the same type of electrolyte.
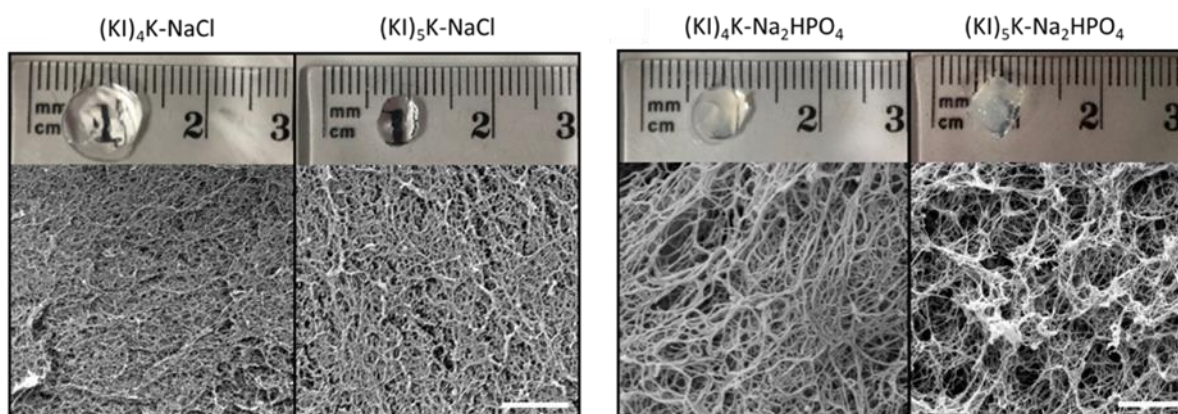
Figure 3.10: The digital and SEM images showing transparent NaCl-triggered peptide hydrogels with homogeneous microstructure and Na_2HPO_4-triggered peptide hydrogels with reduced transparency and a more porous structure. Scale bar= 2 μm.

3.3. Supramolecular peptide-polymer hybrid hydrogel

To further exploit hydrogel formation in presence of polyelectrolytes (PEs), different anionic PEs, including alginate, HA, PSS and PAA, were used to trigger the self-assembly of $(KI)_nK$, peptides. Four PEs and five peptides ($(KI)_2K$, $(KI)_3K$, $(KI)_4K$, $(KI)_5K$ and $(KI)_6K$), and their combinations, were investigated resulting in 20 different peptide-PE combinations, which were studied in both salt-free (ultrapure water) and PBS condition. The results on the

formation of gels can be found in **Table 3.2**. (KI)$_2$K peptide was not able to form a hybrid hydrogel with any of the PEs because of its limited self-assembly capacity. Longer peptides, especially (KI)$_5$K and (KI)$_6$K, were more likely to form hydrogel with PEs, probably due to a stronger β-sheet formation propensity.

Table 3.2: *Hydrogel formation of peptide-PE self-assembling system in salt-free (water) and PBS environment.*

Peptide in water	Polyelectrolyte							
	PSS		PAA		Alginate		HA	
	In water	In PBS	In water	In PBS	In water	In PBS	In water	In PBS
(KI)$_2$K	No gel	No gel	No gel	No gel	No gel	No gel	No gel	No gel
(KI)$_3$K	No gel	No gel	No gel	No gel	Gel	Gel	No gel	No gel
(KI)$_4$K	No gel	Gel	No gel	Gel	Gel	Gel	No gel	Gel
(KI)$_5$K	No gel	Gel	Gel	Gel	Gel	Gel	Gel	Gel
(KI)$_6$K	No gel	Gel	Gel	Gel	Gel	Gel	Gel	Gel

Legend: Red = No gel formed; Green = Gel formed.

3.3.1. Anionic polyelectrolytes

In the supramolecular peptide-PE system, the viscosity and charge of PE solutions can play an important role in mediating the self-assembly process. For example, the high viscosity of PE can slow down the mixing process and limit the self-assembly at the interface of both solutions (19). The viscosity of HA, alginate, PSS and PAA solutions was determined by rheometry in presence and absence of electrolytes (**Figure 3.11**).

Alginate, HA and PAA in water and PBS exhibited shear viscosity behaviour, typical of many polymer solutions. For alginate solutions, a Newtonian plateau is observed at low shear rates followed by a region of shear thinning at higher shear rates, where the zero-shear rate viscosity was at 1.84 Pa·s for polymer solution in water and 0.76 Pa·s for PBS solution. For HA

and PAA solutions, there was no visible plateau within the observed shear rate range, and the viscosity was continuously decreasing as shear rate increased. However, the viscosity measurements of PSS solutions showed considerable noise without the apparent shear-thinning behaviour, probably because the viscosity of PSS is very low, and the data collected from the rheometer is less accurate.
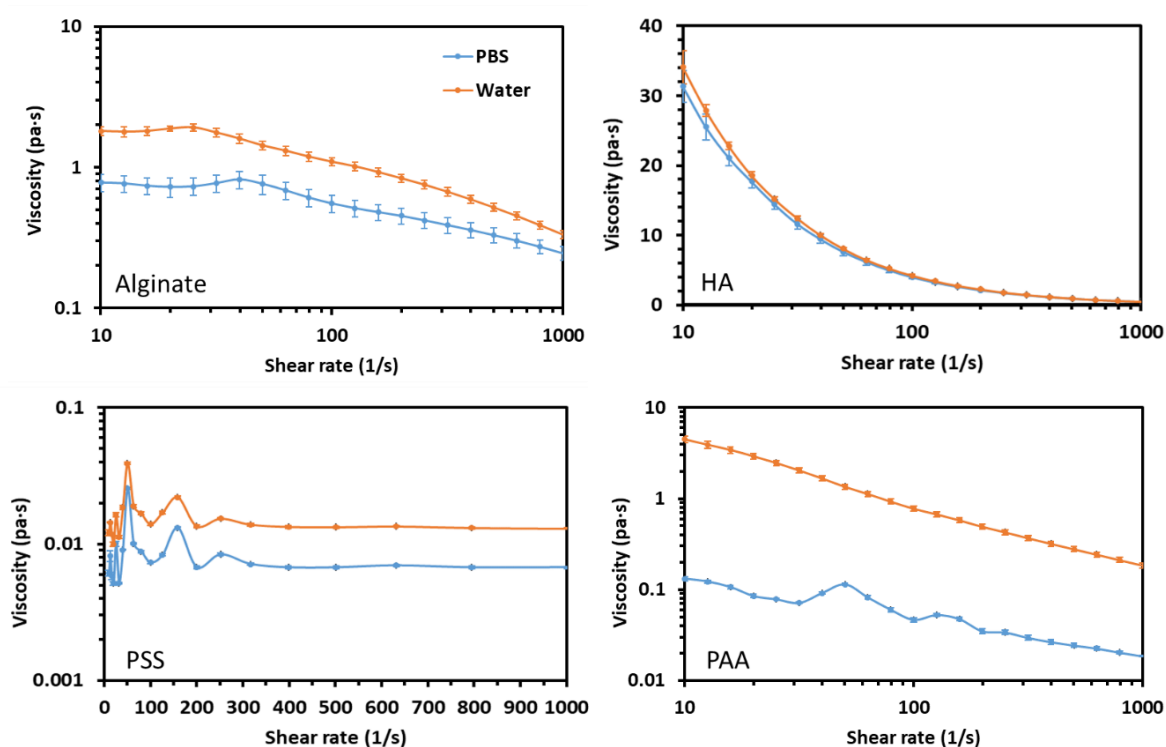
Figure 3.11: *Viscosity as a function of shear rate for PE solutions with concentration of 2 wt% in PBS or water at room temperature. Standard deviation is indicated by error bars and measurements were performed in triplicate.*

The viscosity of PEs in PBS is lower than salt-free PE solution. In salt free solution, like charges along the PE produce strong Coulombic repulsions, which lead to the PE backbone to stretch and elongate. The addition of counterions screens the Coulombic repulsion so the PE conformation can change, where the chain can fold up to form a smaller and more compact

118

conformation leading to viscosity reduction in the dilute and semi-dilute concentration regimes (20). For PAA, precipitates were observed once the polyelectrolyte is dissolved in PBS which may contributed to the decrease viscosity.

The viscosity of PEs has a great impact on the peptide-PE self-assembling system. In this work, HA (in water and PBS), alginate (in water and PBS) and PAA (in water) were considered as highly viscous solutions, while PSS (in water and PBS) and PAA (in PBS) showed low viscosity. Since the peptide solution also had the viscosity close to water, they were miscible with PE solution with low viscosity.

3.3.2. Supramolecular (KI)$_n$K-alginate complex

The most used physical alginate hydrogel is Ca^{2+}-alginate system, as divalent cations can easily ionically crosslink the alginate to form the hydrogel which has wide biological applications. In the supramolecular (KI)$_n$K-alginate hydrogel system, it is assumed that alginate can screen the positive charges on the side chain of (KI)$_n$K and their self-assembly will enable the network formation. The (KI)$_3$K, (KI)$_4$K, (KI)$_5$K and (KI)$_6$K peptides are able to form hydrogels with alginate (**Figure 3.12**) in the salt-free environment (referred as (KI)$_n$K-alginate). Alginate could form hydrogel with four (KI)$_n$K peptides, while other PEs would only form hydrogels with two or three peptides, probably because alginate solution has the strongest negative zeta potential. All (KI)$_n$K-alginate hydrogels have nanofibrous structure, which is similar to Ca^{2+}-alginate hydrogel, though the network density in (KI)$_n$K-alginate is more loose compared to Ca^{2+}-alginate hydrogel. It is hypothesized that Ca^{2+} can easily diffuse, due to its small size, promote rapid crosslink and leading to a more homogeneous structure, while in (KI)$_n$K-alginate system the diffusion of (KI)$_n$K in the alginate solution might be prevented by the peptide self-assembly. In fact, it was also observed that Ca^{2+}-alginate hydrogels form faster than peptide-alginate ones.
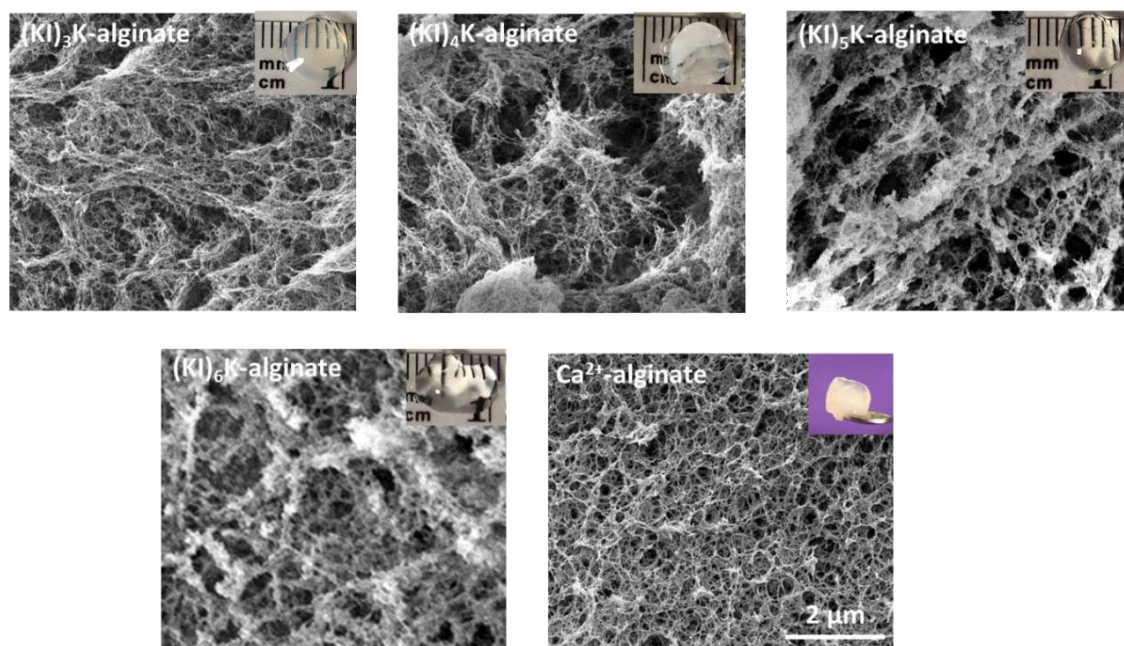
Figure 3.12: *The digital and SEM images of (KI)$_n$K-alginate hydrogels formed in salt-free (ultrapure water) environment. Ca^{2+}-alginate hydrogel was made of alginate solution and 0.5 M CaCl$_2$.*

Although there are not evident differences in the microstructures of (KI)$_n$K-alginate hydrogels, difference in mechanical properties were observed (**Figure 3.13**). G' is larger than G'' for all hydrogels, within the observed frequency, indicating the gel status, where (KI)$_4$K-alginate hydrogel has the largest G' (~20 kPa) followed by (KI)$_5$K-alginate hydrogel with G' around 5 kPa. (KI)$_3$K-alginate hydrogel is relatively weaker, with G' only around 1 kPa while G' increases as frequency is becoming higher (at high frequency range). Since shorter (KI)$_n$K peptides have lower β-sheet formation propensity, it is possible that in (KI)$_3$K-alginate hydrogel the peptide is not fully in the assembled state. G' of (KI)$_6$K-alginate is the lowest probably because (KI)$_6$K is only able to self-assemble into short fibril compromising the mechanical properties.
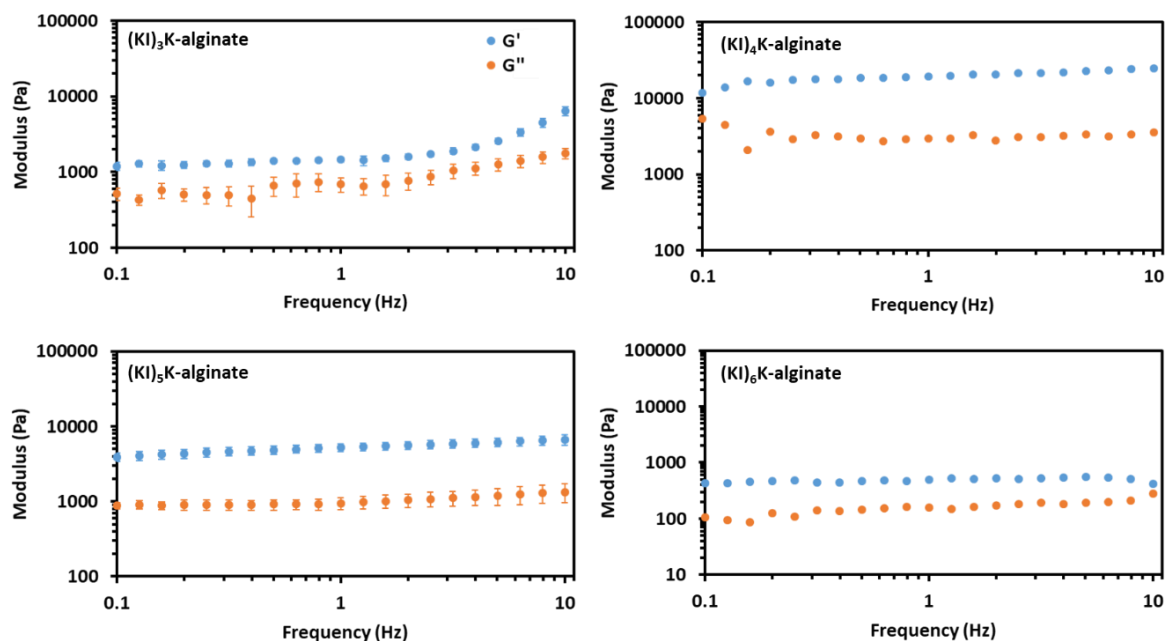
Figure 3.13: *Rheology analysis of (KI)$_n$K-alginate hydrogels formed in salt-free (ultrapure water) environment. Standard deviation is indicated by error bars and measurements were performed in triplicate.*

The supramolecular (KI)$_n$K-alginate system in PBS ((KI)$_n$K-alginate-PBS) was also investigated, where alginate was first dissolved in PBS and then the peptide solution in water was added. The microstructure of (KI)$_n$K-alginate-PBS hydrogels revealed by SEM shows fibrils which tend to be thicker and longer, and PBS is assumed to further screen the charges of peptides and encourage the fibril bundling and elongation (**Figure 3.14**), which might explain the increase of G' in (KI)$_3$K-alginate-PBS, (KI)$_5$K-alginate-PBS and (KI)$_6$K-alginate-PBS compared to the peptide-alginate hydrogel formed in the salt-free environment (**Figure 3.15**). (KI)$_6$K-alginate-PBS and (KI)$_5$K-alginate-PBS hydrogels were found to be the most rigid, followed by (KI)$_4$K-alginate-PBS and (KI)$_3$K-alginate-PBS, which is in good agreement with microstructures shown in SEM images where fibrils in (KI)$_4$K-alginate-PBS and (KI)$_3$K-alginate-PBS appeared to be thinner and shorter. (KI)$_3$K-alginate-PBS, (KI)$_4$K-alginate-PBS and (KI)$_5$K-alginate-PBS hydrogels have a relatively homogeneous cross-section, while (KI)$_6$K-alginate-PBS was found to have

121

overlapped fibrous layers. Generally, $(KI)_nK$-alginate-PBS hydrogels have a denser network structure than $(KI)_nK$-alginate, probably due to alginate dissolved in PBS reducing the viscosity thus promoting the diffusion between peptide and alginate solution.
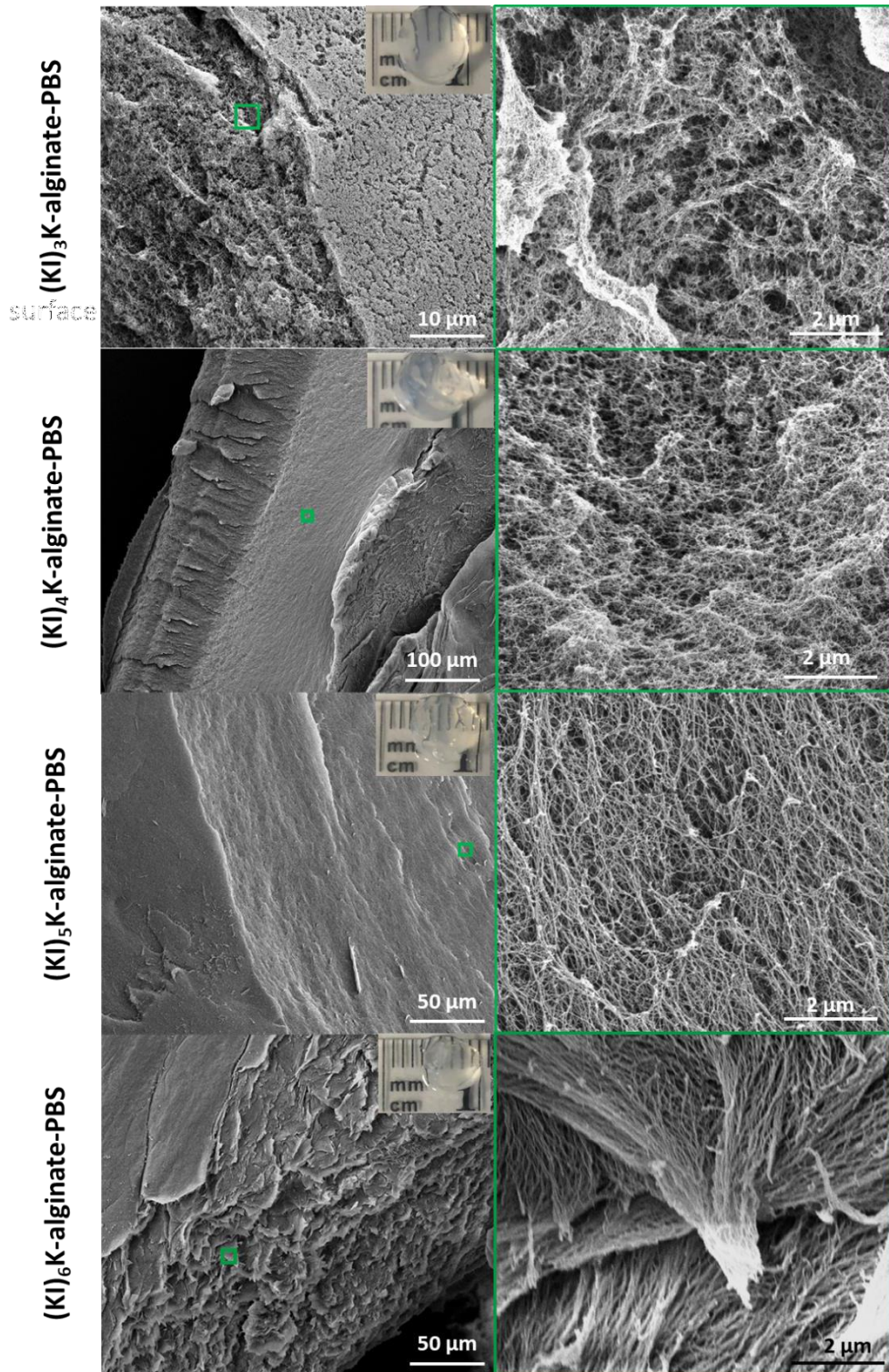
Figure 3.14: The digital and SEM cross-section images of (KI)$_n$K-alginate-PBS hydrogels.
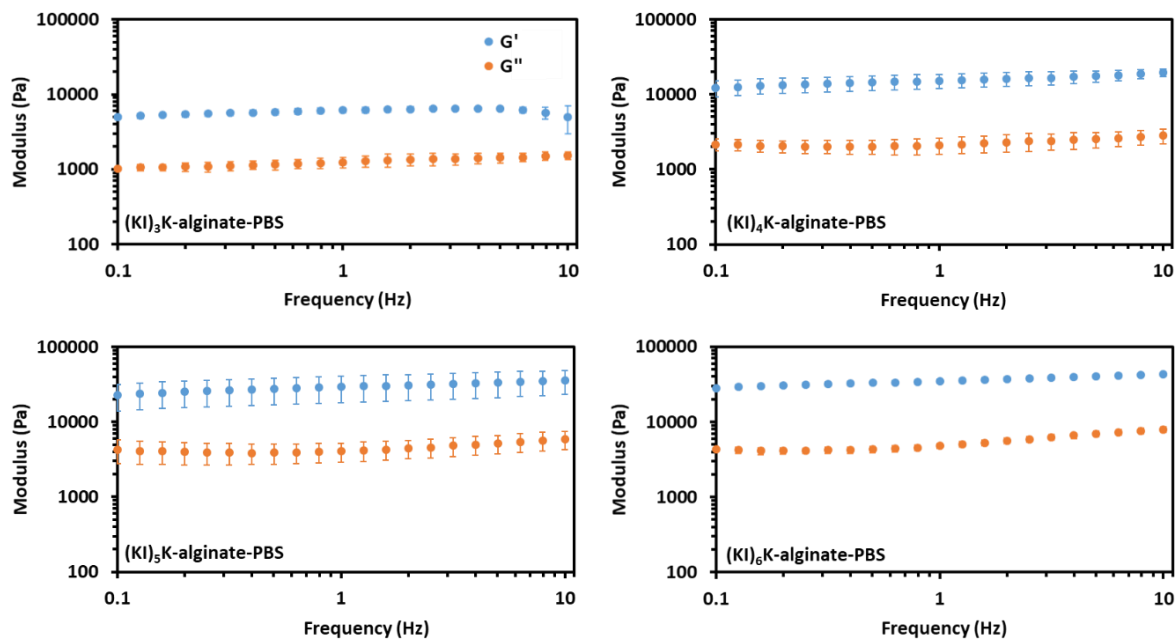
Figure 3.15: *Rheological analysis of (KI)$_n$K-alginate-PBS hydrogels. Standard deviation is indicated by error bars and measurements were performed in triplicate.*

3.3.3. Supramolecular (KI)$_n$K-PAA complex

(KI)$_5$K and (KI)$_6$K peptides form hydrogel with PAA in both salt-free and PBS environment. Microstructures of (KI)$_5$K-PAA and (KI)$_6$K-PAA hydrogels show clusters of assemblies present in the porous network, while in PBS environment (KI)$_5$K-PAA-PBS had fibril-like structures and (KI)$_6$K-PAA-PBS showed branch-like structures (**Figure 3.16**). Typical fibrils were not found in (KI)$_n$K-PAA and (KI)$_n$K-PAA-PBS hydrogels, probably because of the high flexibility of PAA favouring the smaller and more compact aggregation.
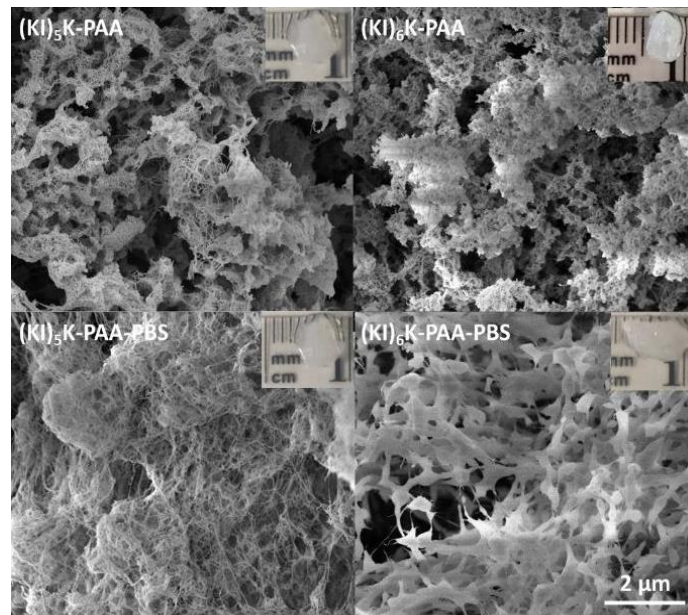
Figure 3.16: *The digital and SEM cross-section images of (KI)$_n$K-PAA and (KI)$_n$K-PAA-PBS hydrogels.*
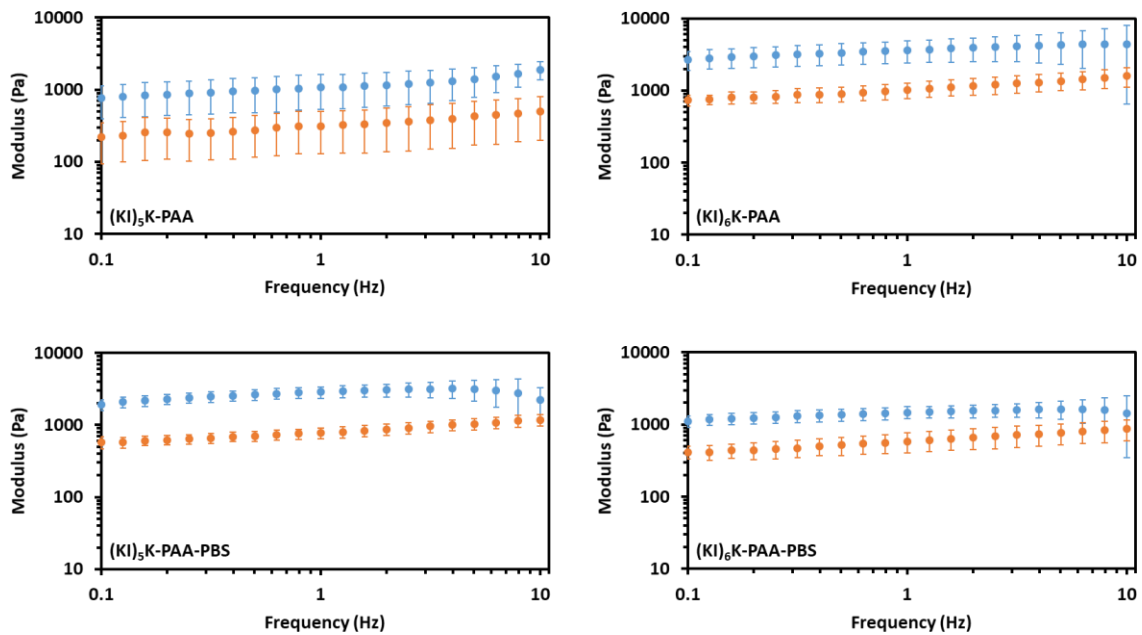
Figure 3.17: *Rheological analysis of (KI)$_n$K-PAA and (KI)$_n$K-PAA -PBS hydrogels. Standard deviation is indicated by error bars and measurements were performed in triplicate.*

(KI)$_5$K-PAA-PBS had a slightly higher G' than (KI)$_5$K-PAA which is likely to be caused by the more homogeneous and dense structure seen for (KI)$_5$K-PAA-PBS, while (KI)$_6$K-PAA-PBS was weaker than (KI)$_6$K-PAA, probably because the branch-like structures seen in (KI)$_6$K-PAA-PBS are likely to be less robust (**Figure 3.17**).

3.3.4. Supramolecular (KI)$_n$K-PSS complex

The previous rheological analysis has shown that PSS solutions have much lower viscosity than alginate, HA and PAA solutions, and once (KI)$_n$K peptides were added on the top of PSS salt-free (ultrapure water) solution, a white precipitate was formed immediately, unlike the other supramolecular (KI)$_n$K-PE complexes where the diffusion of peptide and PE solution take longer time due to their high viscosity. However, after overnight incubation no hydrogel was formed, and it is probably because the electrostatic interaction between PSS and peptide occurs immediately leaving less time for the supramolecular system to reorganize. Interestingly, (KI)$_4$K, (KI)$_5$K and (KI)$_6$K form hydrogels with PSS in PBS, whose microstructures and rheology properties are shown in **Figure 3.18**.

Figure 3.18: (A) The rheology of (KI)$_n$K-PSS-PBS hydrogels. Standard deviation is indicated by error bars and measurements were performed in triplicate. (B) SEM and digital images of (KI)$_n$K-PSS-PBS hydrogels.

It was observed that (KI)$_4$K-PSS-PBS and (KI)$_5$K-PSS-PBS hydrogels present short fibrils, forming relatively loose network, while (KI)$_6$K-PSS-PBS hydrogel has a more homogeneous structure with long entangled fibrils. (KI)$_5$K-PSS-PBS and (KI)$_6$K-PSS-PBS have similar rheological properties, being stiffer than (KI)$_4$K-PSS-PBS. The presence of PBS may promote the fibril bundling which result in a stable network. PBS also increased the flexibility of PSS by screening the charges, thus there is a higher chance for PSS to adopt a better conformation to fit in the self-assembling peptide system.

3.3.5. Supramolecular (KI)$_n$K-HA complex

Supramolecular (KI)$_n$K-HA hydrogels could be produced by adding (KI)$_5$K and (KI)$_6$K on HA solution. SEM images of (KI)$_5$K-HA showed the presence of two distinct layers at the cross-section, where one layer shows a network rich of long and entangled fibrils, whereas the other layer is mainly composed of clusters of dense assemblies (**Figure 3.19**). However, sample shrinkage was observed during the SEM sample preparation which may affect the accuracy of the SEM micrographs. Heterogeneous morphology would also be observed in (KI)$_6$K-HA hydrogel.
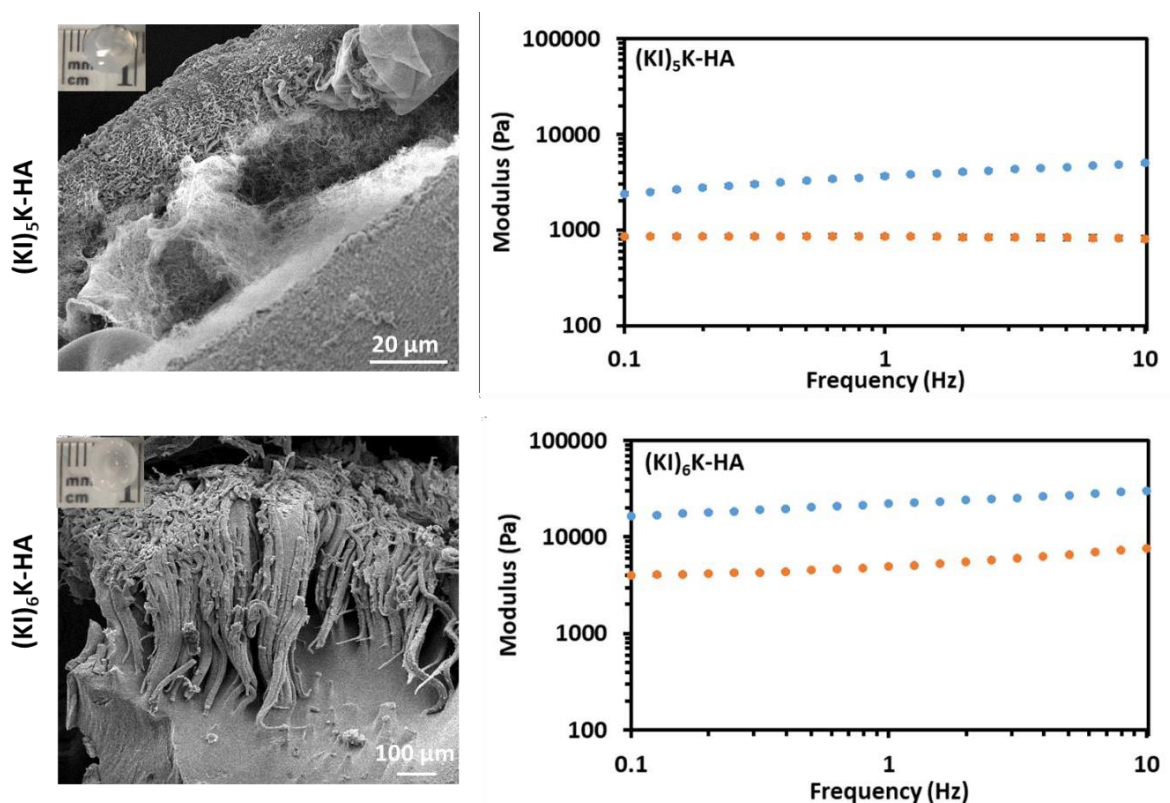
Figure 3.19: *The digital images, SEM images and rheology of (A) (KI)$_5$K-HA and (B) (KI)$_6$K-HA hydrogels. Standard deviation is indicated by error bars and measurements were performed in triplicate.*

The microstructures of (KI)$_n$K-HA-PBS hydrogels show a porous network formed by long and thick fibrils at cross-section. However, the dense fibre network found in (KI)$_n$K-HA could not

be observed in (KI)$_n$K-HA-PBS (**Figure 3.20**). Rheology showed that (KI)$_n$K-HA-PBS are generally much softer than (KI)$_n$K-HA, unlike other (KI)$_n$K-polyelectrolyte where the presence of PBS would often stiffen the hydrogels. More detailed studies on (KI)$_n$K-HA system will be described in chapter 4.

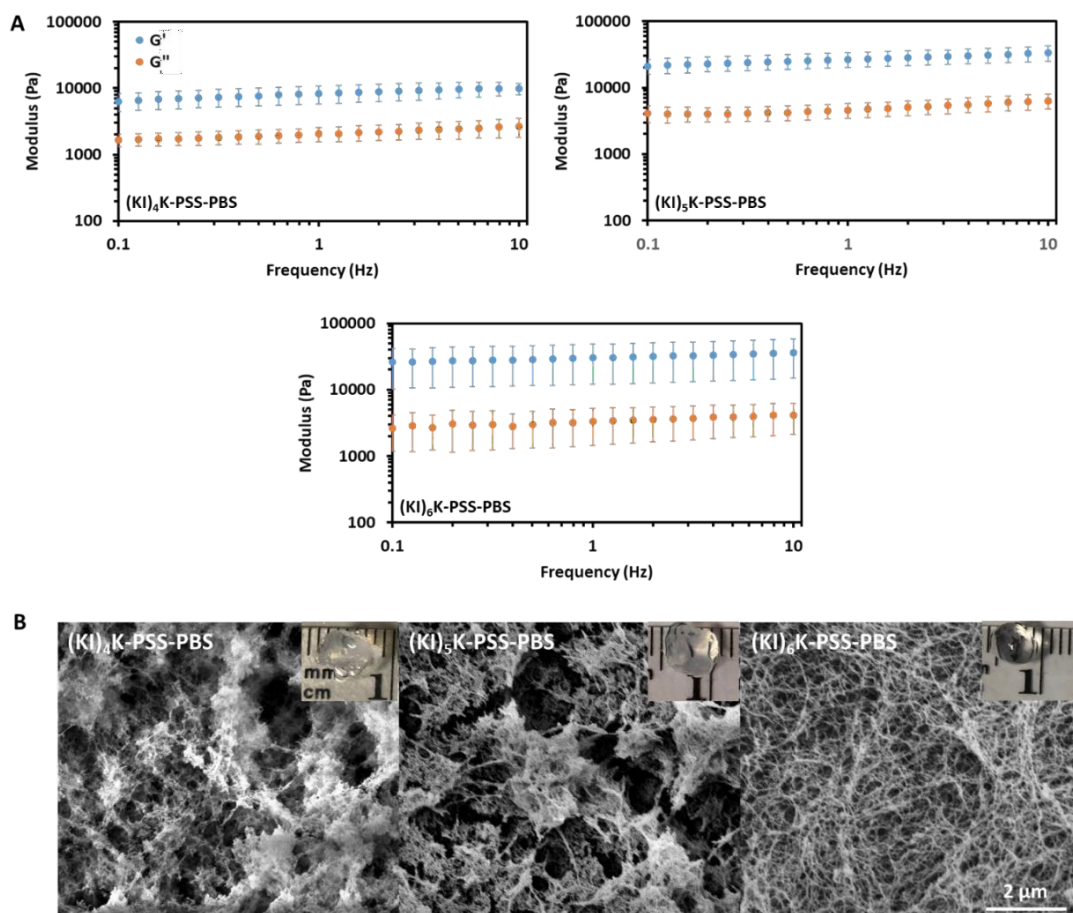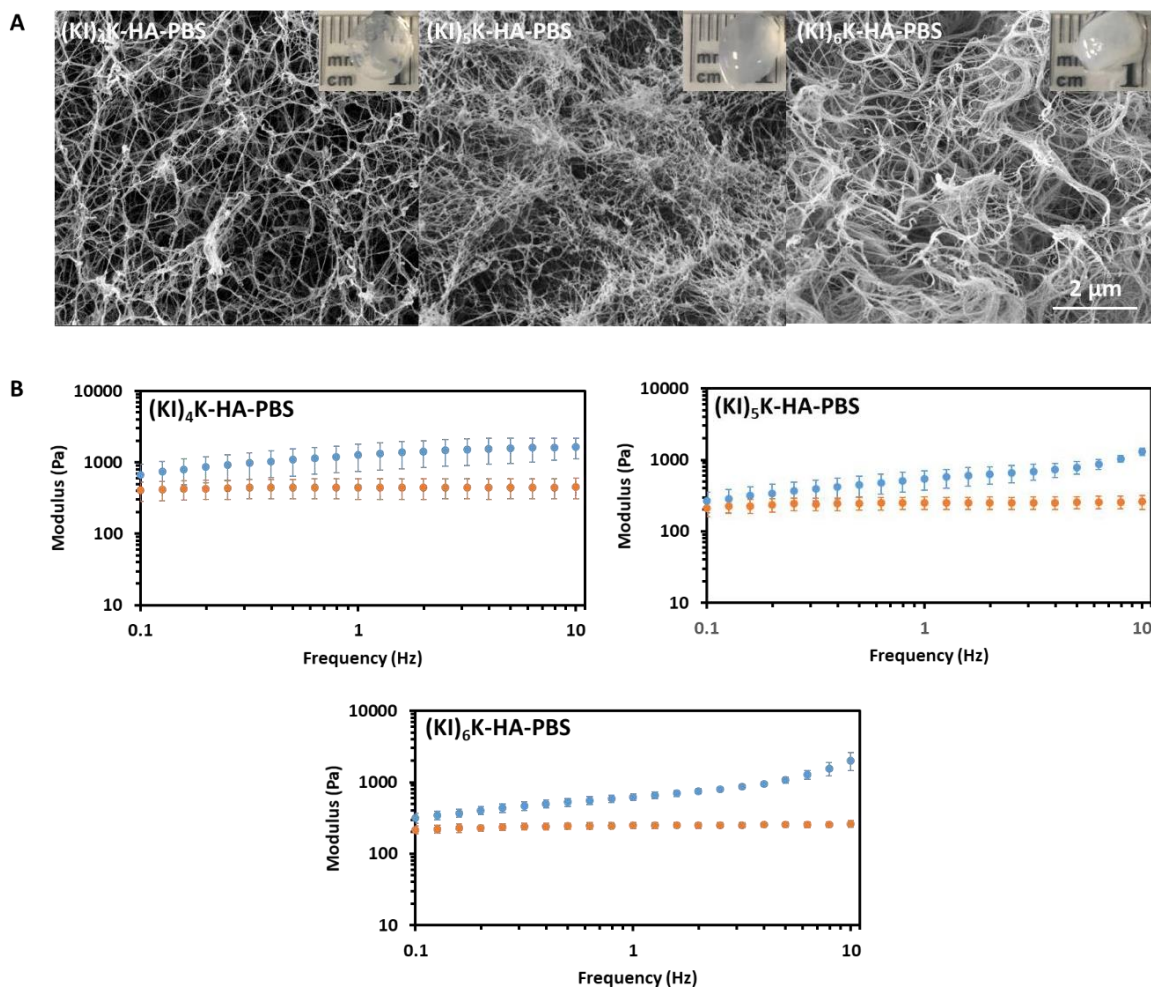**Figure 3.20:** *(A) The digital images and cross-section SEM images of (KI)$_n$K-HA-PBS hydrogels. (B) The rheology of (KI)$_n$K-HA-PBS hydrogels. Standard deviation is indicated by error bars and measurements were performed in triplicate.*

3.4. Conclusions

In this work a library of cationic $(KI)_nK$ (n=2 to 6) peptides were designed. By increasing pH and ionic strength $(KI)_nK$ peptides were able to form β-sheet rich nanofibril. Increasing length of $(KI)_nK$ peptides result in the higher hydrophobicity and enhanced β-sheet forming ability, however, as longer $(KI)_nK$ carries higher number of charges it would also form into the shorter and thinner nanofibril. $(KI)_nK$ peptides could self-assemble with four anionic polyelectrolytes (HA, alginate, PAA, PSS) in both PBS and salt-free environment. In general, longer $(KI)_nK$ peptides are more likely to form the hybrid peptide-polymer hydrogel, whose rheological results show higher G' than G'' indicating the gel state.

3.5. References

1.   Dong H, Paramonov SE, Aulisa L, Bakota EL, Hartgerink JD. Self-assembly of multidomain peptides: Balancing molecular frustration controls conformation and nanostructure. Journal of the American Chemical Society. 2007;129(41):12468-72.

2.   Schneider JP, Pochan DJ, Ozbas B, Rajagopal K, Pakstis L, Kretsinger J. Responsive hydrogels from the intramolecular folding and self-assembly of a designed peptide. Journal of the American Chemical Society. 2002;124(50):15030-7.

3.   Bowerman CJ, Liyanage W, Federation AJ, Nilsson BL. Tuning beta-Sheet Peptide Self-Assembly and Hydrogelation Behavior by Modification of Sequence Hydrophobicity and Aromaticity. Biomacromolecules. 2011;12(7):2735-45.

4.   Sinthuvanich C, Haines-Butterick LA, Nagy KJ, Schneider JP. Iterative design of peptide-based hydrogels and the effect of network electrostatics on primary chondrocyte behavior. Biomaterials. 2012;33(30):7478-88.

5.   Wickremasinghe NC, Kumar VA, Hartgerink JD. Two-Step Self-Assembly of Liposome-Multidomain Peptide Nanofiber Hydrogel for Time-Controlled Release. Biomacromolecules. 2014;15(10):3587-95.

6.   Jiang LH, Xu DW, Sellati TJ, Dong H. Self-assembly of cationic multidomain peptide hydrogels: supramolecular nanostructure and rheological properties dictate antimicrobial activity. Nanoscale. 2015;7(45):19160-9.

7.   Moore AN, Hartgerink JD. Self-Assembling Multidomain Peptide Nanofibers for Delivery of Bioactive Molecules and Tissue Regeneration. Accounts of Chemical Research. 2017;50(4):714-22.

8.   Sarkar B, Siddiqui Z, Nguyen PK, Dube N, Fu W, Park S, et al. Membrane-Disrupting Nano-fibrous Peptide Hydrogels. ACS Biomaterials Science & Engineering. 2019;5(9):4657-70.

9.   Radvar E, Azevedo HS. Supramolecular Peptide/Polymer Hybrid Hydrogels for Biomedical Applications. Macromolecular Bioscience. 2019;19(1):1800221.

10.   Tang C, Smith AM, Collins RF, Ulijn RV, Saiani A. Fmoc-Diphenylalanine Self-Assembly Mechanism Induces Apparent pKa Shifts. Langmuir. 2009;25(16):9447-53.

11.   Urry D.W. LC. Proteins: Structure, folding and function. In: Lenaz G. MG, editor. Bioelectrochemistry of Biomacromolecules Bioelectrochemistry: Principles and Practice. 5: Birkhäuser Basel; 1997.

12.   Sha Y, Li Y, Wang Q, Fan K, Liu D, Lai L, et al. CD evidence of a peptide ongoing α/β/random transition in different solutions. Protein and Peptide Letters. 1999(3):137-40.

13.   Altman M, Lee P, Rich A, Zhang S. Conformational behavior of ionic self-complementary peptides. Protein Sci. 2000;9(6):1095-105.

14.   Surewicz WK, Mantsch HH, Chapman D. Determination of protein secondary structure by Fourier transform infrared spectroscopy: a critical assessment. Biochemistry. 1993;32(2):389-94.

15.   Korshavn KJ, Satriano C, Lin Y, Zhang R, Dulchavsky M, Bhunia A, et al. Reduced Lipid Bilayer Thickness Regulates the Aggregation and Cytotoxicity of Amyloid-β. J Biol Chem. 2017;292(11):4638-50.

16.   Arad E, Green H, Jelinek R, Rapaport H. Revisiting thioflavin T (ThT) fluorescence as a marker of protein fibrillation – The prominent role of electrostatic interactions. Journal of Colloid and Interface Science. 2020;573:87-95.

17.   Zandomeneghi G, Krebs MR, McCammon MG, Fändrich M. FTIR reveals structural differences between native beta-sheet proteins and amyloid fibrils. Protein Sci. 2004;13(12):3314-21.

18.   Bowerman CJ, Nilsson BL. Self-assembly of amphipathic β-sheet peptides: insights and applications. Biopolymers. 2012;98(3):169-84.

19.   Gong X, Branford-White C, Tao L, Li S, Quan J, Nie H, et al. Preparation and characterization of a novel sodium alginate incorporated self-assembled Fmoc-FF composite hydrogel. Materials Science and Engineering: C. 2016;58:478-86.

20.   Wyatt NB, Gunther CM, Liberatore MW. Increasing viscosity in entangled polyelectrolyte solutions by the addition of salt. Polymer. 2011;52(11):2437-44.

Chapter 4

Supramolecular peptide-hyaluronan complexes and hydrogels

4. Supramolecular peptide-hyaluronan complexes and hydrogels

4.1. Introduction

Chapter 3 described various types of supramolecular peptide-polyelectrolyte hydrogels, from which the peptide-HA hydrogel system is of particular interest as HA is a naturally occurring polymer with the advantage of inherent biocompatibility, biodegradability, and non-immunogenic characteristics. In fact, HA-based hydrogels have attracted large interest in a wide range of biomedical applications (1). To impart stability and improve functions of HA hydrogels, covalent and noncovalent crosslinking approaches have been exploited, requiring chemical modification of HA (2). In this work, the formation of supramolecular peptide-HA hydrogels is driven by electrostatic interactions between opposite charged components, which do not require any chemical modification of HA. Supramolecular peptide-HA complex was first introduced in Stupp's group, where a cationic PA was shown to self-assemble in presence of HA forming 2D membranes or sacs (3). It was found that most supramolecular peptide-HA membranes adopted a hierarchical structure composed of distinct two or three layers (**Figure 1.4**) (3-7). In this chapter, the possibility to alter the structure of $(KI)_nK$-HA hydrogels by adjusting the peptide sequence and concentration was investigated. On the other hand, to gain insight on the formation process kinetics of the supramolecular peptide-HA hybrid complex, as well as to probe the mechanism leading to the varied structures, fluorescently-labelled peptide and HA are used to study their diffusion along the time, which also offers the possibility to study hydrogel structure in hydrated state as sample dehydration is required in for conventional SEM which may introduce artefacts.

Tissue engineering requires artificial materials able to biomechanically mimic the native tissue (8). Therefore, tuning the mechanical properties of supramolecular hydrogels is an important goal in biomaterial engineering, which could often be achieved by changing the concentration of building blocks or ionic cross-linkers (9, 10). In this work, the mechanical properties of $(KI)_nK$-HA complexes could be adjusted by changing the concentration of peptide or HA.

The ECM is a three-dimensional network consisting of macromolecules, where collagen and HA are chief components. As supramolecular $(KI)_nK$-HA hydrogels resemble the structure and composition of native ECM, they could be applied as an artificial scaffold for cell culture. To exploit this possibility, the stability of hydrogels was investigated in physiological conditions, as well as their susceptibility to enzymatic degradation. The matrix degradation is a key characteristic of native ECMs in which matrix components are degraded by enzymes expressed by surrounding cells, so the artificial scaffold is also expected to be biodegradable.

Anisotropic organisation is a common feature of many human tissues (e.g. bone, tendons, annulus fibrosus, cornea, muscle and blood vessels). Mimicking the structural organization of tissues via biomaterials engineering approaches is expected to promote enhanced tissue regeneration. In fact, it was found that anisotropic artificial scaffolds could induce the alignment of cells which in turn produced oriented deposition of ECM by cells, also promoting cell proliferation and differentiation (11). As such, the structural alignment of the supramolecular hybrid peptide-HA hydrogel was also explored in this work.

4.2. Engineering the mechanical properties of supramolecular $(KI)_nK$-HA complexes

Chapter 3 described the properties of peptide-HA hydrogels formed by 2 wt% HA and 2 wt% peptide. In order to evaluate the effect of peptide concentration on the properties of this supramolecular peptide-HA hydrogel system, peptide solutions with lower concentrations (1 wt%) along with the 2 wt% HA solutions were also used to fabricate the hybrid hydrogel (**Figure 4.1**). As the HA solution has high viscosity, due to the large molecular weight (2 MDa), the two solutions are not expected to immediately mix. After incubation at room temperature overnight, it was found that either single-phase homogeneous complex was observed, or a phase separation occurred in the $(KI)_nK$-HA self-assembling system. A gel-like phase emerged at the interface between HA and peptide solutions with 2 wt% $(KI)_5K$, 2 wt% $(KI)_6K$ or 1 wt% $(KI)_6K$. As shown in chapter 3, hydrogels were formed for 2 wt% $(KI)_5K$-HA and 2 wt% $(KI)_6K$-

HA self-assembling system which could be easily taken out from the low viscosity supernatant phase. Though distinguished phases were also observed in the supramolecular 1 wt% $(KI)_6$K-HA system, the supernatant phase below the gel phase has a high viscosity and the two phases were stick together. However, phase separation did not occur in 2 wt% $(KI)_2$K-HA, 2 wt% $(KI)_3$K-HA and 2 wt% $(KI)_4$K-HA systems. Similarly, it was also found that only clear single phase was formed by HA and 1 wt% $(KI)_2$K, $(KI)_3$K, $(KI)_4$K or $(KI)_5$K. Since the longer $(KI)_n$K peptide has a stronger β-sheet forming ability, whose repulsive positive charges could be more readily screened, it is plausible that phase separation can only occur in the supramolecular system with HA and longer peptides.
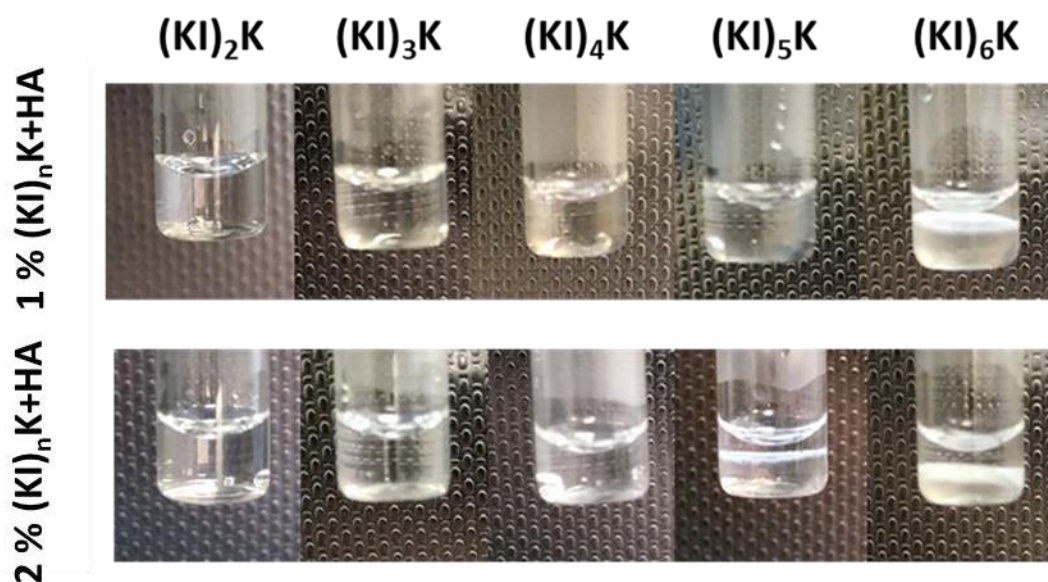
Figure 4.1: *Supramolecular $(KI)_n$K-HA complexes formed in a glass vial when $(KI)_n$K peptide solutions (1 and 2 wt%) are added on top of HA solution (2 wt%) and incubated overnight. Gel-like phases between the two liquid layers were visible in 2 wt% $(KI)_5$K-HA, 2 wt% $(KI)_6$K-HA or 1 wt% $(KI)_6$K-HA.*

The mechanical properties of $(KI)_n$K-HA complexes were then investigated by conventional rheology (for the two-phase complex, only the gel-like phase was measured). It was found that all mixtures with HA and 1 wt% $(KI)_n$K, have rheological behaviour like pure HA,

independent of the peptide sequence, indicating minor contribution of the self-assembling peptides, and with HA dominating the mechanical properties of the mixtures (**Figure 4.2**). Large molecular weight HA is known to have higher G'' than G' in low frequency region, but G' then predominates over G'' at higher frequencies due to the transient HA network formed by increased molecular entanglement in the short period of oscillation (12).
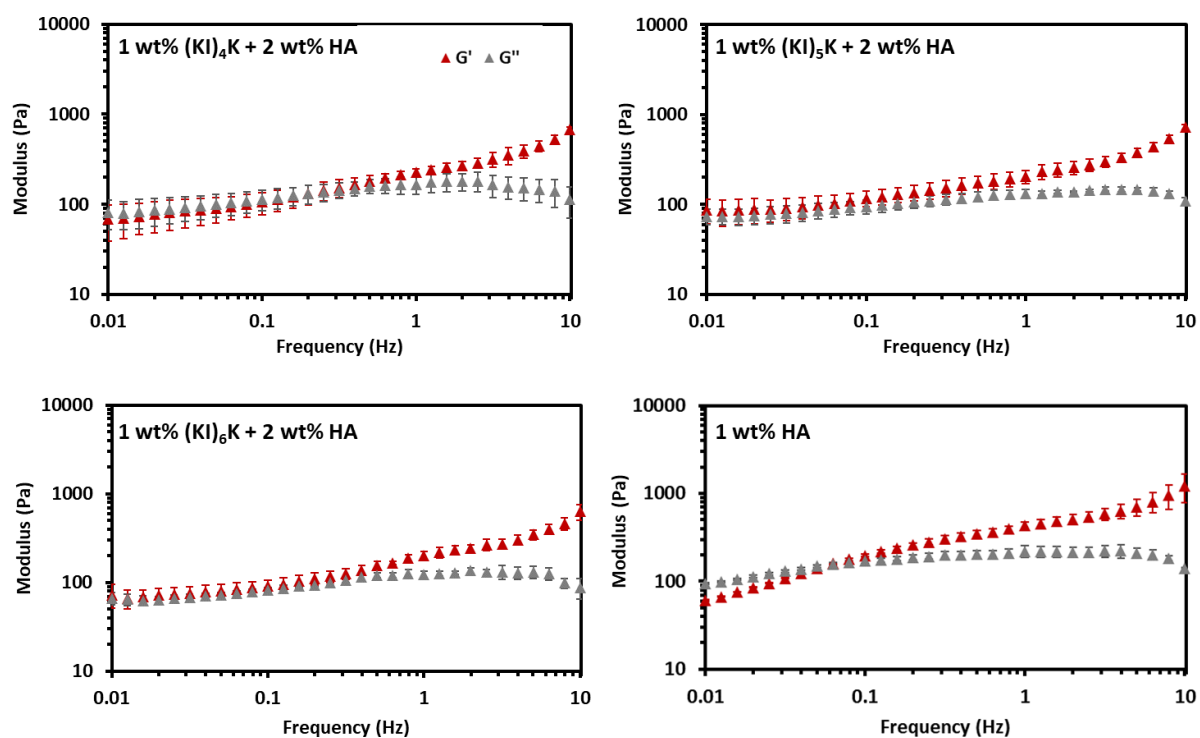
Figure 4.2: *Rheological analysis of 1 wt% (KI)$_n$K-2 wt% HA complexes and 1 wt% HA solution. Standard deviation is indicated by error bars and measurements were performed in triplicate.*

Mixtures composed of HA and 2 wt% (KI)$_2$K, (KI)$_3$K and (KI)$_4$K also exhibit HA-like rheological behaviour (**Figure 4.3**). While the cross-over frequency (when G'=G'') for 2 wt% (KI)$_2$K-HA and 2 wt% (KI)$_3$K-HA was found at around 0.1 Hz, for 2 wt% (KI)$_4$K-HA mixture the cross-over point was observed at lower frequency (~0.01 Hz) probably due to relatively weak peptide self-assembly turning the viscoelastic liquid into a form closer to a gel. The rheological behaviour of 2 wt% (KI)$_5$K-HA and 2 wt% (KI)$_6$K-HA hydrogels is significantly different from the other

single-phase system, as there is a dramatic increase of both G' and G'' being also much less frequency dependant, where the contribution of self-assembling peptides dominates the mechanical properties of the hydrogels. Generally, longer $(KI)_nK$ shifted the viscoelastic spectrum of the hydrogels towards lower frequencies and led to higher stiffness in 2 wt% $(KI)_nK$-HA complex.
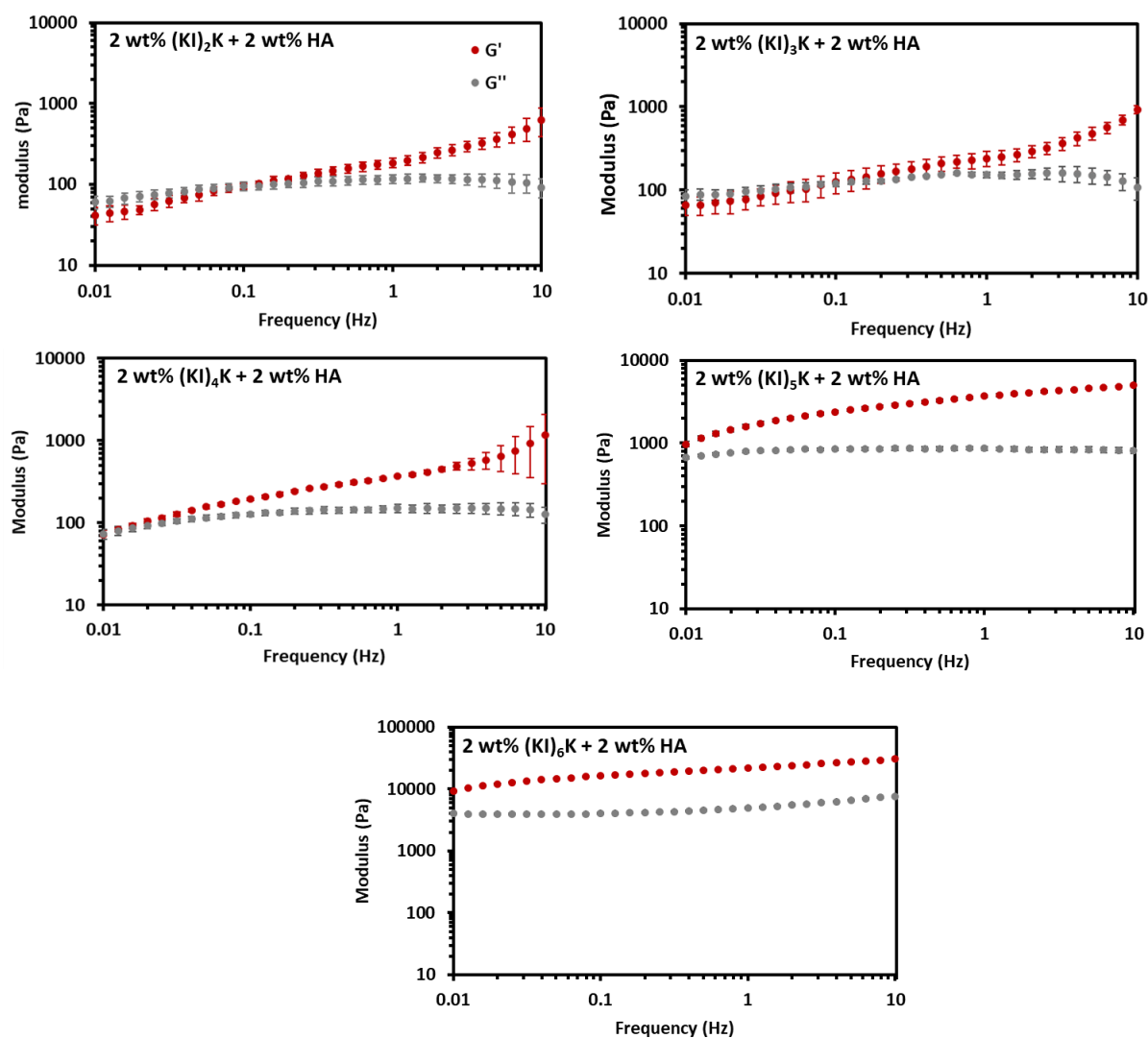
Figure 4.3: *Rheological analysis of 2 wt% $(KI)_nK$-2 wt% HA complexes or hydrogels. Standard deviation is indicated by error bars and measurements were performed in triplicate.*

The effect of HA concentration on the $(KI)_nK$-HA complex was also investigated. Two supramolecular system, 2 wt% $(KI)_4K$ and $(KI)_5K$ in combination with HA of different concentrations, were chosen as representation of single-phase and two-phase system, respectively, and their rheological properties were compared (**Figure 4.4**). It was found that changing the HA concentration from 2 wt% to 1 wt% would not affect the phase behaviour of the two systems, as 2 wt% $(KI)_4K$-1 wt% HA and 2 wt% $(KI)_5K$-1 wt% HA remained to behave as single-phase and two-phase respectively.
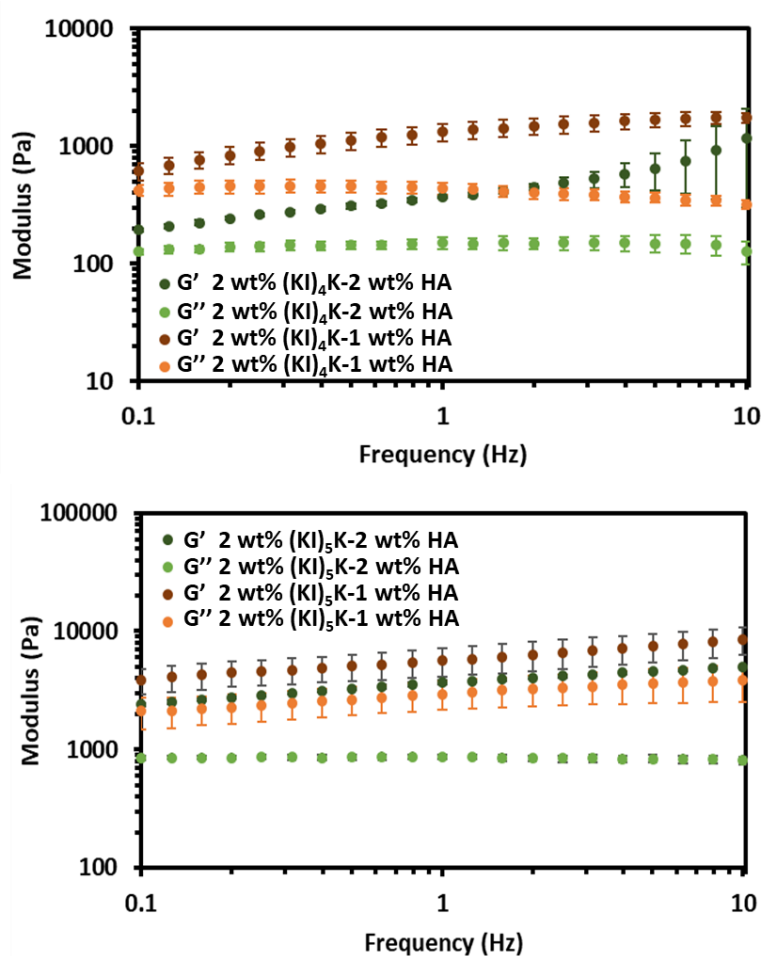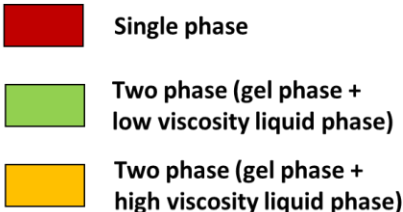
Figure 4.4: *Comparison of the rheological behaviour of 2 wt% $(KI)_nK$-2 wt% HA and 2 wt% $(KI)_nK$-1 wt% HA. Standard deviation is indicated by error bars and measurements were performed in triplicate.*

Increasing concentration of hydrogel components is often thought to promote the stiffness of the self-assembling hydrogel. However, in supramolecular polymer-peptide system this correlation is not as simple. For example, in a PA-chitosan hydrogel, increased PA concentration was found to decrease the G' of the hybrid hydrogel, because higher concentration PA resulted in greater viscosity, disturbing solution mixing (13). In this work, it was also found that lower HA concentration led to the higher G' and G'' for $(KI)_4K$-HA and $(KI)_5K$-HA complexes. Less concentrated HA solution has a lower viscosity which results in a better diffusion between peptide and HA. Additionally, increasing polymer content may decrease the entanglement among self-assembling peptide fibrils and weaken the strength of hybrid peptide-polymer complex (14).

4.3. Tuning the structure of supramolecular $(KI)_nK$-HA hydrogels

In order to explore the potential application of $(KI)_nK$-HA as stem cell substrate, cell culture media (DMEM) and PBS were added to all $(KI)_nK$-HA complexes to investigate the stability in physiological-like conditions. In this section, the HA concentration of $(KI)_nK$-HA complex is 2 wt%. It was found that 1 wt% $(KI)_6K$-HA, 2 wt% $(KI)_5K$-HA and 2 wt% $(KI)_6K$-HA hydrogels remained stable in these conditions, while some liquid-like single-phase complex (1 wt% $(KI)_4K$-HA, 1 wt% $(KI)_5K$-HA, and 2 wt% $(KI)_4K$-HA) were able to transform into hydrogels with the addition of DMEM and PBS as phase separation occurred, but none of the $(KI)_2K$-HA and $(KI)_3K$-HA complex formed any self-supporting hydrogel and finally dissolved in DMEM and PBS, probably due to the limited β-sheet formation ability of the peptides (**Table 4.1**). It is postulated that counterions (e.g. Cl^- and HPO_4^{2-}) in DMEM and PBS could further screen repulsive positive charges of the peptides and finally trigger the hydrogel formation.

Table 4.1: *The state of the supramolecular $(KI)_nK$-HA complexes before and after overnight incubation in physiological-like conditions at room temperature.*

	1 wt% $(KI)_nK$ + 2 wt% HA		2 wt% $(KI)_nK$ + 2 wt% HA	
	Original	In DMEM or PBS	Original	In DMEM or PBS
$(KI)_2K$	Single phase	Single phase	Single phase	Single phase
$(KI)_3K$	Single phase	Single phase	Single phase	Single phase
$(KI)_4K$	Single phase	Two phase (low visc.)	Single phase	Two phase (low visc.)
$(KI)_5K$	Single phase	Two phase (low visc.)	Two phase (low visc.)	Two phase (low visc.)
$(KI)_6K$	Two phase (high visc.)	Two phase (low visc.)	Two phase (low visc.)	Two phase (low visc.)

Legend:
- Single phase (red)
- Two phase (gel phase + low viscosity liquid phase) (green)
- Two phase (gel phase + high viscosity liquid phase) (orange)

To study the swelling behaviour of supramolecular $(KI)_nK$-HA complex in physiological condition, 2 wt% $(KI)_4K$-HA and 2 wt% $(KI)_5K$-HA were taken as examples and immersed in PBS. After one hour, the weight of 2 wt% $(KI)_4K$-HA and 2 wt% $(KI)_5K$-HA increased 116.2% and 192.5%, respectively (**Figure 4.5-A**). Since $(KI)_nK$-HA complexes are composed of polyelectrolyte and charged peptide network, the counterions trapped inside the complex exerting osmotic pressure triggered the swelling behaviour (15). The initial transparency of $(KI)_4K$-HA reduced dramatically and $(KI)_5K$-HA significantly increased in size after swelling (**Figure 4.5-B**).

Morphology study found that supramolecular hydrogel formed by HA and peptide with different sequences would exhibit varied structures. However, it was challenging to obtain SEM images of single-phase $(KI)_nK$-HA complexes, as they were not stable during the sample preparation. Consequently, SEM images of 1 wt% $(KI)_4K$-HA, 1 wt% $(KI)_5K$-HA and 2 wt% $(KI)_4K$-HA were only available after gelation in PBS or DMEM. Two distinct layers were observed at the cross-section of 2 wt% $(KI)_4K$-HA and 2 wt% $(KI)_5K$-HA (**Figure 4.5-C**). However, it was found that at the cross-section of 2 wt% $(KI)_4K$-HA and 2 wt% $(KI)_5K$- HA incubated in PBS, porous structures formed by thin fibrils were observed, in contrast to most supramolecular peptide-HA membranes composed of distinct layers with oriented fibrils (5-7). Since increase transmittance of hydrogel may be related to homogeneous morphology (16), the reduced

transparency found in 2 wt% $(KI)_4$K-HA when swollen in PBS is likely to be ascribed to structural heterogeneity. 2 wt% $(KI)_5$K-HA hydrogel also shown two distinct layers in salt-free (ultrapure water) environment, but with different morphologies from the hydrogel incubated in the water. In 2 wt% $(KI)_5$K-HA hydrogel incubated in PBS, large and small pores were visible at each side of the hydrogel cross-section, while the porous structures were not visible in salt-free condition. As the hydrogel in salt-free environment suffered from the dramatic shrinkage during sample preparation for SEM, it was possible that larger pores were damaged. The formation of small pores in 2 wt% $(KI)_5$K-HA incubated in PBS may be due to the presence of counterions like HPO_4^{2-} and Cl^- promoting fibril bundling.
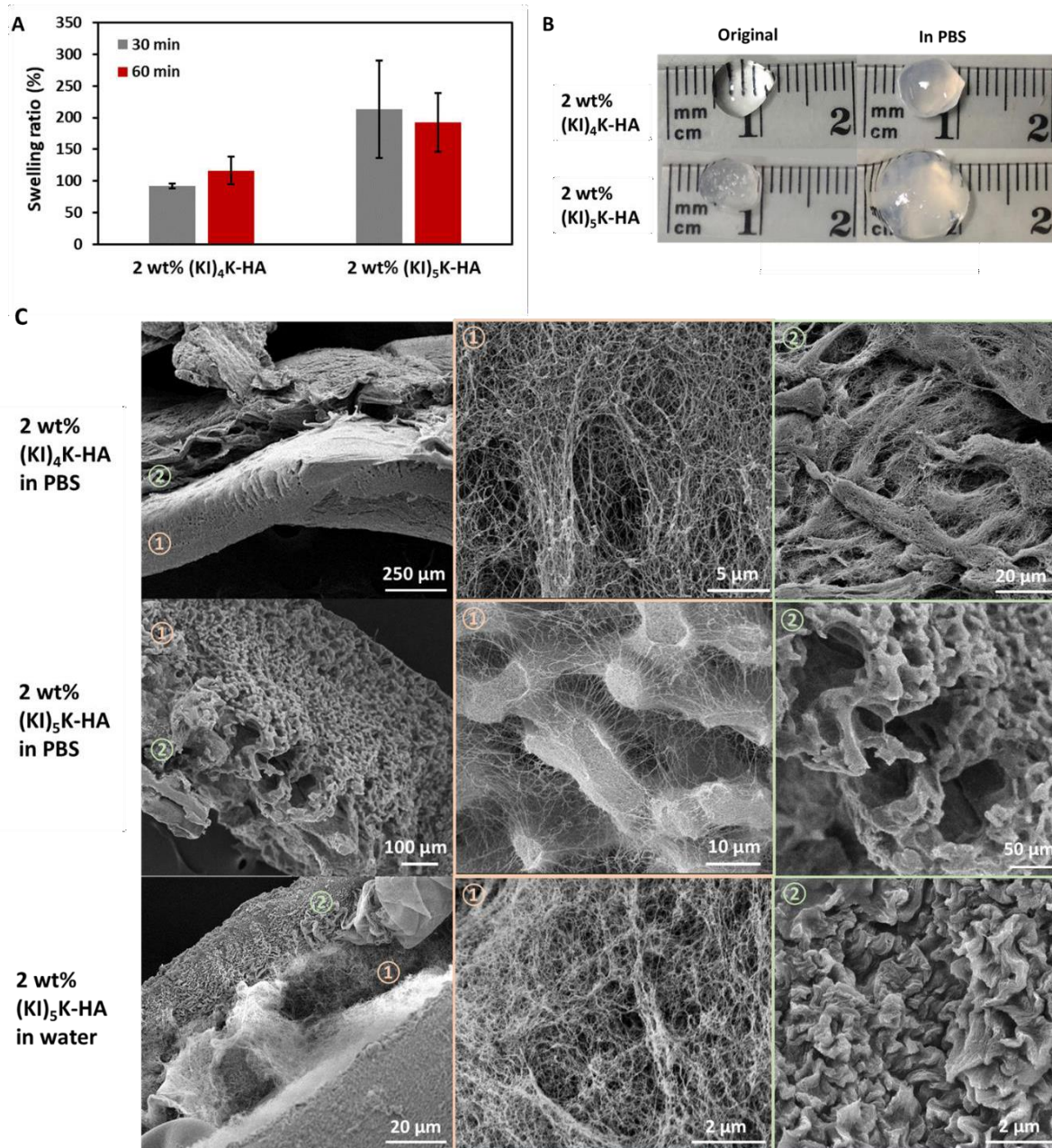
Figure 4.5: *Study of 2 wt% (KI)₄K-HA and 2 wt% (KI)₅K-HA hybrid hydrogel (A) Swelling ratio of the supramolecular complexes measured at 30 and 60 min after incubation in PBS. Standard deviation is indicated by error bars and measurements were performed in triplicate. (B) Digital images of original and swollen gels incubated in PBS for 60 min. (C) SEM images of cross-section of water or PBS incubated hydrogels.*

The microstructure investigation of 1 wt% $(KI)_4K$-HA and 1 wt% $(KI)_5K$-HA found that both hydrogels incubated in PBS have a homogeneous structure without distinctive layers, and the magnified image show that they were composed of nanofibrous structure, in which 1 wt% $(KI)_5K$-HA was denser than 1 wt% $(KI)_4K$-HA hydrogel (**Figure 4.6**).
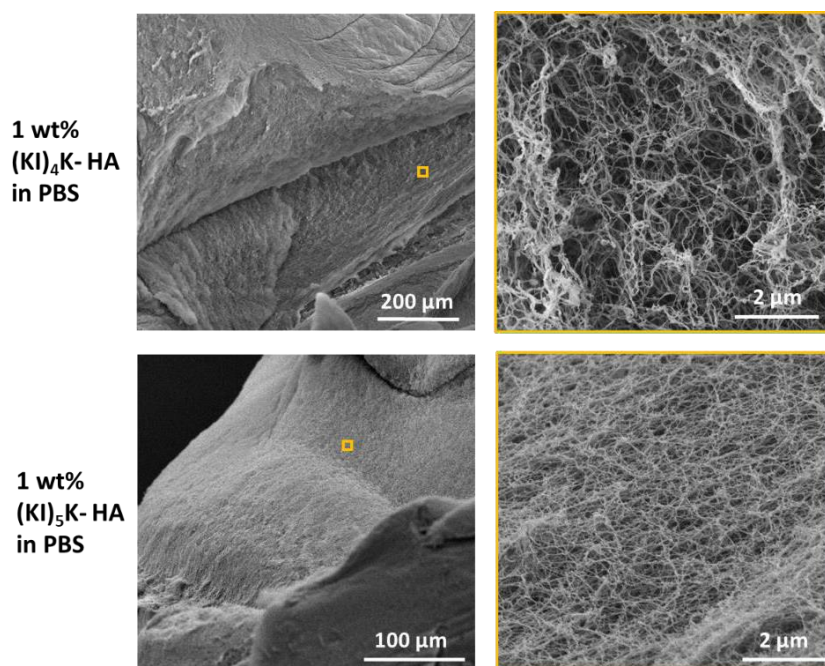
Figure 4.6: *SEM images of cross-section of 1 wt% $(KI)_4K$-HA and 1 wt% $(KI)_5K$-HA hydrogels incubated in PBS.*

Examination of the microstructure of 1 wt% $(KI)_6K$-HA and 2 wt% $(KI)_6K$-HA hydrogels incubated in both water and PBS was also performed. However, little structural differences were observed between water and PBS incubated hydrogels. In **Figure 4.7**, it was found that at the edge of the hydrogels hierarchical structures with distinct layers were displayed, which is similar with the morphology of supramolecular PA-HA and MDP-HA membranes (3-6). 1 wt% $(KI)_6K$-HA hydrogel was composed of three different zones, which are amorphous layer, parallel and perpendicular aligned fibre regions. In 2 wt% $(KI)_6K$-HA hydrogel there were two distinct regions, with the central part of the hydrogel consisted of randomly entangled nanofibrils and the oriented fibre at the edge.
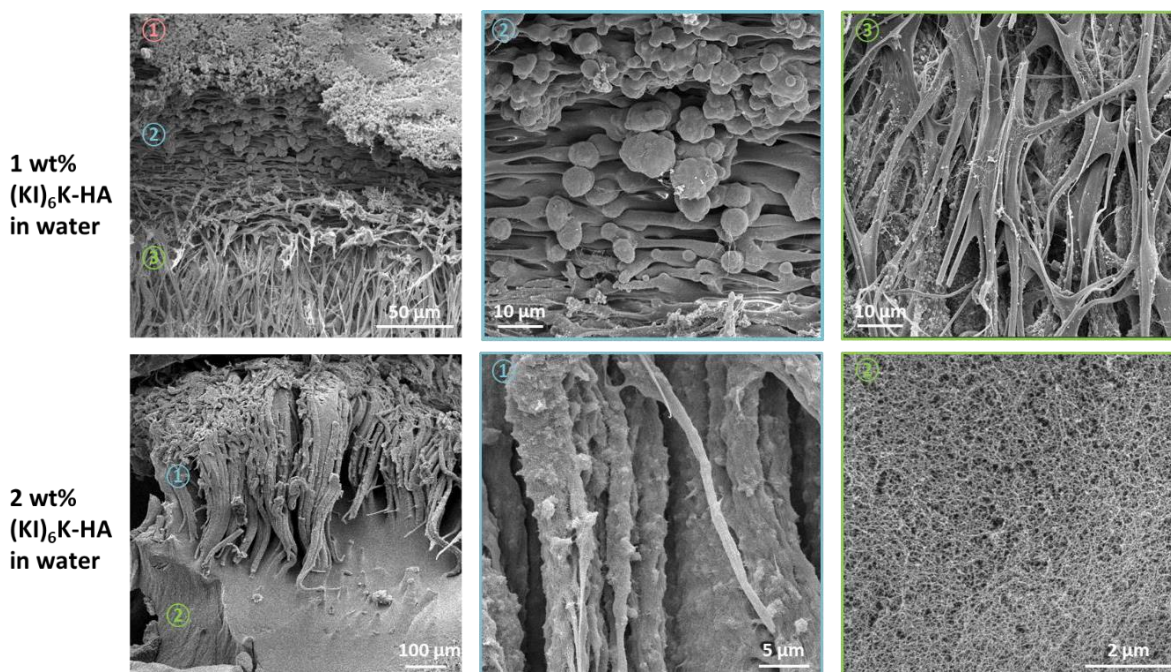
Figure 4.7: *SEM images showing heterogeneous structures at the edge of 1 wt% (KI)$_6$K-HA and 2 wt% (KI)$_6$K-HA hydrogels.*

For all the work described above, the hybrid supramolecular hydrogels were produced by casting peptide solution on the top of HA solution. It was hypothesised if the order of adding these components would affect the morphology in the (KI)$_n$K-HA hydrogels, by adding HA solution on the top of (KI)$_n$K solution and then immersed in PBS (referred as HA-(KI)$_n$K, **Figure 4.8**). It was found that 2 wt% HA-(KI)$_4$K hydrogels exhibited a very dense and homogeneous network structure formed by thin fibrils, while in 2 wt% HA-(KI)$_5$K microporous structure could be found and fibrils appeared to be longer and thicker. When denser HA solution was placed on the (KI)$_n$K solution, HA solution could directly penetrate into the peptide solution, so the typical horizontal liquid-liquid interface was not formed upon contact of the two components, and the distinct two-layer structure was also not observed in the final hydrogel structure. Stupp's group also found that the order of adding solutions could alter the formation of supramolecular PA-HA complex, where a membrane was formed by adding PA

on HA whereas placing HA in PA led to the sac formation (3). The differences in mixing kinetics were caused by the different viscosities of the solutions of the two building blocks.
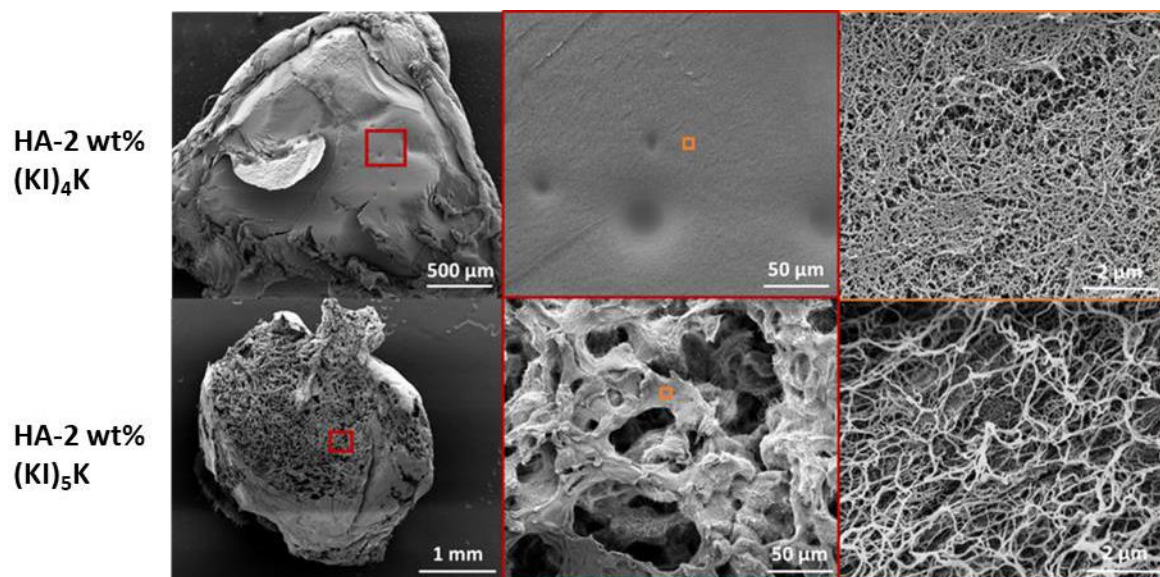
Figure 4.8: SEM images of the hydrogels cross-section obtained in the reverse order (adding HA on the top of peptide solution) in PBS environment.

4.4. Kinetics of the supramolecular formation of $(KI)_nK$-HA complexes

In order to investigate the kinetics of the supramolecular formation of the $(KI)_nK$-HA complex, along with the peptide and HA distribution, rhodamine and fluorescamine fluorescent dyes were conjugated to $(KI)_nK$ and HA to produce fluorescent probes (Rhod-$(KI)_nK$, **Figure 4.15**) and fluorescein-HA) respectively (**Figure 4.9-A**). The kinetic of the typical $(KI)_nK$-HA single-phase system is shown in **Figure 4.9-B**. No defined structure was observed at the interface, suggesting the relatively weak interaction between the peptide and HA, and the overlap of red and green signal reflects the homogeneous mixing of the two components.

It is noticeable that in PA-HA self-assembling system, the formation of dense diffusion barrier between peptide and HA was considered an important factor causing the hierarchical distinct layer structure, with one rich in HA and the other in self-assembling peptides (5, 17). However,

145

in the single-phase system, no diffusion barrier could be observed, thus the free diffusion was enabled, which resulted in the homogeneous morphology.
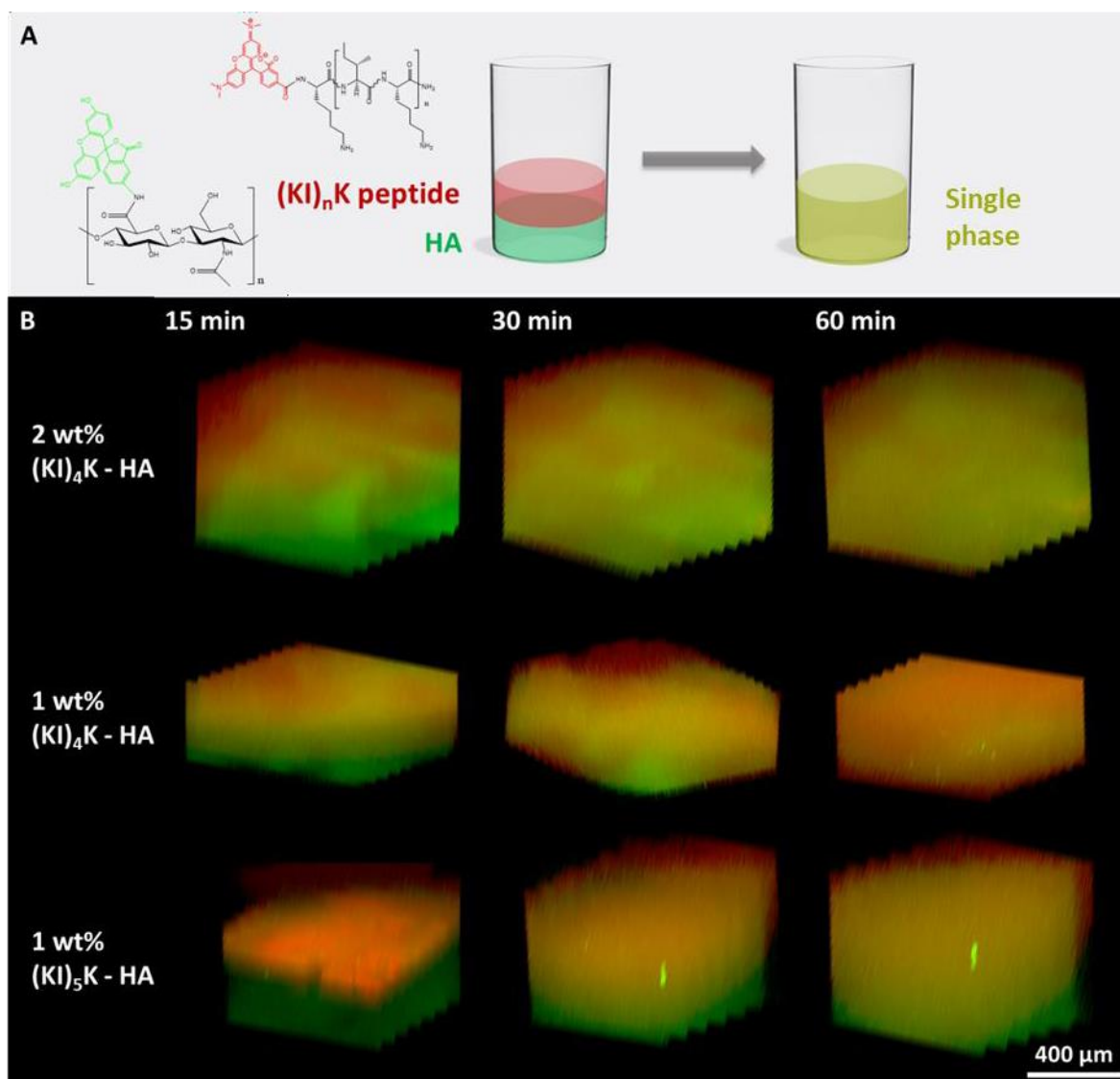
Figure 4.9: *(A) Schematic representation of single-phase $(KI)_nK$-HA formation. (B) Reconstructed 3D images of CLSM used to study the kinetic of single-phase $(KI)_nK$-HA complex (salt-free environment) at three time points in merged channel. Red and green signals represent $(KI)_nK$ and HA, respectively.*

Using the same experimental approach, it was found that in the supramolecular 2 wt% $(KI)_5K$-HA system, where phase separation and hydrogel formation were observed, a porous layer

forms shortly after the addition of peptide on the HA solution, and the layer continues to grow in thickness until the formation of a microporous 3D network was observed on one hour (**Figure 4.10**). The porous layer was rarely observed in supramolecular peptide-polymer complex, and it may promote the continuous diffusion between $(KI)_nK$ and HA allowing the relatively sufficient mix.
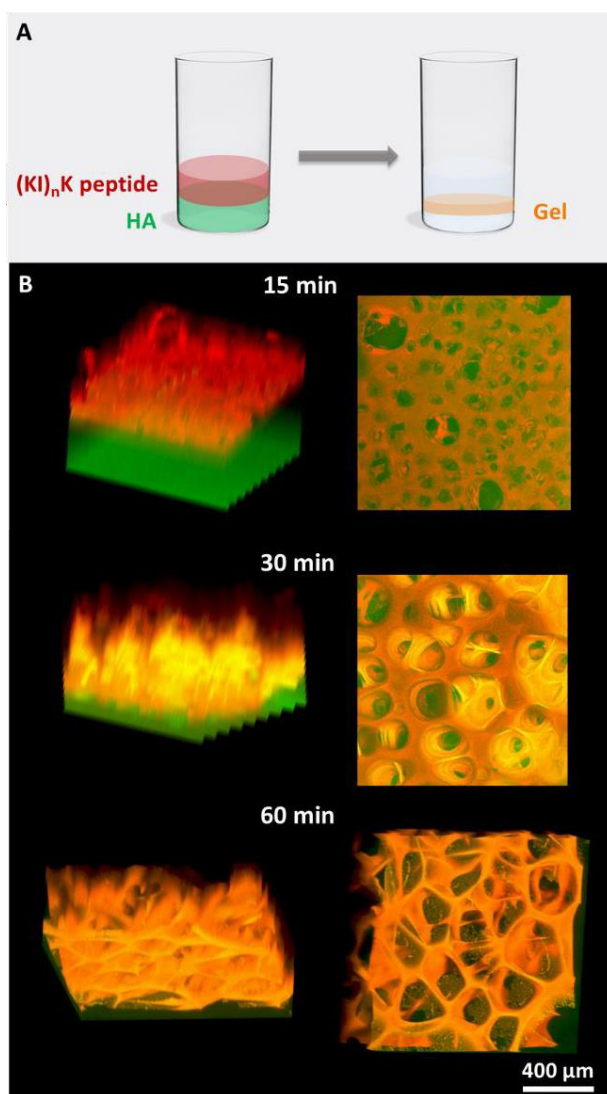
Figure 4.10: *(A) Schematic representation of $(KI)_nK$-HA hydrogel formation (B) CLSM used to study the kinetic of 2 wt% $(KI)_5K$-HA hydrogel formation (salt-free environment) showing the reconstructed 3D structures and stacking 2D images at three time points in merged channel. Red and green signals represent $(KI)_5K$ and HA, respectively.*

The CLSM images were also taken 24 hours after 2 wt% (KI)$_5$K-HA hydrogel formation shown in **Figure 4.11**. The microporous network was found to be at the bottom of the gel (HA side), while on the top of the gel (peptide side) the structure appears relatively dense. The CLSM image of 2 wt% (KI)$_5$K-HA hydrogel in salt-free environment along with SEM images reveal that the hydrogel may have dense nanofibrous structures at the peptide side, and microporous network at the HA side where both of (KI)$_5$K and HA build up the pore walls. The microporous network would form first, and then the dense nanofibrous structure gradually formed as the hybrid hydrogel continues to grow.
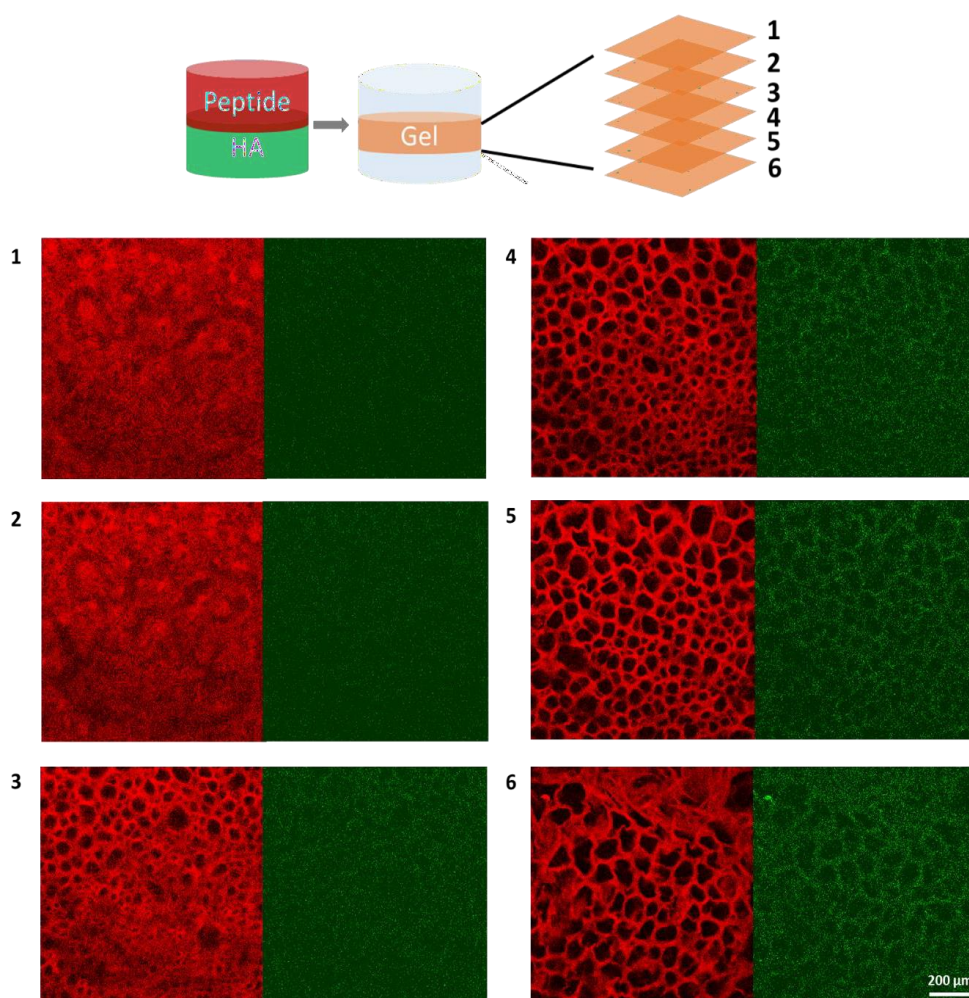
Figure 4.11: *CLSM images in red ((KI)$_5$K) and green (HA) channels of 2 wt% (KI)$_5$K-HA hydrogel at different layers after 24 hours incubation in salt-free condition. Hydrogel was taken out of the supernatant and observed on the glass slide.*
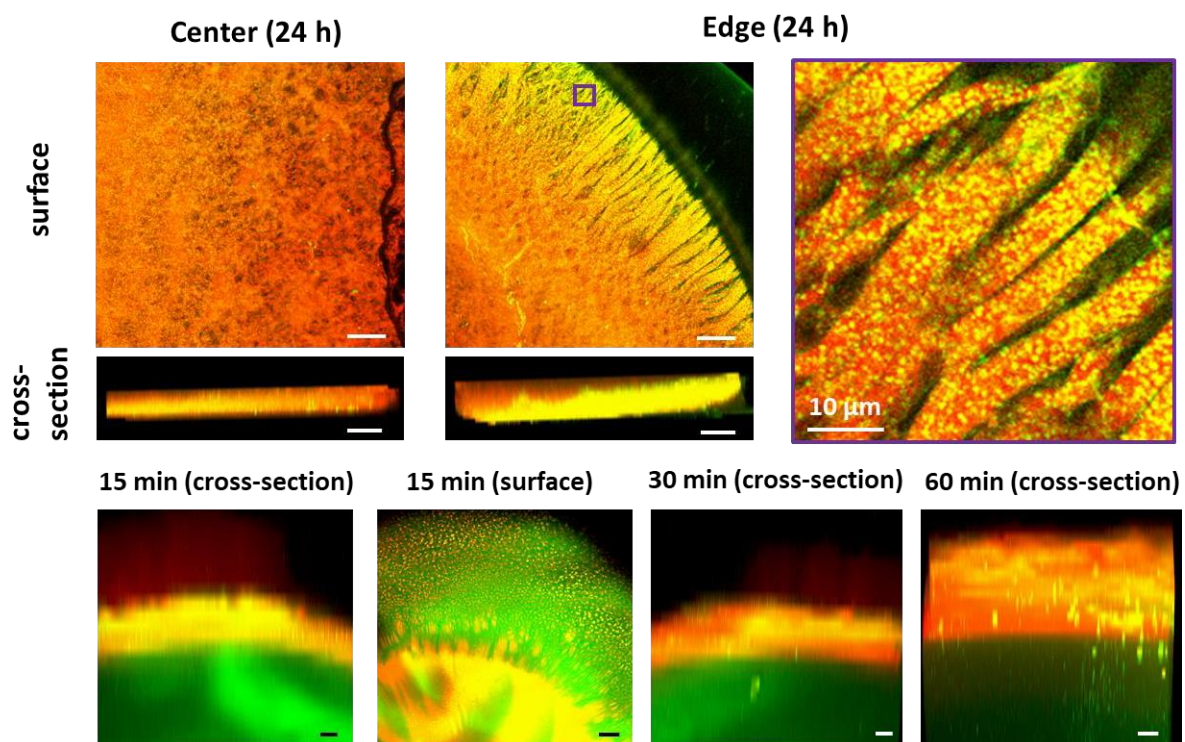
Figure 4.12: *CLSM used to study the kinetic of 2 wt% (KI)$_6$K-HA hydrogel formation (salt-free environment) showing the reconstructed 3D structures and stacking 2D images at four time points in merged channel. The morphologies of the centre and edge of the hydrogel are shown for 24 h. Red and green signals represent (KI)$_6$K and HA, respectively (scale bar=100 µm unless otherwise state).*

The CLSM image of 2 wt% (KI)$_6$K-HA hydrogel after 24 hours (**Figure 4.12**) reveals that the hydrogel has an amorphous central part while oriented fibre-like structure could be found at the periphery of the hydrogel (image with purple frame). The magnified image of the fibre structures showed that there were HA-rich assemblies attached to the peptide-rich fibre structure. It was found that after 24 hours the peptide and HA were not fully mixed, where the bottom and the edge of the hydrogel were HA-rich and peptide were more likely to be observed at the centre of the hydrogel. The heterogeneous structure of the hydrogel might be caused by the diffusion barrier during the hydrogel formation. The presence of diffusion barrier has also been considered an important factor leading to the formation of peptide-HA membrane with hierarchical structure (3-5). Though 2 wt% (KI)$_5$K-HA hydrogel also exhibited two structurally different zones, the typical aligned fibre structure was not present and a

149

porous structure was found instead. In this work, the absence of aligned fibre structure in 2 wt% $(KI)_5K$-HA hydrogel was probably due to the porous layer at the interface allowing the chaotic mixing between HA and $(KI)_5K$ peptide, while the interfacial diffusion barrier in 2 wt% $(KI)_6K$-HA hydrogel enabled the formation of oriented fibre structure.

Through the kinetic study of the supramolecular peptide-HA hydrogel, it was found that the formation of a diffusion barrier at the peptide-HA interface may be associated with peptide sequence and concentration. It has been described in chapter 3 that longer $(KI)_nK$ peptide exhibit stronger β-sheet forming tendency. Among $(KI)_4K$, $(KI)_5K$ and $(KI)_6K$ peptides, $(KI)_4K$ shows relatively poor self-assembling ability, so no structure could form at the $(KI)_4K$-HA interface leading to completely free diffusion. $(KI)_5K$ has an increased β-sheet forming tendency compared to $(KI)_4K$, which resulted in the porous layer formed in 2 wt% $(KI)_5K$-HA self-assembling system. The dense diffusion barrier could be formed by 2 wt% $(KI)_6K$ and HA due to the stronger self-assembling ability of $(KI)_6K$.

4.5. Enzymatic degradation of $(KI)_nK$-HA hydrogels

Hyaluronidase was used to assess if the peptide-HA hydrogels are susceptible to enzymatic degradation. HAase is known to be present in varied organs of the human body and catalyse the cleavage of HA into oligosaccharides (18). The degradation behaviour of the 2 wt% $(KI)_5K$-1 wt% HA hydrogel was studied in three different conditions, PBS only (0 U/ml), PBS containing 2.6 U/mL (physiological enzyme level) (19) and 50 U/ml HAase. The HAase and PBS solutions were refreshed every 72 hours.

HA oligosaccharides would release from the hydrolysis of HA present in the hydrogels. Therefore, the degradation was monitored by quantifying the concentration of NAG reducing ends (**Figure 2.9**) in the supernatant (**Figure 4.13-A**). On day 0.8 and day 3, evident hydrogel degradation was observed when the hydrogels were incubated in both enzyme solutions, where higher concentration of NAG reducing ends were found in 50 U/ml HAase solution and

indicating enhanced degradation. However, after day three, degradation was not observed, even in presence of the enzyme. In fact, the hybrid hydrogels did not completely degrade as part of the hydrogels still remained in the HAase solution after day 14 (**Figure 4.13-B**). $(KI)_nK$-HA hydrogels incubated in PBS were only assessed on day 7 and 14, with relatively low concentration of NAG reducing ends detected in the supernatant, indicating the hydrogel remained stable in enzyme-free physiological conditions. Compared to the hybrid hydrogels incubated in PBS, which were relatively intact, hydrogels in HAase solutions have disintegrated into pieces. However, no evident changes on the hydrogel nanofiber structure were observed after enzyme incubation for 14 days (**Figure 4.13-C**).

The supramolecular peptide-HA assemblies were often observed to degrade in enzyme solutions. For example, in a study combining the self-assembling Fmoc-FF peptide system with HA, the resulting hydrogel also showed retarded degradation in HAase/PBS solution (20). However, the lack of hydrogel stability in physiological conditions makes degradation of hybrid hydrogel was evident even in the absence of the enzyme. Degradation of supramolecular PA-HA membrane in presence of HAase was observed within 14 days, but it remained stable in enzyme-free condition (5). In order for HAase to degrade HA, the enzyme would have to accommodate the polymer in its active site (21). It was hypothesised that the incomplete degradation of $(KI)_nK$-HA hydrogel could be due to interaction of some HA chains with peptide, remaining immobilized in the gel, while other HA chains were freer in the gel. The complete degradation of HA in the supramolecular hybrid hydrogel by HAase was supressed as the β-1,4 linkages (HAase cleavage site) in the immobilized HA were not accessible to the enzyme, corresponding to the intact nanofiber structures observed in SEM after incubation in the presence of HAase. Generally, the degradation test confirms that $(KI)_nK$-HA hydrogel is sensitive to HAase and would be able to be partially degraded in the presence of the enzyme under physiological conditions.
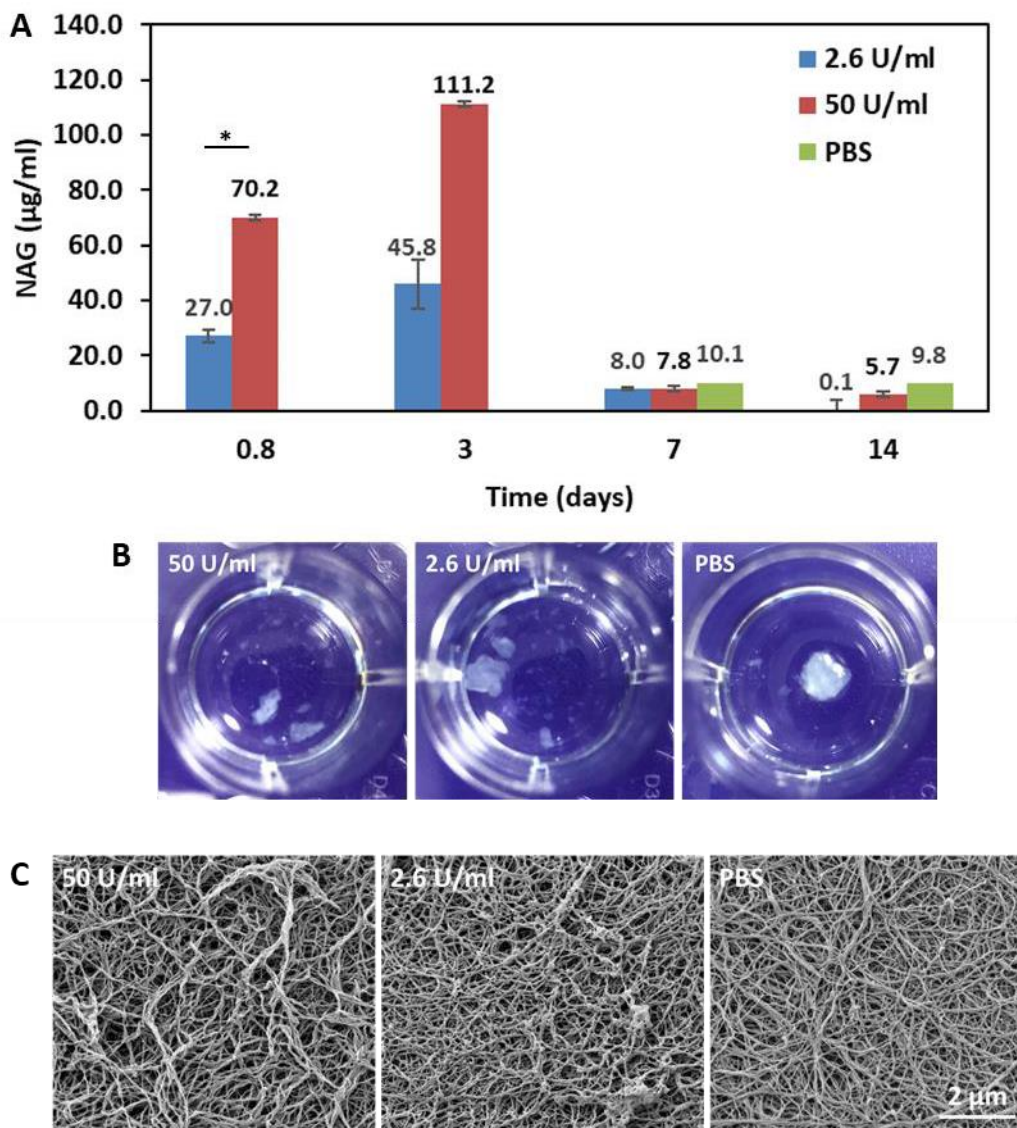
Figure 4.13: *Degradation of 2 wt% (KI)$_5$K-1 wt% HA hydrogel in PBS or PBS containing 2.6 U/ml and 50 U/ml HAase. (A) Quantification of N-acetylamino sugars released from the hydrogels. (*=p < 0.0332, error bars in 2.6 U/ml and 50 U/ml represent standard deviation (n = 3), and only one hydrogel sample was tested in PBS on day 7 and 14). (B) Digital and (C) SEM images of hydrogels after 14 days of incubation.*

4.6. Fabrication of (KI)$_n$K-HA hydrogel under shear stress

To develop anisotropic supramolecular peptide-HA membranes, either soft lithography (7) or electric field (22) has been used. However, these techniques are relatively complex requiring

152

the use of additional equipment for the experiment setting up, not always available in common labs. Consequently, it is worth to explore simpler methods to align nanofibers in the peptide-HA hydrogel. External shearing forces, which could be generated from varied approaches, including extruding, drawing, microfluid and electrospinning, offer the possibility to introduce long-range aligned nanofibers in an easier way. In order to create the anisotropic self-assembling peptide hydrogel, shear forces were often applied by pushing the peptide solution through the tip or needle. For example, Hartgerink's group reported MDP hydrogels achieving macroscopic anisotropy assisted by shearing forces through syringe delivery (23). When Stupp's group demonstrated the fabrication of an anisotropic self-assembled hydrogel using thermally treated liquid crystalline PA, the low strain forces produced by dragging the solution from a pipette tip contributed to the macroscopic alignment (24). However, this simple method was not used in the supramolecular peptide-HA systems probably due to the lack of injectability.

Supramolecular $(KI)_nK$-HA viscoelastic complex showed similar rheological behaviour as pure HA, with high independency of G' and G'' with frequency and large loss factor. Therefore, similar to HA, the liquid-like $(KI)_nK$-HA hybrid complex could be easily injected through a needle or tip. As the complex had a high viscous component, the recovery of deformation caused by the external force is likely to be slow, and it was found that the slow dynamic recovery could lead to the fibre alignment in self-assembling peptide system (25). The aligned nanofiber structure could be captured by covalent or ionic cross-linking (23, 24). Since the $(KI)_nK$-HA viscoelastic complexes, such as 2 wt% $(KI)_4K$-2 wt% HA, were shown to gelate in PBS, the shear induced deformation could be stabilized by the presence of counterions before recovery. In this study, 2 wt% $(KI)_4K$-2 wt% HA was injected through the tip using a micropipette, and the formed peptide-HA string was easily lifted by tweezers without breaking (**Figure 4.14-B**). Under the polarized microscope the string showed a birefringence indicative of a microscopically anisotropic structure (**Figure 4.14-A**) and aligned nanofibers were observed by SEM at the cross-section of the string (**Figure 4.14-C**).
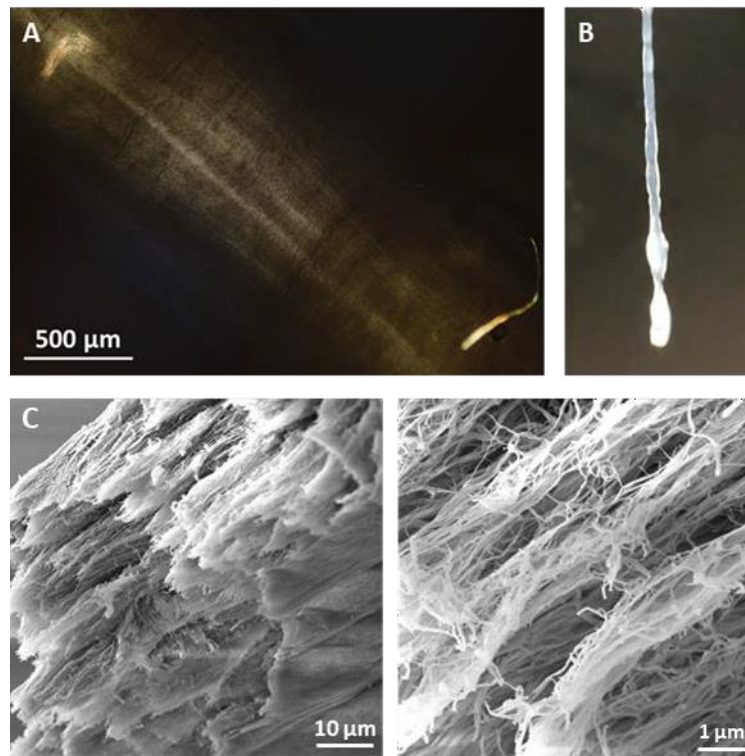
Figure 4.14: *(A) Polarized microscopy images and (B) digital image of 2 wt% (KI)$_4$K-2 wt% HA string. (C) SEM images showing the microstructures of the peptide-HA string.*

4.7. Conclusions

This chapter investigated the self-assembling (KI)$_n$K-HA system and demonstrated various approaches to form either single-phase or two-phase complexes, whose mechanical properties could be tuned by adjusting the concentration of the building blocks. By changing the peptide sequence and concentration, peptide-HA hydrogels with varied structures (homogeneous fibrous structure, porous and hierarchical structure) could be formed. These hybrid hydrogels were stable in physiological conditions where some transparent viscoelastic liquid-like complexes transformed into more cloudy hydrogels. Partial degradation of the hydrogel was enabled in presence of HA-degrading enzyme. Additionally, the formation of anisotropic peptide-HA string offers the possibility of using the hydrogel in hierarchical tissue regeneration (e.g. nerve). Generally, the biomimetic composition and structure of the

peptide-HA indicate the potential of peptide-HA hydrogels as physiological and pathologically relevant *in vitro* models. Their exploitation as *in vitro* models will be described in chapter 5.

4.8. References

1.   Burdick JA, Prestwich GD. Hyaluronic Acid Hydrogels for Biomedical Applications. Advanced Materials. 2011;23(12):H41-H56.

2.   Azevedo HS. Engineering Hyaluronan (HA) Hydrogels with Bioactive and Mechanical Signals. In: Singh TRR, Laverty, G., & Donnelly, R., editor. Hydrogels: Design, Synthesis and Application in Drug Delivery and Regenerative Medicine2017.

3.   Capito RM, Azevedo HS, Velichko YS, Mata A, Stupp SI. Self-assembly of large and small molecules into hierarchically ordered sacs and membranes. Science. 2008;319(5871):1812-6.

4.   Carvajal D, Bitton R, Mantei JR, Velichko YS, Stupp SI, Shull KR. Physical properties of hierarchically ordered self-assembled planar and spherical membranes. Soft Matter. 2010;6(8):1816-23.

5.   Ferreira DS, Marques AP, Reis RL, Azevedo HS. Hyaluronan and self-assembling peptides as building blocks to reconstruct the extracellular environment in skin tissue. Biomaterials Science. 2013;1(9):952-64.

6.   Ribeiro S, Radvar E, Shi Y, Borges J, Pirraco RP, Leonor IB, et al. Nanostructured interfacial self-assembled peptide-polymer membranes for enhanced mineralization and cell adhesion. Nanoscale. 2017;9(36):13670-82.

7.   Mendes AC, Smith KH, Tejeda-Montes E, Engel E, Reis RL, Azevedo HS, et al. Co-Assembled and Microfabricated Bioactive Membranes. Advanced Functional Materials. 2013;23(4):430-8.

8.   Guimarães CF, Gasperini L, Marques AP, Reis RL. The stiffness of living tissues and its implications for tissue engineering. Nature Reviews Materials. 2020;5(5):351-70.

9.   Ozbas B, Rajagopal K, Schneider JP, Pochan DJ. Semiflexible chain networks formed via self-assembly of beta-hairpin molecules. Phys Rev Lett. 2004;93(26 Pt 1):268106.

10.   Ozbas B, Kretsinger J, Rajagopal K, Schneider JP, Pochan DJ. Salt-Triggered Peptide Folding and Consequent Self-Assembly into Hydrogels with Tunable Modulus. Macromolecules. 2004;37(19):7331-7.

11.   Gouveia RM, Koudouna E, Jester J, Figueiredo F, Connon CJ. Template Curvature Influences Cell Alignment to Create Improved Human Corneal Tissue Equivalents. Advanced Biosystems. 2017;1(12):1700135.

12.   Kobayashi Y, Okamoto A, Nishinari K. Viscoelasticity of hyaluronic acid with different molecular weights. Biorheology. 1994;31(3):235-44.

13.   Cotey TJ, Sai H, Perez C, Palmer LC, Stupp SI. Hybrid gels via bulk interfacial complexation of supramolecular polymers and polyelectrolytes. Soft Matter. 2021;17(19):4949-56.

14.   Nadernezhad A, Forster L, Netti F, Adler-Abramovich L, Teßmar J, Groll J. Rheological analysis of the interplay between the molecular weight and concentration of hyaluronic acid in formulations of supramolecular HA/FmocFF hybrid hydrogels. Polymer Journal. 2020;52(8):1007-12.

15.   Mann BA, Kremer K, Holm C. The Swelling Behavior of Charged Hydrogels. Macromolecular Symposia. 2006;237(1):90-107.

16.   Calderón-Colón X, Xia Z, Breidenich JL, Mulreany DG, Guo Q, Uy OM, et al. Structure and properties of collagen vitrigel membranes for ocular repair and regeneration applications. Biomaterials. 2012;33(33):8286-95.

17.   Bitton R, Chow LW, Zha RH, Velichko YS, Pashuck ET, Stupp SI. Electrostatic Control of Structure in Self-Assembled Membranes. Small. 2014;10(3):500-5.

18.   Astériou T, Vincent JC, Tranchepain F, Deschrevel B. Inhibition of hyaluronan hydrolysis catalysed by hyaluronidase at high substrate concentration and low ionic strength. Matrix Biol. 2006;25(3):166-74.

19.   Delpech B, Bertrand P, Chauzy C. An indirect enzymoimmunological assay for hyaluronidase. J Immunol Methods. 1987;104(1-2):223-9.

20.   Aviv M, Halperin-Sternfeld M, Grigoriants I, Buzhansky L, Mironi-Harpaz I, Seliktar D, et al. Improving the Mechanical Rigidity of Hyaluronic Acid by Integration of a Supramolecular Peptide Matrix. ACS Applied Materials & Interfaces. 2018;10(49):41883-91.

21.   Stern R, Jedrzejas MJ. Hyaluronidases: their genomics, structures, and mechanisms of action. Chem Rev. 2006;106(3):818-39.

22.   Velichko YS, Mantei JR, Bitton R, Carvajal D, Shull KR, Stupp SI. Electric Field Controlled Self-Assembly of Hierarchically Ordered Membranes. Advanced Functional Materials. 2012;22(2):369-77.

23.   Li IC, Hartgerink JD. Covalent Capture of Aligned Self-Assembling Nanofibers. Journal of the American Chemical Society. 2017;139(23):8044-50.

24.   Zhang S, Greenfield MA, Mata A, Palmer LC, Bitton R, Mantei JR, et al. A self-assembly pathway to aligned monodomain gels. Nat Mater. 2010;9(7):594-601.

25.   Wychowaniec JK, Smith AM, Ligorio C, Mykhaylyk OO, Miller AF, Saiani A. Role of Sheet-Edge Interactions in β-sheet Self-Assembling Peptide Hydrogels. Biomacromolecules. 2020;21(6):2285-97.

4.9. Appendix
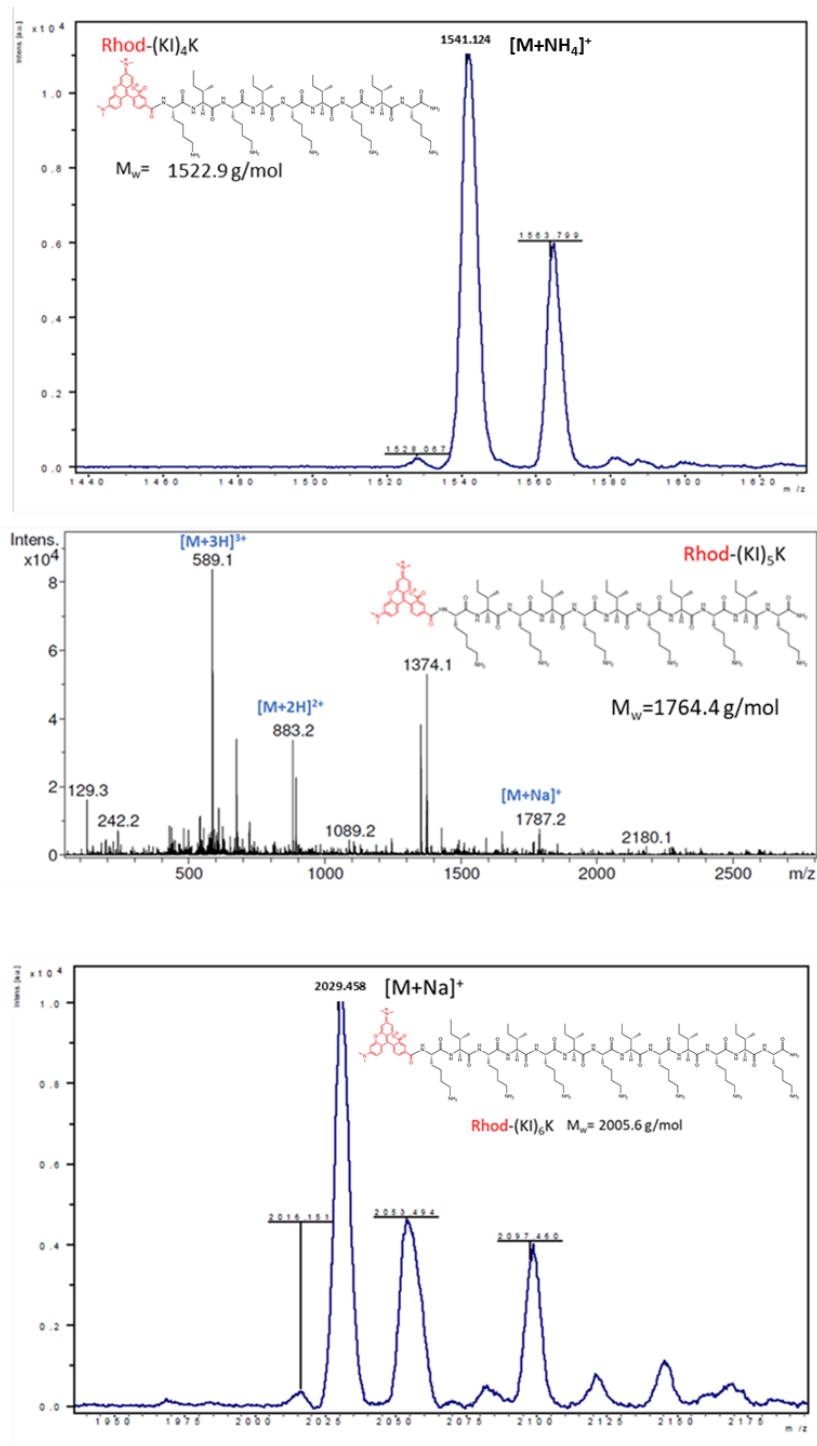
Figure 4.15: *The mass spectrum and chemical structures of Rhod-(KI)$_4$K, Rhod-(KI)$_5$K and Rhod-(KI)$_6$K.*

Chapter 5

In vitro applications of supramolecular peptide-hyaluronan hydrogels

5. *In vitro* applications of supramolecular peptide-hyaluronan hydrogels

5.1. Introduction

The compositional and structural similarity of supramolecular peptide-HA hydrogels with native extracellular matrices (ECMs) suggests the possibility of exploiting them as *in vitro* models of tissues. For example, they could be used as surrogate of the human vitreous, the transparent hydrogel filling the space between the lens and the retina (**Figure 5.1-A**), which is vital to the eye in terms of its mechanical stability, biochemical transport, and optical clarity (1, 2). Additionally, the treatment of posterior segment diseases often relies on the direct via injection of drugs into the vitreous, where their diffusion in the vitreous would depend on the interactions with vitreous components and movement through the vitreous network.
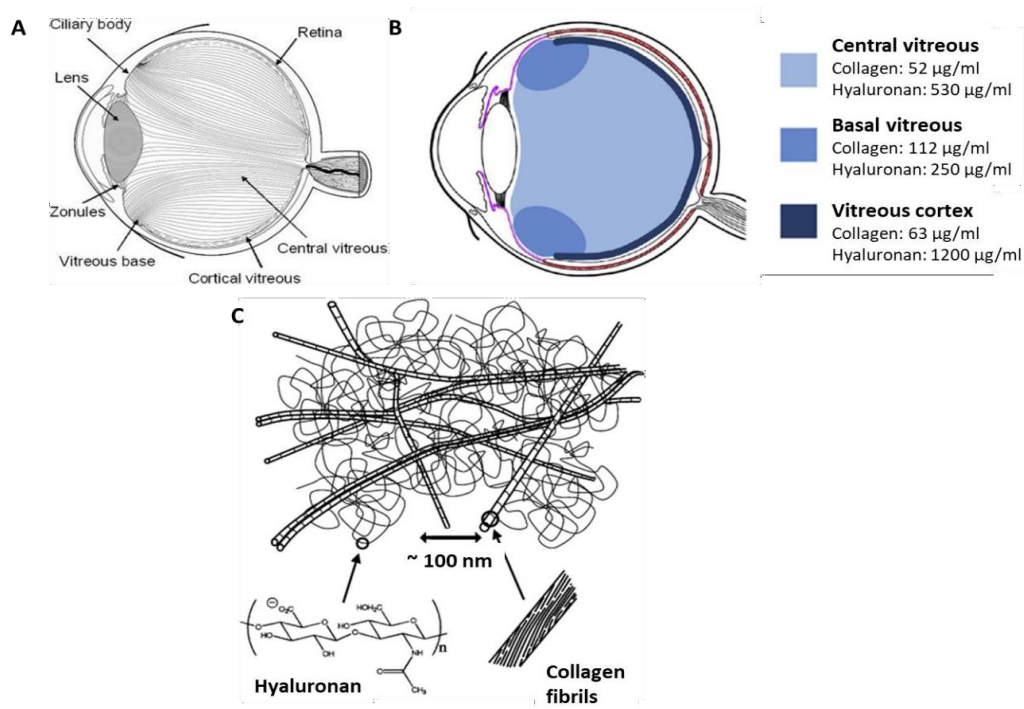
Figure 5.1: *(A) Schematic overview of the human eye (adapted from ref (2)). (B) The vitreous is anatomically subdivided into three different regions: central vitreous, basal vitreous and vitreous cortex (adapted from ref (3)). (C) Schematic representation of the cooperation between two networks responsible for the gel structure of the vitreous (adapted from ref (4)).*

The human vitreous is composed of a double network of collagen fibrils and HA (**Figure 5.1-C**), where the collagen network maintains the gel state and provides the vitreous with tensile strength, and the HA network fills the spaces between the collagen fibrils and provides a swelling pressure to inflate the gel (4), and the vitreous has a heterogeneous structure as the concentration of collagen and HA are varied in different part of the vitreous (**Figure 5.1-B**). The supramolecular peptide-HA hydrogels are expected to replicate the collagen-HA complex of the human vitreous, which could be further developed as *in vitro* vitreous model for drug diffusion studies.

On the other hand, the supramolecular peptide-HA hydrogel can also offer a 3D culturing platform for studying the behaviour of stem cells. It is well known that mesenchymal stem cells (MSCs) are able to differentiate into many mesodermal tissues, such as bone, cartilage, fat, neuron, and muscle, and have been regarded as promising cell source for cell-based tissue repair and regeneration. The conventional technique to maintain MSCs *in vitro* is 2D adherent cell culture. However, this culture setup limits cell-cell and cell-substrate interactions which may compromise cell viability and differentiation potential (5). Compared to the traditional 2D monolayer cell culture, 3D multicellular MSC spheroids often exhibit enhanced anti-inflammatory effects, improved differentiation capacity and increased cell survival after transplantation with the advantage of promoting cell–cell communication, as well as increased secretion of pro-angiogenic factors and ECM by the inner cells due to the hypoxic microenvironment (6, 7). The biological significance of MSC spheroids is becoming a new trend in tissue engineering. Stem cell spheroids can be generated through hanging drop, non-adherent surfaces, micropatterned surfaces, suspension culture, microfluidic system and polycation coated surface (e.g. chitosan coated well plate) (5). However, these technologies fail to provide an ECM-like environment for MSC spheroid formation. The ECM is a dynamic hybrid structure composed of various fibrillar proteins and glycosaminoglycans, which would serve as 3D substrate for cell adhesion and migration (8). Introduction of MSC spheroids into 3D scaffolds has become increasingly popular in tissue regeneration studies since the 3D

environment can often promote cell differentiation. For example, MSC spheroid-loaded macroporous scaffolds secreted more cartilage-associated ECM than single-cell seeded scaffold in the corresponding induction medium, and showed superior cartilage regeneration *in vivo* (9). MSC spheroids were found to more effectively encourage to differentiation of neuronal stem cell in collagen hydrogel than dissociated MSC, which shed insight in the development of neural regeneration (10). Hydrogels are excellent scaffolds for cell culture as they can mimic salient elements of native ECM and mechanically resemble the soft tissue (11). However, hydrogel-based MSC spheroids culture often requires transferring the pre-formed MSC spheroids into the desired place, which is time-consuming and may also disturb and damage the MSC spheroids. In this work, a novel and easy method of *in situ* generating MSC spheroids on hydrogel is presented, where MSC would spontaneously form spheroids directly on the hydrogel. As demonstrated in the former chapters, the supramolecular peptide-HA hydrogel resembles structure and component of native ECMs, which could provide an ECM-like microenvironment to MSC spheroids. To further elucidate the ability of peptide-HA to induce MSC spheroid formation, peptide-alginate hydrogels and peptide-polymer membranes were also used in this work.

This chapter reports the potential of peptide-HA hydrogels, whose physico-chemical properties were described in previous chapters, as *in vitro* models for biomedical applications.

5.2. Supramolecular peptide-HA hydrogel as *in vitro* vitreous model

Considering the composition and nanoarchitecture of peptide-HA hydrogels, their potential as an *in vitro* vitreous model for studying drug diffusion was exploited. Animal (*ex vivo*) vitreous are the gold standard used in intravitreal drug delivery research. To make direct comparisons in terms of structural and rheological properties, ovine and porcine vitreous were obtained. It was found that liquid flowed out of the vitreous immediately after being removed from the eyeball. The liquid was collected, and its zeta potential measured, revealing

negative zeta potential (-10.2 ± 1.3 mV) and indicating the liquid might contain HA-based complex. This observation also highlights the fragility of the vitreous and the need of a trained person to properly dissect the vitreous from the eye without altering its properties.

SEM images showed a nanofiber network structure of the animal vitreous (**Figure 5.2**). Previous studies showed that vitreous is not a homogeneous structure, with the cortex vitreous being the densest part, followed by basal vitreous and central vitreous (12). However, in this experiment, the density of the nanofibers from the different vitreous parts was found to be similar. The possible reason could be that the areas were not correctly identified. Because the vitreous samples suffered from serious shrinkage during sample preparation, SEM images may not represent the real nanofiber density.
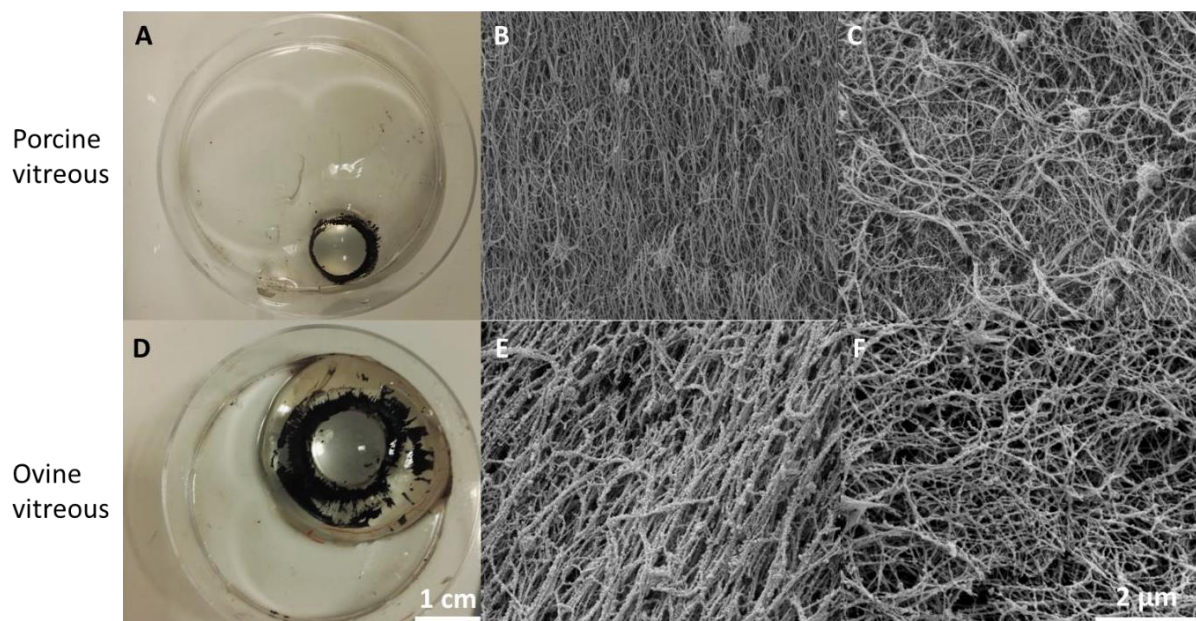
Figure 5.2: *Photographs of porcine (A) and ovine (D) vitreous attached to the lens and iris. SEM images showing the microstructure of porcine basal vitreous (B), porcine central vitreous (C), ovine basal vitreous (E) and ovine central vitreous (F). Small globules in the image could be vitreous cells (hyalocytes) which are sparsely found in the vitreous.*

Rheology is an important property for the characterization of the vitreous. In this study, the frequency varied from 0.1 to 10 Hz, while the amplitude of the shear stress was kept constant

at 0.1% strain which was found to be within the LVR. At a low frequency of 0.1 Hz, ovine vitreous had G' of 17.63 Pa and G'' of 12.38 Pa and porcine vitreous had G' of 0.78 Pa and G'' of 0.34 Pa. Both animal vitreous showed higher G' than G'' within the measured frequency range, indicating their gel state (**Figure 5.3-A and B**).

Suitable *in vitro* vitreous model should structurally and mechanically mimic the natural vitreous. It has been shown that supramolecular $(KI)_nK$-HA hydrogels share the similar nanofibrous network structures with animal vitreous according to the SEM images. However, rheological studies suggests that animal vitreous are super soft viscoelastic materials, and all the $(KI)_nK$-HA hydrogels designed in this work are far stiffer than vitreous. It is worth to notice that vitreous exhibit relatively large loss factor (G''/G') indicating the high viscous component, and the similar behaviour is also observed in some of $(KI)_nK$-HA hydrogels (**Figure 5.3-C**). However, lowering down the stiffness of $(KI)_nK$-HA hydrogel and at the same time maintaining the gel state (G'>G'') still remains a challenge. Though it was found that the concentration of collagen and HA is low in the vitreous (52 µg/ml of collagen and 530 µg/ml of HA in the central vitreous) (3), mixing low concentration peptide and HA solutions would not form the hydrogel (data not shown). Instead, it often led to the formation of a white precipitation. Enzymatic degradation of hydrogel might be another strategy to soften the hydrogel as lower G' was found in enzyme (collagenase, trypsin or HAase) treated vitreous compared to the untreated one (13). However, in this work the peptide-HA hydrogel was only found to collapse into small pieces after incubation in HAase solution, as shown in **Figure 4.10-B**.

It is arguable that microrheology may better reflect the mechanical properties of the vitreous compared to the conventional bulk rheology, which probe the local rheological properties in an extended frequency range by analysing the mobilities of nanoparticels with varied sizes and charges in the vitreous. It would also be possible to explore the microstructure of the vitreous by microrheology, as Xu et al. estimated that the average size of bovine vitreous to be 550±50 nm by analysing the nanoparticle diffusion (14). Meanwhile, Kosdarf et al. found that the diffusion of positively charged nanoparticles in the vitreous were supressed as the

vitreous carries an overall negative charge due to the existence of polyanionic GAGs (e.g. HA) (15).
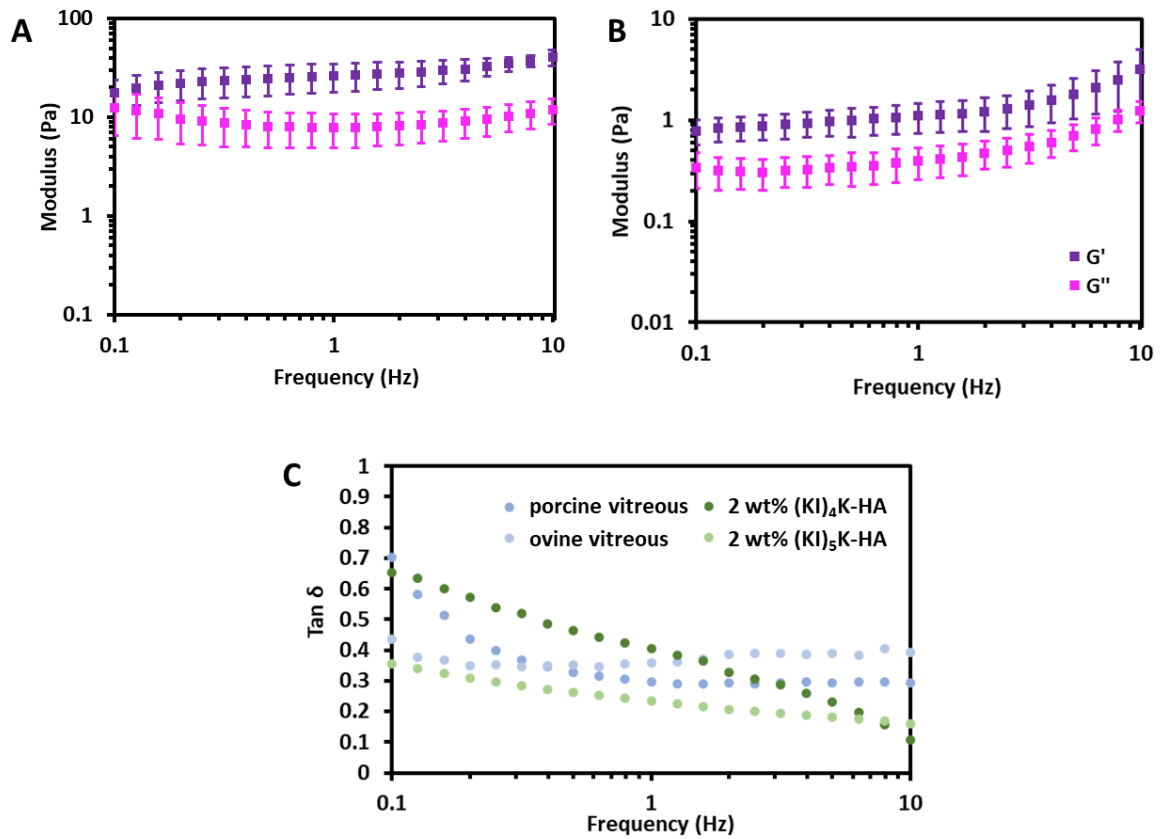
Figure 5.3: *Bulk rheology study of (A) porcine and (B) ovine vitreous (Error bars represent standard deviation (n = 3)). (C) Loss factor (Tan δ) of vitreous and hydrogel measured by frequency sweep using rheometer.*

Ideally, the *in vitro* vitreous model should have a similar mesh size with the natural vitreous and also carry negative charges, so comparing the microrheology data of vitreous and *in vitro* vitreous model would be important.

5.3. MSCs culture on supramolecular peptide-polymer hydrogel

5.3.1. Formation of MSC spheroids on supramolecular peptide-HA hydrogel

As described in Chapter IV, the supramolecular hybrid hydrogel $(KI)_4K$-HA, $(KI)_5K$-HA and $(KI)_6K$-HA were shown to be stable in cell culture media (DMEM). Therefore MSCs, which were trypsinized from the standard 2D adherent cell culture, were added on the top of 1 wt% $(KI)_4K$-HA, 1 wt% $(KI)_5K$-HA and 1 wt% $(KI)_6K$-HA hydrogels. However, it was found that the cell-seeded 1 wt% $(KI)_4K$-HA hydrogels were not stable and easily collapsed. Cell spheroids were observed on day 3, on both 1 wt% $(KI)_5K$-HA and 1 wt% $(KI)_6K$-HA hydrogel (**Figure 5.4-A and B**). In some of the spheroids, cells on the exterior and interior have different morphology, with cells on the border of the spheroids tending to be more elongated and extended. Additionally, some elongated cells on the border would gradually migrate out of the spheroid in the following days (**Figure 5.4-D and E**), which is commonly observed in MSC spheroids when maintained in the growth media (16, 17). The diameter of spheroids on 1 wt% $(KI)_5K$-HA hydrogel is 89.0 ± 30.1 µm, which appears to be significantly larger than 1 wt% $(KI)_6K$-HA hydrogel (42.2 ± 15.2 µm). (**Figure 5.4-C**). In the MSC spheroids, there could be a reduced diffusion of nutrients, oxygen, and waste as aggregated cells creating spatial hindrance, thus the viability of cells, especially the cells at the core of the spheroids might be comprised (6). The viability of MSC in the spheroid was examined (**Figure 5.5**) where live cells were stained green and dead cells-stained red. It can be observed that dissociated cells and cell spheroids on both peptide-HA hydrogels have good viability, and the morphology change of the cells is over time is also evident. On day 1, the majority of the cells adopted a round shape in contrast to the standard 2D monolayer culture (**Figure 5.14**), where MSCs often exhibit spindle-like morphology.
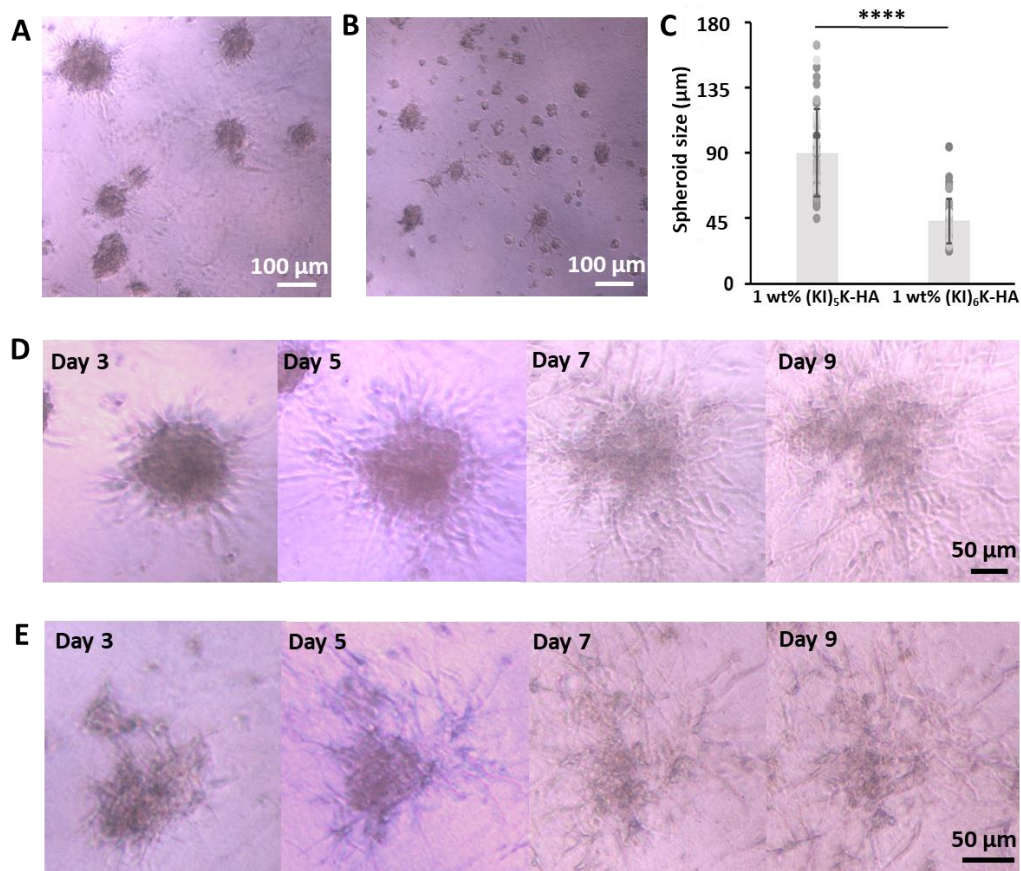
Figure 5.4: *MSC spheroids formed on the (A) 1 wt% (KI)$_5$K-HA and (B) 1 wt% (KI)$_6$K-HA hydrogel observed by optical microscope on day 3, and (C) the analysis of spheroid size (****=p < 0.0001, and error bars represent standard deviation (n = 40)). The disassembly of the MSC spheroid on (D) 1 wt% (KI)$_5$K- HA and (E) 1 wt% (KI)$_6$K-HA hydrogels was also observed around 9 days.*

The initial round morphology induces spheroid formation, as 'cell rounding' is known to be the initial step of self-assembly of multicellular aggregates (7), and cells already showed aggregation tendency on 1 wt% (KI)$_5$K-HA hydrogel. On day 3, MSC spheroids were found on both hydrogels, and on day 7 the core of the spheroid on 1 wt% (KI)$_5$K-HA hydrogel appeared to be looser, while on 1 wt% (KI)$_6$K-HA hydrogel only some cell assemblies remained, and dissociated cells exhibited an extended morphology.
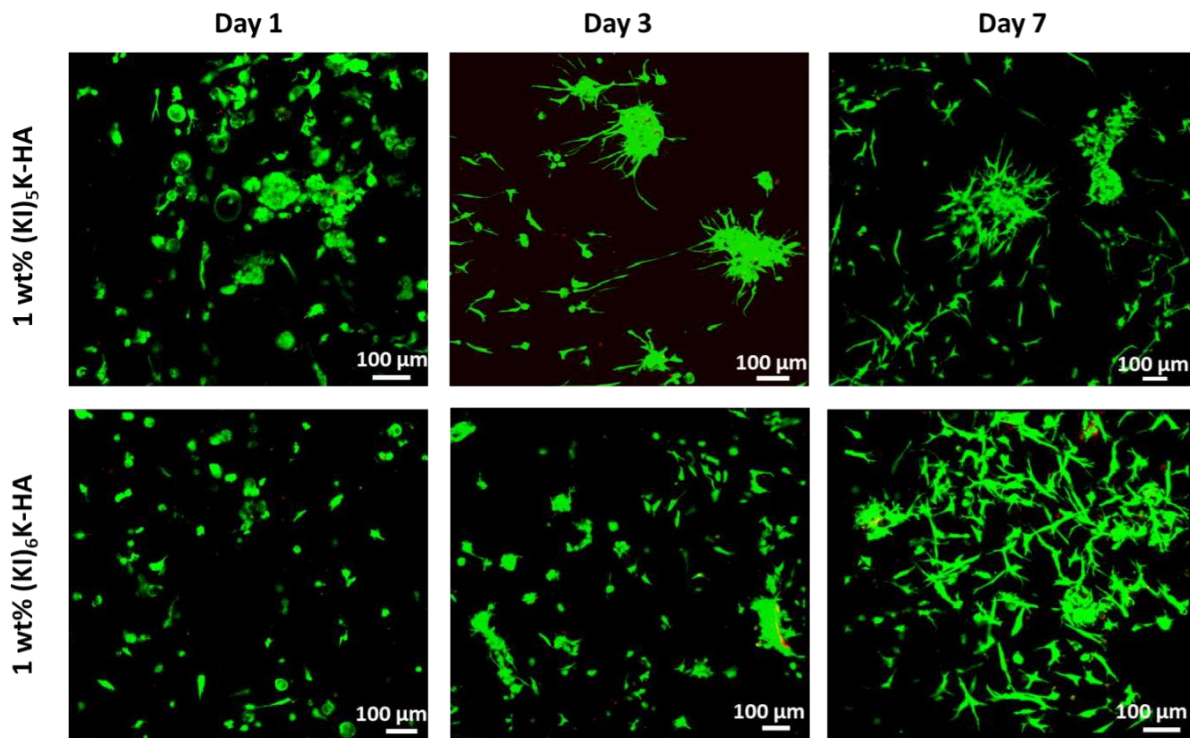
Figure 5.5: CLSM of calcein-stained live MSCs (green) and ethidium homodimer-stained dead cells (red) on peptide-HA hydrogels.

SEM images were obtained to observe the interaction between the spheroid and the hydrogel substrate, as shown in **Figure 5.6** on day 7. In 1 wt% (KI)$_5$K-HA hydrogel, MSC spheroid were found trapped inside the hydrogel. At the edge of the spheroid, some of the cells were found to extend outward and entangle with nanofibers of the hydrogel (white arrow), while round cells could also be observed inside the spheroid. Cells at the core of the cell spheroid often displayed spherical morphology whose size is significantly smaller than in 2D monolayer culture (6). On 1 wt% (KI)$_6$K-HA hydrogel, MSC assembles were found on the surface of the hydrogel, and there was the formation of filopodia at the outskirt of the cell assembly was observed. Filopodia on the edge of cells is typically prominent during initial cell adhesion on 2D substrate and might also indicate further cell migration (18, 19). The existence of filopodia may suggest cells were migrating out of the cell assemblies and adhering to the hydrogel surface on day 7. It is interesting to notice that cell assemblies on 1 wt% (KI)$_6$K-HA hydrogel

display the typical cell behaviour of both 2D (presence of filopodia and relatively higher flattening degree) and 3D (cells aggregated and stacked), which is likely caused by the 'competition' between cell-substrate and cell-cell adhesion, as the cell aggregation fate is determined by cell-substrate and cell-cell adhesion interactions (20).

1 wt% $(KI)_5K$-HA

1 wt% $(KI)_6K$-HA
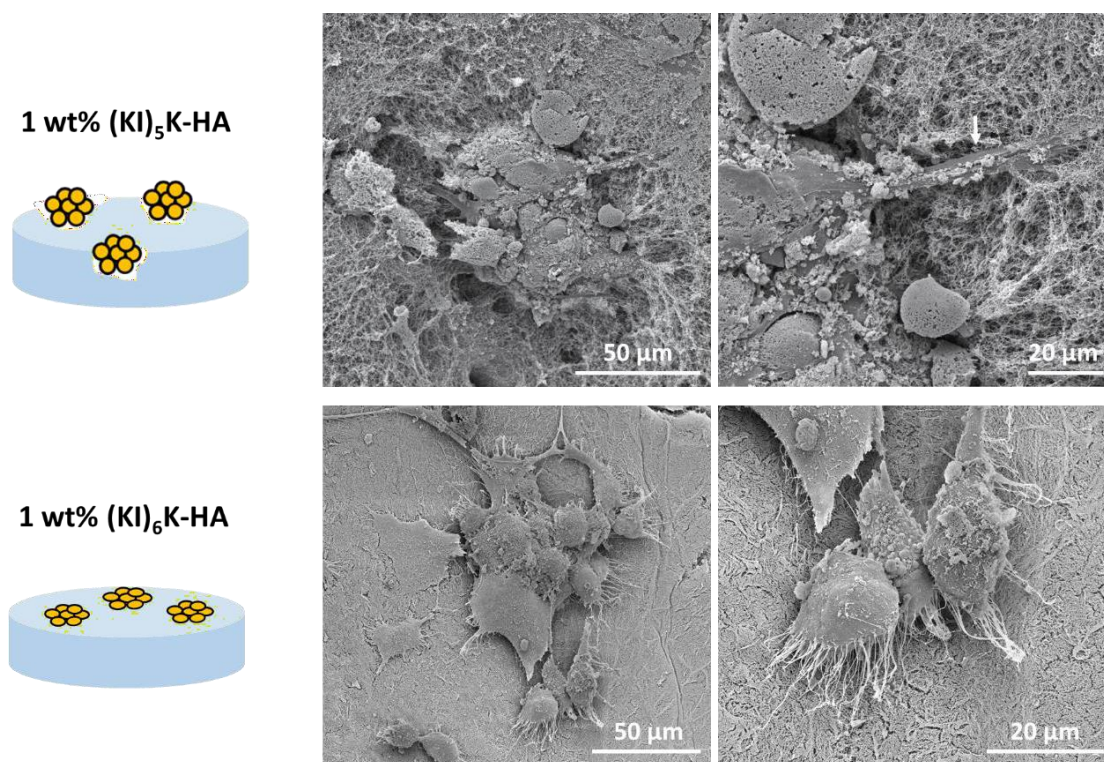
Figure 5.6: SEM images of MSC assemblies on supramolecular peptide-HA hydrogels on day 7.

It is noticeable that many disassociate cells were also present on day 7, which are composed of cells migrating out of the spheroid and cells not involved in the spheroid formation, exhibiting spindle-like or spreading morphology indicating the good cell adhesion (**Figure 5.7**). Disassociated cells on 1 wt% $(KI)_5K$-HA hydrogel (white arrows) were not completely visible as they were entrapped in the hydrogel, while cells on 1 wt% $(KI)_6K$-HA hydrogel were clearly residing on the hydrogel surface.
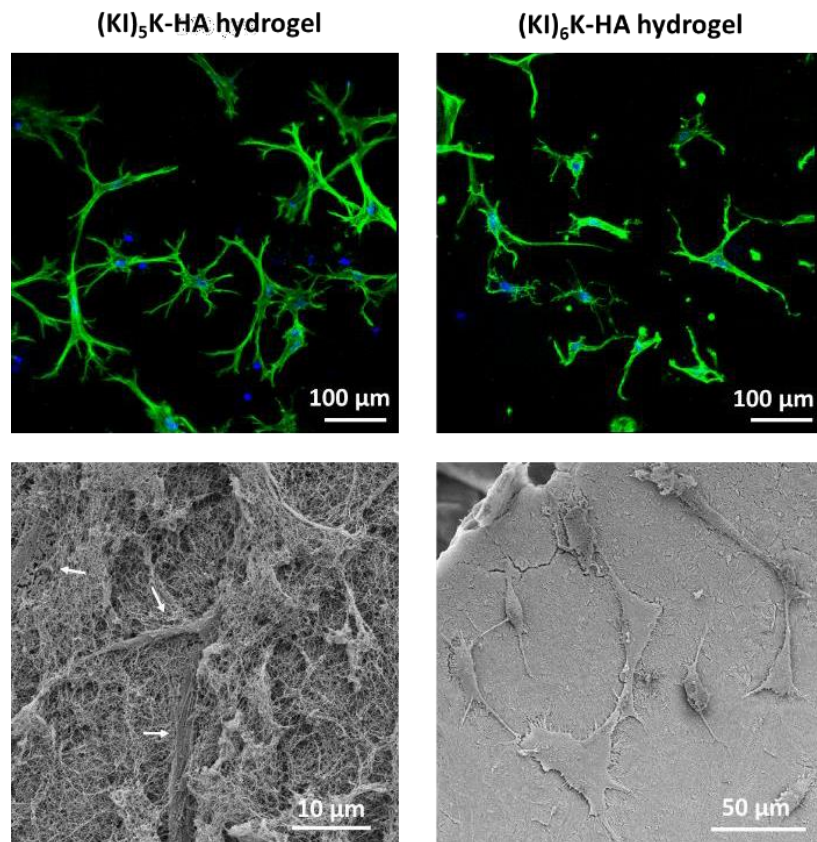
Figure 5.7: *CLSM and SEM images of disassociated MSCs cultured on peptide-HA hydrogels on day 7. F-actin was labelled with FITC-phalloidin (green) and nuclei with DAPI (blue).*

The mechanical environment surrounding the cell spheroids is considered an important factor regulating the cell behaviour. The rheology of the supramolecular peptide-HA hydrogel incubated in culture media overnight is shown in **Figure 5.8**. Both hydrogels exhibit viscoelastic behaviour, where hydrogels generally have small G' and large loss factor (0.57 for 1 wt% $(KI)_5K$-HA and 0.52 for 1 wt% $(KI)_6K$-HA at 0.1 Hz). The hydrogels showed frequency-dependent rheology performance, which would behave as elastic solids at short time scales (high frequency) and viscous fluids at long time scale (low frequency) mechanically mimic the soft tissue. The formation of cell spheroid on the substrate could be analogous to the liquid drop in the suspension method for obtaining spheroid shape (20). The large viscous

component of the hydrogel at low frequencies is assumed to contribute to the MSC spheroid formation as it offers viscous liquid-like microenvironment at long time scale.

The bulk rheology study shows that 1 wt% $(KI)_6K$-HA (0.4 kPa at 0.1 Hz) has a relatively lower G' than 1 wt% $(KI)_5K$-HA hydrogel (0.7 kPa at 0.1 Hz). However, it is assumed that not only bulk rheology but also surface microstructure could affect the morphology of MSC assemblies. It is noticeable that 1 wt% $(KI)_6K$-HA hydrogel has a denser surface than 1 wt% $(KI)_5K$-HA (**Figure 5.8**), in which the denser surface might exhibit a larger yield stress. Consequently, the stress (caused by the gravity of the cell spheroid) applied on the surface might be higher than the yield stress of 1 wt% $(KI)_5K$-HA hydrogel surface, which lead to the permanent surface deformation so that spheroid was found trapped inside the hydrogel. While for 1 wt% $(KI)_6K$-HA, the applied stress may be lower than the surface yield stress, thus the spheroid would reside on the surface of the hydrogel.
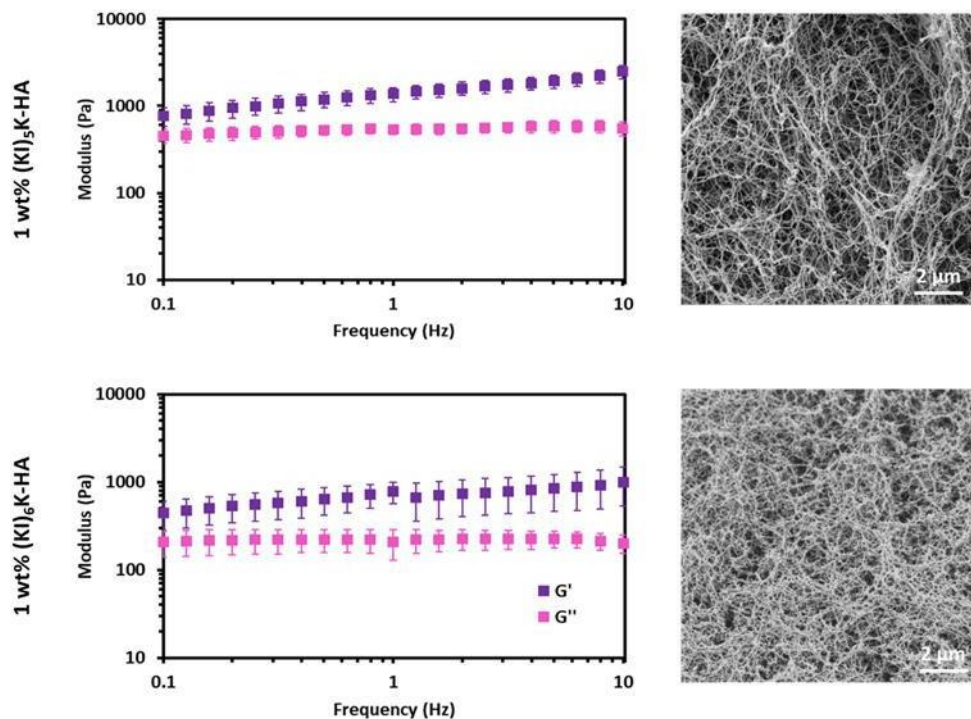
Figure 5.8: Bulk rheology property and surface SEM images of 1 wt% $(KI)_5K$-HA and 1 wt% $(KI)_6K$-HA cell-free hydrogel. Both hydrogels were incubated in DMEM with 10% FBS overnight. Error bars represent standard deviation (n = 3).

As describe in chapter 4, increasing concentration of the peptide enhanced the bulk stiffness of the supramolecular peptide-HA hydrogel. 2 wt% $(KI)_5K$-HA hydrogel has bulk G' around 2.0 kPa at 0.1 Hz in water (**Figure 4.3**), and based on the typical supramolecular hydrogels are often stiffer in physiological conditions (e.g. DMEM and PBS) than in water. Though G' of 2 wt% $(KI)_5K$-HA hydrogel is much higher than of 1 wt% $(KI)_5K$-HA or 1 wt% $(KI)_6K$-HA hydrogel, the rheology behaviour of 2 wt% $(KI)_5K$-HA also exhibits frequency dependency as G' and G'' increased with the frequencies. It was observed that sphere-like structures could be found 3 days after MSCs seeding on the surface of 2 wt% $(KI)_5K$-HA (**Figure-5.9 A**). However, after 7 days, the sphere-like structure disappeared and most cells exhibited fully spreading morphology (**Figure 5.9-B and D**) confirming the strong interaction between the cell and the substrate, which could often be observed in typical 2D cell culture (21).
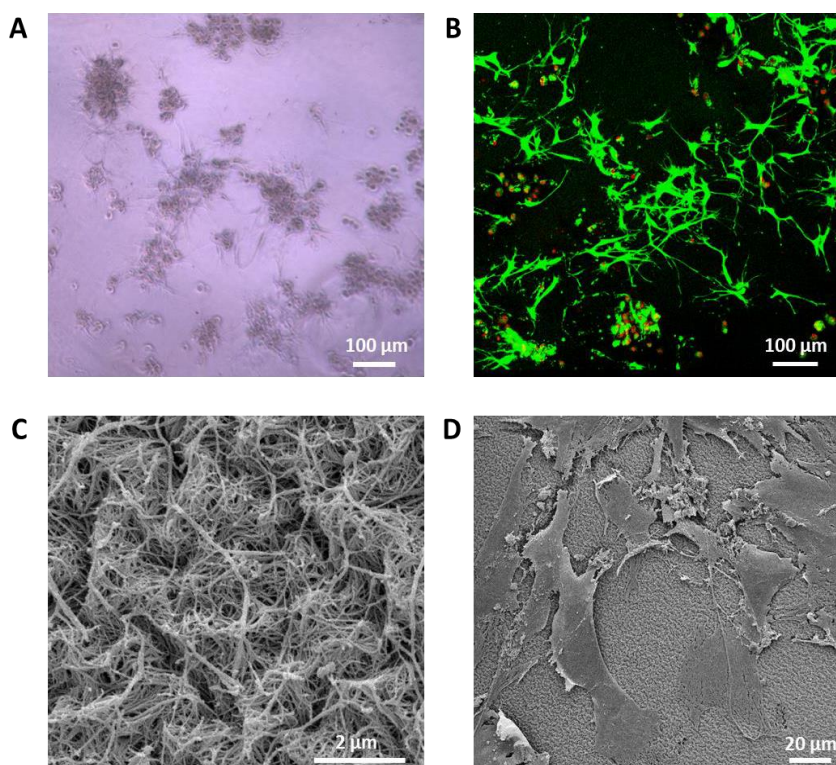
Figure 5.9: *MSCs on 2 wt% $(KI)_5K$-HA hydrogel observed by (A) optical microscopy on day 3 and (B) CLSM of calcein-stained live cells (green) and ethidium homodimer-stained dead cells (red) on day 7. (C) SEM image of the hydrogel surface after incubated in DMEM with 10% FBS overnight. (D) SEM image of cells on the hydrogel on day 7.*

The denser surface of 2 wt% (KI)$_5$K-HA (**Figure 5.9-C)** and the relatively higher hydrogel stiffness may, altogether, contribute to the flat morphology of MSCs on day 7. This experiment indicates that MSCs are still able to self-assemble on a relatively stiffer supramolecular peptide-HA hydrogels.

**5.3.2. MSC morphology on supramolecular peptide-alginate hydrogel**

Cells seeded on other supramolecular peptide-HA hydrogel or membrane have never been observed to form spheroid. For example, periosteum-derived cells showed good adhesion on K$_3$(QL)$_6$E$_2$-HA membrane with or without the presence of serum and C$_{16}$V$_3$A$_3$K$_3$-HA membrane also supported the adherence of human dermal fibroblasts in DMEM with 10% FBS, and cell on both membrane exhibit spreading morphology (22, 23). On K$_2$(QL)$_6$K$_2$-HA membrane it was found that MSCs would exhibit round-shape morphology (24). Therefore, it is hypothesized that (KI)$_n$K peptide plays an important role in the spheroid formation. On the other hand, it was found that chitosan-HA membrane would induce the formation of MSC spheroid, where the increasing HA content would lead to the larger size of the spheroid, indicating that HA may also encouraged the spheroid formation (17). To gain insights on the mechanism of cell spheroid formation on 1 wt% (KI)$_5$K-HA and 1 wt% (KI)$_6$K-HA hydrogels, supramolecular peptide-alginate hydrogels were also utilized as scaffold for the MSC seeding in order to explore the compositional contribution to the spheroid formation on peptide-HA hydrogel. MSCs were seeded on supramolecular hybrid hydrogel 1 wt% (KI)$_3$K-alginate, 1 wt% (KI)$_4$K-alginate, 1 wt% (KI)$_5$K-alginate and 1 wt% (KI)$_6$K-alginate. All hydrogels were stable in cell culture media DMEM except (KI)$_3$K-alginate hydrogel. It was found that most MSCs remained to be round in 7 days of culture on the supramolecular peptide-alginate hydrogels. The viability of cells on day 7 is shown in **Figure 5.10**. Cells showed good overall viability on the hydrogels but most cells showed little aggregation tendency.
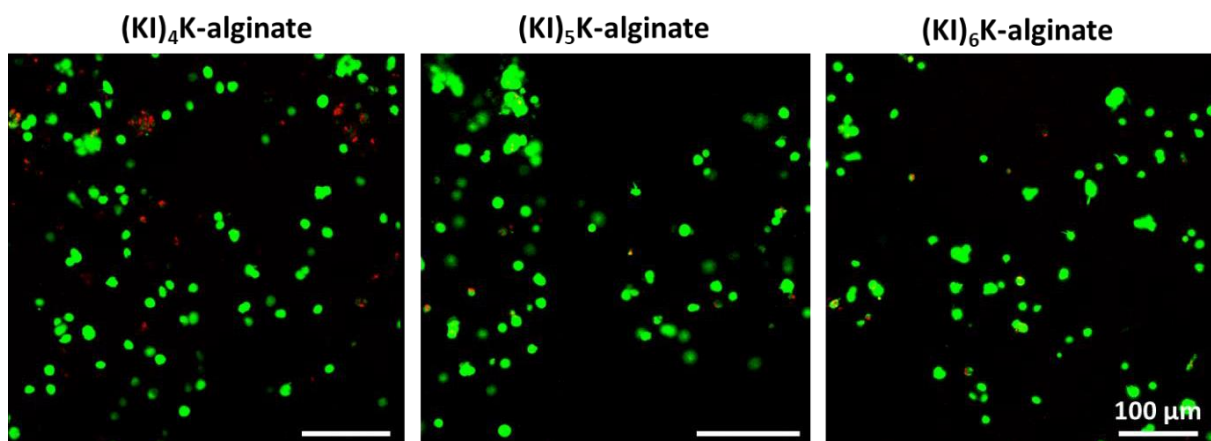
Figure 5.10: *CLSM of calcein-stained live cells (green) and ethidium homodimer-stained dead cells (red) on peptide-alginate hydrogels on day 7.*

SEM images show that MSCs are easily identified on the surface of three peptide-alginate hydrogels on day 7 existing as morphological heterogeneous population (**Figure 5.11 A-C**). Most cells tend to be round (**Figure 5.11-E, G, H and I**), while some of cells are flat and adhere to the surface (**Figure 5.11-D and F**). **Figure 5.11-J** shows that more than half of cells were round on the surface of all peptide-alginate hydrogels on day 7, where (KI)$_4$K-alginate hydrogel has the lowest ratio of cells exhibiting flat morphology. The formation of filopodia and lamellipodia (red arrow) indicates good cell-substrate communication. Meanwhile, blebs (green arrow, round-shape structures) and microspikes (yellow arrow, short fibril-like structures), which often appeared at the early stage of cell adhesion, could be found on the surface of round cells (18). In particular, the existence of blebs may also suggest loss of substrate adhesion ability of the cells (25). It is noticeable that pseudopodia (white arrow), which is often associated with the transient adhesion during migration, was also occasionally found on the cells (18). Generally, the SEM images of the cells at high magnification reveals that MSCs are still capable of attaching to the surface of peptide-alginate hydrogel with intense cell-substrate communication and a potential migration ability.

The three supramolecular peptide-alginate hydrogels show similar bulk rheology behaviour (**Figure 5.11 K**). Compared to the peptide-HA hydrogels, peptide-alginate hydrogels have

higher G' (5.3 kPa for (KI)$_4$K-alginate, 3.6 kPa for (KI)$_5$K-alginate and 4.7 kPa for (KI)$_6$K-alginate hydrogel at 0.1 Hz) relatively independent with the frequency change, and lower loss factor (0.29 for (KI)$_4$K-alginate, 0.30 for (KI)$_5$K-alginate and 0.28 for (KI)$_6$K-alginate hydrogel at 0.1 Hz). In addition, peptide-alginate hydrogels also exhibit denser surfaces (**Figure 5.15**). Generally, peptide-alginate hydrogels display relatively higher stiffness and more elastic performance compared to peptide-HA hydrogels, especially 1 wt% (KI)$_5$K-HA and 1 wt% (KI)$_6$K-HA hydrogel. For common 2D cell culture soft surfaces are more likely to result in poor cell adhesion compared to stiffer surfaces (26, 27). However, in this work disassociated MSCs on peptide-HA hydrogels showed better adhesion than cells on peptide-alginate hydrogels on day 7, despite the latter hydrogel tends to be stiffer.

The majority of MSCs on peptide-HA hydrogels remained round on day 1 and the self-aggregation of cells could be observed on day 3. However, cell spheroid disassembly was observed on day 7. However, on peptide-alginate hydrogel, most cells kept a globular shape, and no obvious aggregation could be observed up to day 7. As HA is known to strongly involve in cell adhesion and migration (28), it is believed that HA plays an essential role in the formation of MSC spheroid on the supramolecular peptide-HA hydrogel.
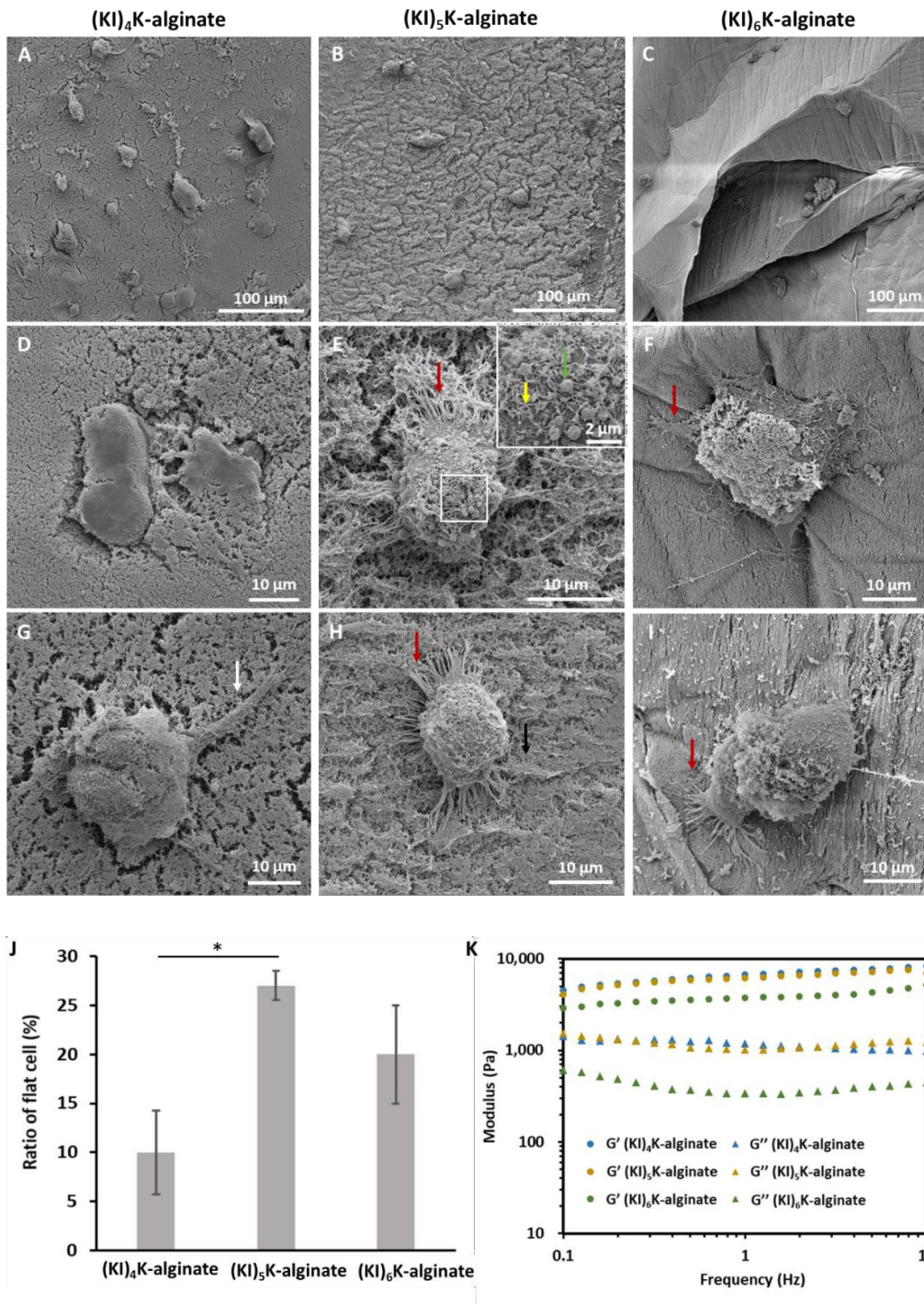
Figure 5.11: *(A-I) SEM images of MSCs on peptide-alginate hydrogels on day 7, and the higher magnified image in (E) shows the cell surface. (J) The analysis of ratio of cell exhibiting flat morphology on peptide-alginate hydrogels on day 7. (K) Bulk rheology measurement of 1 wt% peptide-alginate cell-free hydrogels incubated in DMEM with 10% FBS overnight. (*=p < 0.0332, and error bars represent standard deviation (n = 3)).*

In order to explore if MSCs would migrate on the supramolecular peptide-alginate hydrogels and aggregate at longer times, the cell seeded hydrogels were incubated for 14 days. Small cell clusters composed of a few cells could be observed on the hydrogel on day 14, while cells tend to be more separated on day 7 (**Figure 5.12**).
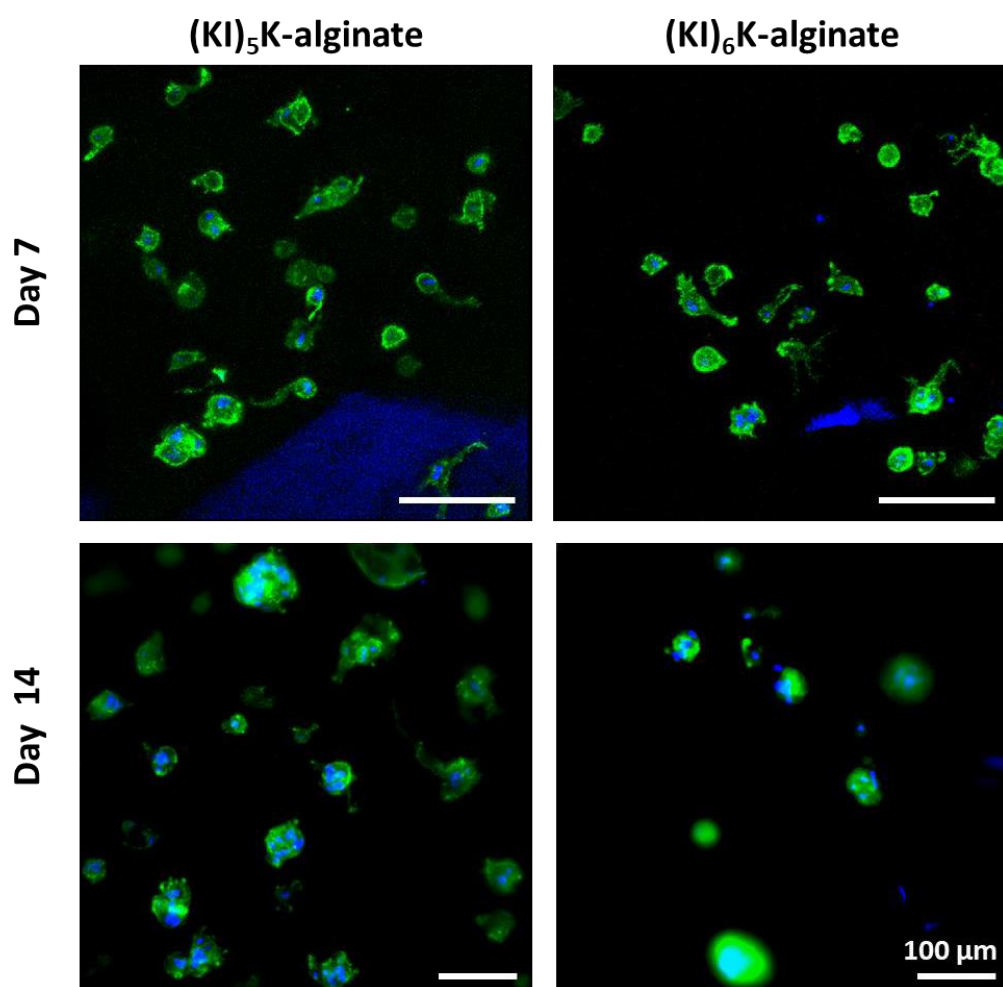
Figure 5.12: *CLSM of MSCs cultured on peptide-alginate hydrogels on days 7 and 14. F-actin was labelled with FITC-phalloidin (green) and nuclei with DAPI (blue). The blue background in the image came from hydrogel autofluorescence.*

To understand the role of $(KI)_nK$ peptides in mediating MSC activities, Ca-alginate hydrogels were used for comparison with peptide-alginate hydrogels. Multivalent cations, such as Ca^{2+},

enable the gelation of alginate solution by ionic cross-linking and whose concentration can affect the hydrogel structure and mechanical properties. Ca-alginate hydrogels are widely used as 3D scaffold for cell encapsulation with good cell viability (29). In this work alginate was cross-linked by 100 mM $CaCl_2$, exhibiting a similar rheological behaviour with $(KI)_nK$-alginate hydrogels (**Figure 5.13-E**). After 7 days of MSCs culture on the surface, lower cell density was found on the Ca-alginate hydrogel than on the three peptide-alginate hydrogels, indicating the lack of cell adhesion (**Figure 5.13-A and F**). No obvious cell aggregation was observed. Cells on the surface could exhibit round-shape and flat-shape, but no cell protrusions were observed, suggesting poor cell-substrate communication (**Figure 5.13-B to D**). Poor cell adhesion and proliferation has been always a challenge when using of Ca-alginate hydrogel as artificial cell scaffold due to the absence of cell adhesion motifs (30). The comparison between supramolecular peptide-alginate and peptide-Ca hydrogel reveals that $(KI)_nK$ peptide may function as bioactive molecule improving the cell adhesion and cell-substrate interaction.
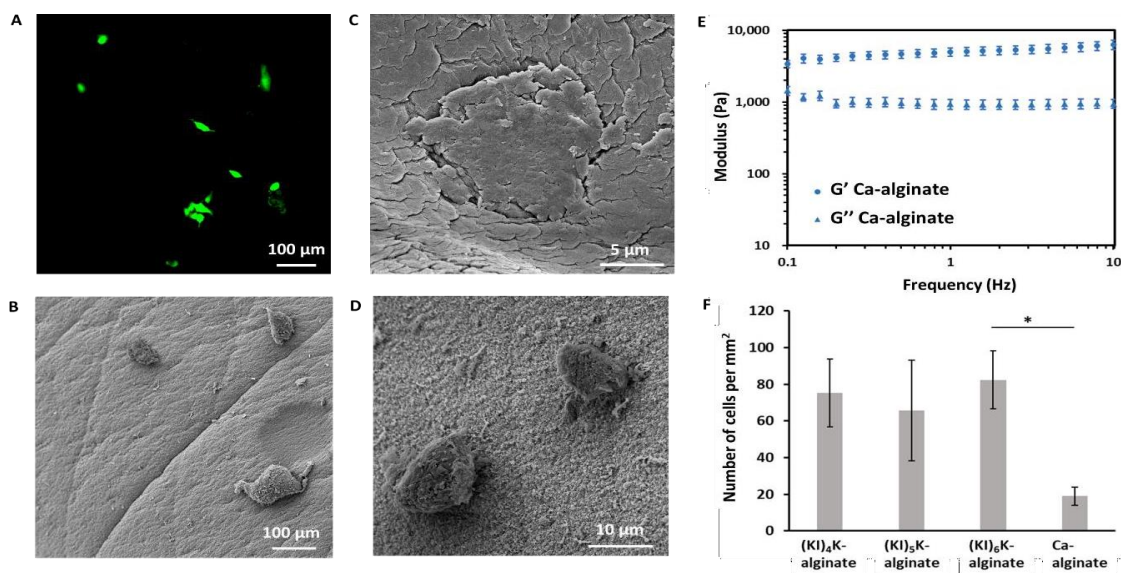
Figure 5.13: *(A) CLSM of calcein-stained live cells (green) and ethidium homodimer-stained dead cells (red) on Ca-alginate hydrogels on day 7. (B-D) SEM images of MSCs on Ca-alginate hydrogels on day 7. (E) Bulk rheology measurement of 1 wt% Ca-alginate cell-free hydrogels incubated in DMEM with 10% FBS overnight. (F) The analysis of cell density on peptide-alginate and Ca-alginate hydrogel. (*=p < 0.0332, and error bars represent standard deviation (n = 3)).*

5.3.3. Culture of MSCs on peptide and peptide-polymer coated well plates

MSCs cultured on supramolecular peptide-HA hydrogels were shown to quickly form sphere-like structures, while on supramolecular peptide-alginate hydrogel most round-shape cells kept separated in 7 days and may probably form small aggregates at longer culture times. Based on these results, the next question would be to investigate if the hydrogel environment is a prerequisite for the MSC spheroid formation, as well as the effect of the self-assembling $(KI)_nK$ on cell behaviour. MSCs were then seeded on the 96 well plate coated with peptide or peptide-polymer mixture solution. **Figure 5.14** shows the morphology and viability of MSCs seeded on peptide-coated surfaces on day 1. It was found that MSCs on $(KI)_4K$-coated and uncoated surfaces adopt a spindle-like morphology, while keeping round shape on $(KI)_5K$-coated and $(KI)_6K$-coated surfaces, at both low and high peptide concentration. The polycation PLL was used as the control for the positively charged $(KI)_nK$ peptides. PLL coated surfaces with high PLL concentration was shown to reduce MSC adhesion, promoting cell sheet detachment and spheroid formation (31). MSC tended to exhibit round shape on PLL-coated surface, like $(KI)_5K$ and $(KI)_6K$, probably because longer $(KI)_nK$ carries more positive charges than the shorter peptides, providing similar a cationic charge as PLL. However, when the coating concentration was raised, PLL showed great cell toxicity due to the disruption of cell membrane as almost all cells were dead. It is worth to notice that MSCs kept good viability on surfaces coated with higher peptide concentration, probably due to $(KI)_nK$ peptide self-assembling into fibrous structures, and the formation of supramolecular fibrils was able to reduce the overall cytotoxicity of cationic self-assembling peptides (32).
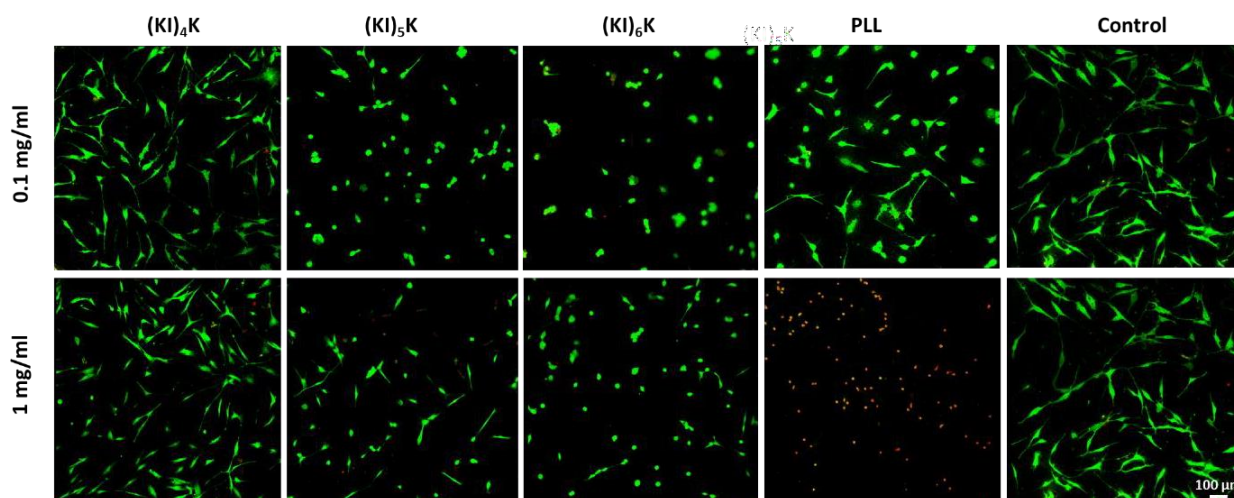
178

Figure 5.14: Fluorescent microscopy images of calcein-stained live cells (green) and ethidium homodimer-stained dead cells (red) cultured on peptide or PLL coated 96 well plate at different coating concentration at day 1. Control are cells cultured on uncoated wells.

The MSC morphology on the 7th day of culture on coated well plates is shown in **Figure 5.15**. For all peptide-coated surfaces, it was found that cells exhibit spreading morphology. Compared to uncoated surface, $(KI)_4K$ showed little influence on MSC adhesion, while the average cell area and cell density decreased as $(KI)_nK$ peptides are longer. Therefore, it is assumed that higher positive charges carried by longer $(KI)_nK$ peptide reduced the MSC adhesion.

In order to make closer comparisons with the supramolecular peptide-polymer hydrogel, peptide-polymer mixtures at low concentrations were used to produce coatings on the 96 well plate. The addition of HA was found to further reduce cell adhesion, as density and cell area of MSCs on $(KI)_5K$-HA and $(KI)_6K$-HA coating were lower than pristine $(KI)_5K$ and $(KI)_6K$ coatings, respectively. Specifically, some small cell clusters could be found on $(KI)_5K$-HA coating. However, cells showed better adhesion on peptide-alginate than on peptide-HA coated well plate, regardless of the peptide sequence. In chapter 3 it has demonstrated that alginate solutions exhibit larger negative zeta potential than HA (**Figure 3.12**), It is therefore plausible to assume that alginate could screen the charges carried by $(KI)_nK$ more effectively,

and no significant differences on cell adhesion could be observed between peptide-alginate coatings and control samples. Some polycation-polymer coated surface have shown to decrease MSC adhesion and induce spheroid formation. For example, both chitosan and chitosan-HA coated coverslip were capable of producing MSC spheroids, while increasing amount of HA in the membrane would promote cellular motility (17). Research also found that glass slides coated with a PLL-HA multilayer was resistant to MSC adhesion, independent of the number of layers, which was ascribed to the low stiffness of soft multilayer membrane (27). The improvement of multilayer stiffness by covalent cross-linking led to better cell adhesion, and similar phenomena was observed on chitosan-alginate multilayer membrane (26). Therefore, the net positive charge of $(KI)_nK$ peptides, the biofunction of HA in improving cell migration, and the soft ECM-like microenvironment provided by the coated surface could all contribute to the reduced adhesion of MSCs on peptide-HA coated well plate.

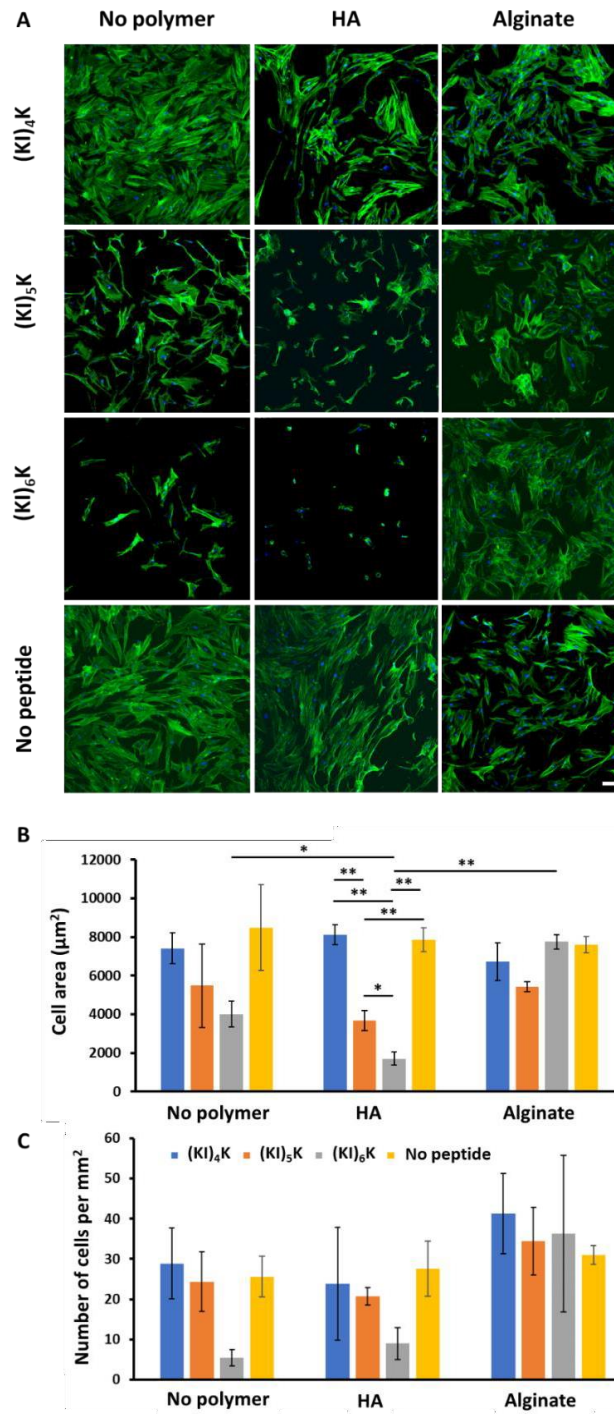**Figure 5.15:** *(A) Fluorescent microscopy images of MSCs seeded on peptide and peptide-polymer coated well plate on day 7 (scale bar =100 µm). F-actin was labelled with FITC-phalloidin (green) and nuclei with DAPI (blue). (B) Cell area and (C) cell density after 7 days cultured on peptide and peptide-polymer membrane. (*=p < 0.0332; **=p < 0.0021, and error bars represent standard deviation (n = 3)).*

181

5.4. Conclusions

It has been demonstrated that the supramolecular peptide-HA hydrogels could potentially be used as an *in vitro* model of the human vitreous considering their compositional and structural similarity. However, engineering a hydrogel mimicking the vitreous mechanical properties still remains a challenge. Supramolecular peptide-polymer hydrogels are promising *in vitro* platform for MSC culture, where $(KI)_nK$ peptides may effectively promote cell-substrate interactions so that cell could well sensor and respond to the surrounding microenvironment. MSCs on peptide-HA hydrogels are capable of self-aggregating into spheroids in 3 days and spheroid disassembly could be observed on day 7, while MSCs on peptide-alginate do not form apparent spheroid on day 7 but may form some small clusters on day 14. It is hypothesized that both bulk rheology and hydrogel surface structure affect the cell spheroid formation, and HA may play an important role in promoting cell migration and encourage cell aggregation. Additionally, no evident cell spheroid could be detected on peptide or peptide-polymer coated well plate confirming that the hydrogel environment also supports the spheroid formation. This work introduces a new method for the effective formation of MSC spheroids *in situ* on supramolecular ECM-like hydrogel without external forces. Since scaffold-based MSC spheroid culture has been successfully applied in nerve regeneration, cartilage repair and vascular repair, the MSC spheroid loaded peptide-HA hydrogels hold promise in the field of regenerative medicine. Besides stem cell spheroid, cancer cell spheroids also raised intense attention as it represents the architecture of native tumours and the cell–cell and cell–ECM interactions that occur in real tumours (5). The supramolecular peptide-HA hydrogels could be also used to fabricate cancer cell spheroid and create *in vitro* tumour models containing an HA-rich environment which is typically overexpressed in a variety of cancer types (e.g. pancreatic and ovarian cancers).

5.5. References

1.   Swindle-Reilly KE, Shah M, Hamilton PD, Eskin TA, Kaushal S, Ravi N. Rabbit Study of an In Situ Forming Hydrogel Vitreous Substitute. Investigative Ophthalmology & Visual Science. 2009;50(10):4840-6.

2.   Le Goff MM, Bishop PN. Adult vitreous structure and postnatal changes. Eye. 2008;22(10):1214-22.

3.   del Amo EM, Rimpelä A-K, Heikkinen E, Kari OK, Ramsay E, Lajunen T, et al. Pharmacokinetic aspects of retinal drug delivery. Progress in Retinal and Eye Research. 2017;57:134-85.

4.   Nickerson CS, Park J, Kornfield JA, Karageozian H. Rheological properties of the vitreous and the role of hyaluronic acid. Journal of Biomechanics. 2008;41(9):1840-6.

5.   Tseng T-C, Wong C-W, Hsieh F-Y, Hsu S-h. Biomaterial Substrate-Mediated Multicellular Spheroid Formation and Their Applications in Tissue Engineering. Biotechnology Journal. 2017;12(12):1700064.

6.   Cesarz Z, Tamama K. Spheroid Culture of Mesenchymal Stem Cells. Stem Cells Int. 2016;2016:9176357-.

7.   Tsai A-C, Liu Y, Yuan X, Ma T. Compaction, fusion, and functional activation of three-dimensional human mesenchymal stem cell aggregate. Tissue Eng Part A. 2015;21(9-10):1705-19.

8.   Kleinman HK, Philp D, Hoffman MP. Role of the extracellular matrix in morphogenesis. Current Opinion in Biotechnology. 2003;14(5):526-32.

9.   Huang GS, Tseng CS, Linju Yen B, Dai LG, Hsieh PS, Hsu Sh. Solid freeform-fabricated scaffolds designed to carry multicellular mesenchymal stem cell spheroids for cartilage regeneration. Eur Cell Mater [Internet]. 2013 2013/10//; 26:[179-94; discussion 94 pp.].

10.   He J, Zhang N, Zhu Y, Jin R, Wu F. MSC spheroids-loaded collagen hydrogels simultaneously promote neuronal differentiation and suppress inflammatory reaction through PI3K-Akt signaling pathway. Biomaterials. 2021;265:120448.

11.   Caliari SR, Burdick JA. A practical guide to hydrogels for cell culture. Nat Methods. 2016;13(5):405-14.

12.   Awwad S, Lockwood A, Brocchini S, Khaw PT. The PK-Eye: A Novel In Vitro Ocular Flow Model for Use in Preclinical Drug Development. J Pharm Sci. 2015;104(10):3330-42.

13.   Huang D, Chen Y-S, Xu Q, Hanes J, Rupenthal ID. Effects of enzymatic degradation on dynamic mechanical properties of the vitreous and intravitreal nanoparticle mobility. European Journal of Pharmaceutical Sciences. 2018;118:124-33.

14.   Xu Q, Boylan NJ, Suk JS, Wang YY, Nance EA, Yang JC, et al. Nanoparticle diffusion in, and microrheology of, the bovine vitreous ex vivo. J Control Release. 2013;167(1):76-84.

15.   Käsdorf BT, Arends F, Lieleg O. Diffusion Regulation in the Vitreous Humor. Biophys J. 2015;109(10):2171-81.

16.   Baraniak PR, McDevitt TC. Scaffold-free culture of mesenchymal stem cell spheroids in suspension preserves multilineage potential. Cell and Tissue Research. 2012;347(3):701-11.

17.   Huang G-S, Dai L-G, Yen BL, Hsu S-h. Spheroid formation of mesenchymal stem cells on chitosan and chitosan-hyaluronan membranes. Biomaterials. 2011;32(29):6929-45.

18.   Suzuki S, Mizuno M, Sakamaki Y, Mimata A, Endo K, Kohno Y, et al. Morphological changes in synovial mesenchymal stem cells during their adhesion to the meniscus. Laboratory Investigation. 2020;100(7):916-27.

19.   Adams JC. Cell-matrix contact structures. Cellular and Molecular Life Sciences CMLS. 2001;58(3):371-92.

20.   Gonzalez-Rodriguez D, Guevorkian K, Douezan S, Brochard-Wyart F. Soft Matter Models of Developing Tissues and Tumors. Science. 2012;338(6109):910-7.

21.   Yamada KM, Cukierman E. Modeling tissue morphogenesis and cancer in 3D. Cell. 2007;130(4):601-10.

22.   Ferreira DS, Marques AP, Reis RL, Azevedo HS. Hyaluronan and self-assembling peptides as building blocks to reconstruct the extracellular environment in skin tissue. Biomaterials Science. 2013;1(9):952-64.

23.   Ribeiro S, Radvar E, Shi Y, Borges J, Pirraco RP, Leonor IB, et al. Nanostructured interfacial self-assembled peptide–polymer membranes for enhanced mineralization and cell adhesion. Nanoscale. 2017;9(36):13670-82.

24.   Mendes AC, Smith KH, Tejeda-Montes E, Engel E, Reis RL, Azevedo HS, et al. Co-Assembled and Microfabricated Bioactive Membranes. Advanced Functional Materials. 2013;23(4):430-8.

25.   Teo GSL, Ankrum JA, Martinelli R, Boetto SE, Simms K, Sciuto TE, et al. Mesenchymal Stem Cells Transmigrate Between and Directly Through Tumor Necrosis Factor-α-Activated Endothelial Cells Via Both Leukocyte-Like and Novel Mechanisms. STEM CELLS. 2012;30(11):2472-86.

26.   Silva JM, Duarte ARC, Caridade SG, Picart C, Reis RL, Mano JF. Tailored Freestanding Multilayered Membranes Based on Chitosan and Alginate. Biomacromolecules. 2014;15(10):3817-26.

27.   Semenov OV, Malek A, Bittermann AG, Vörös J, Zisch AH. Engineered Polyelectrolyte Multilayer Substrates for Adhesion, Proliferation, and Differentiation of Human Mesenchymal Stem Cells. Tissue Engineering Part A. 2009;15(10):2977-90.

28.   Serban MA, Skardal A. Hyaluronan chemistries for three-dimensional matrix applications. Matrix Biol. 2019;78-79:337-45.

29.   Gionet-Gonzales M, Casella A, Diloretto D, Ginnell C, Griffin KH, Bigot A, et al. Sulfated Alginate Hydrogels Prolong the Therapeutic Potential of MSC Spheroids by Sequestering the Secretome. Advanced Healthcare Materials. 2021;10(21):2101048.

30.   Liu Z, Lu M, Takeuchi M, Yue T, Hasegawa Y, Huang Q, et al. In vitro mimicking the morphology of hepatic lobule tissue based on Ca-alginate cell sheets. Biomedical Materials. 2018;13(3):035004.

31.   Lu H, Guo L, Kawazoe N, Tateishi T, Chen G. Effects of Poly(L-lysine), Poly(acrylic acid) and Poly(ethylene glycol) on the Adhesion, Proliferation and Chondrogenic Differentiation of Human Mesenchymal Stem Cells. Journal of Biomaterials Science, Polymer Edition. 2009;20(5-6):577-89.

32.   Xu D, Jiang L, Singh A, Dustin D, Yang M, Liu L, et al. Designed supramolecular filamentous peptides: balance of nanostructure, cytotoxicity and antimicrobial activity. Chemical Communications. 2015;51(7):1289-92.

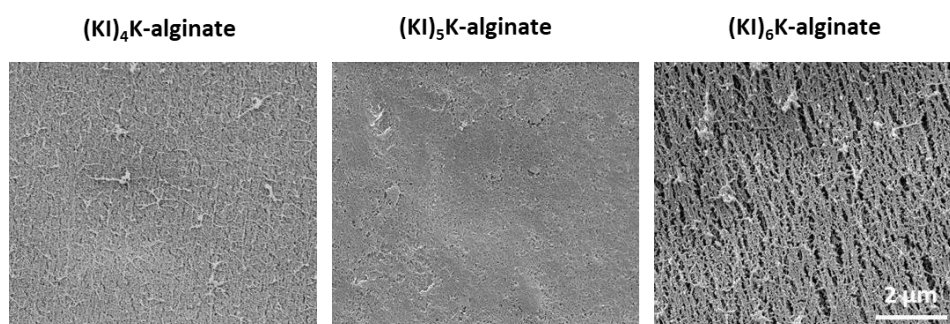## 5.6. Appendix

(KI)$_4$K-alginate   (KI)$_5$K-alginate   (KI)$_6$K-alginate

2 μm

Figure 5.16: *SEM images showing supramolecular peptide-alginate hydrogels with a dense surface.*

Chapter 6

Conclusions and future work

6. Conclusions and future work

In this work, self-assembling β-sheet forming peptides with the generic sequence $(KI)_nK$ were designed (n=2 to 6). The peptides showed good solubility in water due to the high percentage of hydrophilic/cationic residues. The change of pH or ionic strength could induce their self-assembly into nanofibrils. Longer $(KI)_nK$ peptides show increased hydrophobicity and had a stronger tendency to form β-sheet structures. Cationic $(KI)_nK$ peptides were shown to self-assemble with varied anionic polyelectrolytes, including HA, alginate, PSS and PAA, forming supramolecular hybrid peptide-polymer hydrogels with distinct properties and indicating their further exploitation either as control hydrogels or for non-biomedical applications. Among all supramolecular peptide-polymer hydrogels, peptide-HA hydrogels have attracted special attention as it may structurally and compositionally mimic the protein-polymer complexes found in the natural tissues. In particular, the micro- nanostructure of peptide-HA hydrogels could be tuned by changing the peptide sequence and concentration due to different self-assembling ability of $(KI)_nK$ peptides. Peptide-HA complexes exhibit similar viscoelastic properties to HA as they showed frequency-dependant rheological behaviour. *In vitro* application of peptide-HA hydrogel was also explored in this work, including their ability to act as *in vitro* model of the human vitreous. Despite the structural similarities, it still remains challenging to design a proper *in vitro* model using peptide-HA hydrogels as they are much stiffer than human vitreous. Nonetheless, these hydrogels could be eventually used as vitreous substitutes after vitrectomy, but further research are required to assess this possibility. Since the structural and rheological properties of the supramolecular peptide-HA hydrogels could be tuned, these hydrogels were tested in stem cell culture studies. It was shown that the hydrogels could be used as an artificial scaffold and supported the formation of stem cell spheroids. By studying the cell behaviour on peptide-alginate hydrogel and peptide-polymer coated surface as controls, it was assumed that the components (both

peptide and HA), the mechanical properties and the hydrogel environment may all together induce the formation of stem cell spheroid on supramolecular peptide-HA hydrogels.

However, there are some challenges that need to be tackled in the future work. In this work, the mechanical properties of hydrogels were studied using bulk rheology. However, the local rheological properties still remain unclear. It is noticeable that in hydrogel-based cell culture, understanding the microscale mechanical properties is important to elucidate cell interactions with the material (1). Using nanoindentation technology to explore the local Young's modulus of the peptide-polymer hydrogel would be useful to investigate the effect of mechanical properties on cell behaviour and cell spheroid formation. In addition, it also worth to study specific cell functions when cultured on the peptide-HA in more detail (e.g. expression of certain genes and specific cell markers) to ascertain their stemness or their differentiation towards preferential phenotypes. Studies from the literature have demonstrated that MSC-based spheroids often show higher stemness and enhanced multilineage differentiation capacities compared to the disassociate MSCs (2).

The application of scaffold-based MSC spheroids in neuroregeneration strategies has received increased interests (3). In particular, supramolecular peptide-HA hydrogel are soft viscoelastic materials. It is known that the mechanical properties of matrix could direct the stem cell fate, and matrices with low-elasticity (E=0.1-1 kPa) may induce neural differentiation of MSCs (4). Therefore, MSC spheroid-loaded peptide-HA hydrogel may have potential applications in neuroregeneration. Cancer-based spheroids are also being widely used as *in vitro* 3D tumour models, as they mimic the native microenvironment of tumours. Additionally, HA is capable of regulating the cancer cell behaviour (e.g. HA promoted the adhesion migration of breast cancer cell (5)). Therefore, supramolecular peptide-HA hydrogels might be a promising *in vitro* tumour models which may recapitulate 3D spheroid-like microenvironment, where the effect of HA on cancer cell activities could be further investigated in a more realistic manner.

References

1.   Dobre O, Oliva MAG, Ciccone G, Trujillo S, Rodrigo-Navarro A, Venters DC, et al. A Hydrogel Platform that Incorporates Laminin Isoforms for Efficient Presentation of Growth Factors – Neural Growth and Osteogenesis. Advanced Functional Materials. 2021;31(21):2010225.

2.   Tseng T-C, Wong C-W, Hsieh F-Y, Hsu S-h. Biomaterial Substrate-Mediated Multicellular Spheroid Formation and Their Applications in Tissue Engineering. Biotechnology Journal. 2017;12(12):1700064.

3.   He J, Zhang N, Zhu Y, Jin R, Wu F. MSC spheroids-loaded collagen hydrogels simultaneously promote neuronal differentiation and suppress inflammatory reaction through PI3K-Akt signaling pathway. Biomaterials. 2021;265:120448.

4.   Engler AJ, Sen S, Sweeney HL, Discher DE. Matrix elasticity directs stem cell lineage specification. Cell. 2006;126(4):677-89.

5.   Herrera-Gayol A, Jothy S. Effects of hyaluronan on the invasive properties of human breast cancer cells in vitro. Int J Exp Pathol. 2001;82(3):193-200.